

New lipid-based formulation approaches and characterization tools for hot-melt extrusion

Inauguraldissertation

zur

Erlangung der Würde eines Doktors der Philosophie

Vorgelegt der

Philosophisch-Naturwissenschaftlichen Fakultät

der Universität Basel

von

Camille Adler

aus Mulhouse, Frankreich

Basel, 2017

Originaldokument gespeichert auf dem Dokumentenserver der Universität Basel edoc.unibas.ch

Genehmigt von der Philosophisch-Naturwissenschaftlichen Fakultät
auf Antrag von

Fakultätsverantwortlicher	Herrn Prof. Dr. Georgios Imanidis
Korreferentin	Frau Prof. Dr. Karine Mougin

Basel, den 18. April 2017

Prof. Dr. Martin Spiess
Dekan

*“Science is not only a disciple of reason but, also, one of romance
and passion.”*

Stephen Hawking

Abstract

Amorphous solid dispersions (SDs) are considered as one of the most effective strategies for the formulation of poorly water-soluble compounds. The active compound is dispersed in an inert carrier composed of a polymer and active excipients. Since the drug is amorphous, there is typically an increase in apparent solubility as well as dissolution rate. Various methods are employed for manufacturing of SDs, nevertheless, hot-melt extrusion (HME) has become one of the most common process techniques. Indeed, as a solvent-free, one-step continuous process allowing the production of a wide variety of solid dosage forms, HME has emerged as an attractive method. Among the excipients that can be used for SD development, lipid-based excipients are particularly interesting for the formulation of lipophilic compounds. They act as drug solubilizers and stabilizers by improving the chemical and physical stability of drugs. Among poorly water-soluble compounds those exhibiting both high crystallinity and lipophilicity are particularly challenging and require specific formulation considerations. A simple polymeric system might not be sufficient to obtain amorphous SDs. This can lead to sophisticated systems in structure and composition, which are hence rather complex to characterize by means of conventional analysis methods.

The present thesis consists of four studies that aim at developing novel lipid-based formulations for crystalline lipophilic compounds by means of HME and that introduce new characterization methods. For this purpose, β -carotene (BC) was selected as a high melting point, poorly water-soluble model compound.

The objective of the first study was to compare the ability of state-of-the-art methods to detect the presence of low-dose crystalline compounds in lipid matrices. Sensitivity issues were encountered using conventional methods, therefore a new analytical tool was introduced. The novel flow-through cross-polarized imaging combined the advantages of analyzing large sample sizes and the high sensitivity of a microscopic technique. Small amounts of crystalline materials could easily be detected and an upper limit of the kinetic solubility of the model compound could be estimated.

The second study aimed at designing lipid microdomains for drug delivery systems produced by HME. A polymer, a solid fatty acid and an inorganic adsorbent were combined. The acidic lipid was meant to adsorb onto the inorganic carrier to create so called designed lipid microdomains (DLMs) to host an active compound. The employed analytical methods supported the assumption of specific molecular interactions between the fatty acid and the adsorbent. These interactions fostered the amorphization and stabilization of the acidic lipid and lead to the targeted DLM. The novel delivery system appeared to be promising for inclusion of a crystalline lipophilic compound.

In the third study, hot-melt extrudates composed of a polymer, a liquid lipid and different kinds of silica-based adsorbents were produced. Such formulations exhibited a complex microstructure. Since the microstructure can influence the final dosage form quality attributes, the aim was to introduce a mathematical tool for structural analysis of extrudates. This work introduced the multifractal formalism in the field of pharmaceutics and showed that the adsorbent concentration, the type of adsorbent as well as the screw speed had an influence on the microstructure. This study was complemented by self-dispersion analysis since it can condition release of any active compound. We showed that the self-dispersion ability of extrudates can be modified by the lipophilic or hydrophilic nature of the adsorbent. The multifractal and self-dispersion studies appeared to be complementary to better understand complex formulations and future work should evaluate specific effects on drug formulation microstructure.

Finally, in the fourth study a polymer, a liquid lipid and two types of adsorbents were employed as excipients for HME. Using these ingredients, amorphous SDs of BC were produced. The influence of the adsorbent type as well as the presence of amorphous substance on the microstructure was assessed by multifractal analysis. This structural analysis was complemented by mechanical analysis of extrudates. Our results suggested that the type of adsorbent and the presence of amorphous compound had an impact on the extrudate microstructure and thus on the mechanical performance. These findings evidenced the complementarity of the two methods, which could further be used in the development of dosage forms that require knowledge on mechanical properties.

This thesis introduced new lipid-based delivery systems for poorly-water soluble compounds. Novel excipient combinations, involving polymer matrices, lipid-based excipients and inorganic adsorbents, have been suggested for HME and state-of-the-art characterization methods were complemented by new analytical tools to better understand complex formulations. A flow-through cross polarized imaging technique allowed overcoming sensitivity issues encountered otherwise with conventional methods. Moreover, multifractal formalism complemented by self-dispersion imaging provided key insights into pharmaceutical dosage form microstructure that is hardly accessible using conventional methods. These new approaches for HME bear much potential in pharmaceutical technology to tailor dosage form performance.

Contents

Abstract	iii
Contents.....	vi
1) Introduction	1
1.1. Background.....	1
1.2. Objectives	3
2) Theoretical section.....	5
2.1. Solid dispersions.....	5
2.1.1. Solid dispersions containing organic excipients	5
2.1.1.1. Classification.....	5
2.1.1.2. Advantages and limitations	8
2.1.1.3. Manufacturing processes.....	9
2.1.2. Solid dispersions containing inorganic carriers	10
2.2. Hot-melt extrusion.....	12
2.2.1. Equipment and process	13
2.2.2. Advantages and limitations.....	18
2.2.3. Excipients used in HME	18
2.2.4. Selection of excipients	22
2.2.5. Solid-state characterization.....	27
2.2.6. Biopharmaceutical characterization.....	31
2.3. β -carotene	31
3) Flow-through cross-polarized imaging as a new tool to overcome the analytical sensitivity challenges of a low-dose crystalline compound in a lipid matrix.....	34
Summary	34
3.1. Introduction	35
3.2. Materials and methods.....	37
3.2.1. Materials	37
3.2.2. Preparation of the solid dispersions	38

3.2.3. Time-domain NMR.....	38
3.2.4. Differential scanning calorimetry	39
3.2.5. Statistical analysis	39
3.2.6. X-ray powder diffraction	39
3.2.7. Polarized light microscopy in reflection-mode	39
3.2.8. 3D-laser scanning microscopy.....	40
3.2.9. Atomic force microscopy.....	40
3.2.10. Reversed-phase high-performance liquid chromatography (RP-HPLC).....	40
3.2.11. Flow-through cross-polarized imaging in transmission mode.....	41
3.3. Results and discussion	42
3.3.1. Study of the raw materials	42
3.3.2. Solid dispersion characterization with state-of-the-art methods.....	44
3.3.3. Study of the solid dispersions using flow-through cross-polarized imaging	54
3.4. Conclusion	57
4) Molecularly designed lipid microdomains for solid dispersions using a polymer/inorganic carrier matrix produced by hot-melt extrusion.....	58
Summary	58
4.2. Introduction	59
4.3. Materials and methods.....	60
4.3.1. Materials	60
4.3.2. Hot-melt extrusion	61
4.3.3. Time-domain nuclear magnetic resonance	62
4.3.4. X-ray powder diffraction	62
4.3.5. Attenuated total reflectance Fourier-transform infrared spectroscopy	63
4.3.6. Atomic force microscopy.....	63
4.3.7. Scanning electron microscopy and energy dispersive X-ray spectroscopy	63
4.3.8. Reversed phase high-performance liquid chromatography	63
4.4. Results	64
4.4.1. Study of raw materials	64

4.4.2. Characterization of extrudate strands.....	65
4.4.2.1. Evaluation of SA crystallinity by XRPD	65
4.4.2.2. Interaction of SA with AMS	67
SA head group vibrations	67
SA alkyl chain vibrations	68
4.4.2.3. Temperature-variable ATR-FTIR analysis of SA.....	70
SA head group vibrations.	70
SA alkyl chain vibrations	71
4.4.2.4. AFM and SEM/EDS analyses of the extrudates	72
4.4.3. Extrudates containing β -carotene as model compound	74
4.5. Discussion.....	78
4.5.1. Molecular design of lipid microdomains	78
4.5.2. Formulation of a lipophilic, highly crystalline compound using DLM	81
4.6. Conclusion	82
Appendix A	83
5) Multifractal characterization of pharmaceutical hot-melt extrudates.....	85
Summary	85
5.2. Introduction	85
5.3. Essentials of multifractal analysis	88
5.4. Materials and methods.....	90
5.4.1. Materials	90
5.4.2. BET powder specific surface area	90
5.4.3. Hot-melt extrusion	91
5.4.4. Scanning electron microscopy and energy X-ray dispersive spectroscopy	92
5.4.5. Image processing and multifractal analysis	92
5.4.6. Dispersion and erosion of pellets in water.....	93
5.4.7. Statistical analysis	93
5.5. Results and discussion	94
5.5.1. Understanding the microstructure of pharmaceutical extrudates.....	94

5.5.1.1. Multifractal analysis of extrudate pellets containing Aeroperl 300	94
5.5.1.2. Multifractal Analysis of extrudates containing different adsorbents	97
5.5.2. Automated static imaging of pellets self-dispersion	99
5.6. Conclusion	104
Appendix B	105
6) Multifractal and mechanical analysis of amorphous solid dispersions	106
Summary	106
6.1. Introduction	107
6.2. Materials and methods	109
6.2.1. Materials	109
6.2.2. Hot-melt extrusion	109
6.2.3. Oil loading capacity	110
6.2.4. BET powder specific surface area	110
6.2.5. Mercury porosimetry	110
6.2.6. Differential scanning calorimetry	111
6.2.7. X-ray powder diffraction	111
6.2.8. Raman spectroscopy	111
6.2.9. Scanning electron microscopy/energy X-ray dispersive spectroscopy	111
6.2.10. Image processing and multifractal analysis	112
6.2.11. Three point bending test	115
6.2.12. Reversed phase high-performance liquid chromatography	115
6.3. Results and discussion	115
6.3.1. Characterization of BC physical state	115
6.3.2. Understanding the microstructure of hot-melt extrudates	121
6.3.2.1. Multifractal analysis of placebo extrudates	121
6.3.2.2. Multifractal analysis of BC extrudates	123
6.3.3. Mechanical properties of hot-melt extrudates	126
6.4. Conclusion	128
Appendix C	129

7) Final remarks and outlook	130
Bibliography	133
List of abbreviations	150
List of symbols.....	152
List of figures	154
List of tables	157
Acknowledgements.....	158

Chapter 1

Introduction

1.1. Background

Currently, 50-60% of the new active pharmaceutical ingredients (API) exhibit poor aqueous solubility. Therefore, the formulation of such new chemical entities (NCEs) is a substantial challenge for the pharmaceutical industry. Most of these compounds belong to class II according to the Biopharmaceutical Classification System (BCS) introduced by Amidon et al. [1,2]. Class II compounds are characterized by a low aqueous solubility and high effective permeability. The main challenge for delivery of class II substances is to achieve sufficiently high solubility in line with the requirements of the dosage form. Among all routes of administration, oral drug delivery is the preferred and easiest way since it is better accepted by the patients and can be produced in a wide variety of dosage forms [3]. Different approaches have been developed to formulate oral dosage forms of poorly water-soluble APIs, such as complexation, microemulsions, nanoemulsions, micellization, salt formation or solid dispersions (SDs) [4]. Over the last decades, SD which involves the dispersion of a poorly water-soluble compound in a hydrophilic or amphiphilic carrier, appeared as the most successful and promising strategy [1,5,6]. SDs are of high interest for the formulation of high melting point lipophilic compounds that are particularly challenging and require special excipient combinations.

Several types of SDs have been developed over the last decades that are not all equal regarding the physical state of the API in the matrix. The most common and attractive systems are the amorphous solid suspension or solution, where the active compound is in an amorphous form or molecularly dispersed, respectively [4,7]. The amorphous state or the molecular dispersion of an API indeed show typically higher oral bioavailability compared to the crystalline form because of

higher free energy and better thermodynamic activity [8]. Amorphous SDs can be produced by using various manufacturing methods such as solvent evaporation, spray-drying, melting, or hot-melt extrusion (HME).

As a solvent-free, one-step continuous process, HME offers an attractive alternative to other pharmaceutical techniques, therefore a growing interest in this method has been shown in the last 10-15 years [9–11]. During the HME process a material melts or softens under elevated temperature/pressure and is forced through an orifice (i.e. die) by rotating screws [12]. A variety of downstream processes exist that can be even combined, allowing the design of a wide range of dosage forms (e.g. pellets, tablets, granules). The intense mixing imposed by the screws results typically in a uniform dispersion of excipients and active ingredients. The release rate and formulation stability can be tailored according to the choice of polymeric matrix and additives [7]. The major excipient used in HME is a polymeric carrier. In some cases, the selection of the adequate polymer can be challenging and it requires knowledge on the physico-chemical properties. Polymers used in HME should have a thermoplastic behavior, which means that they should soften without decomposing at the processing temperature and solidify while exiting the die. One drawback of the HME process is the rather low number of available polymers that are approved for pharmaceutical use and exhibit sufficient thermal stability [12,13].

The selection of appropriate polymer and functional excipients (e.g. plasticizer, antioxidant, pore formers) is of high importance in the development of amorphous SDs [14]. Thermal stability is a first prerequisite, however, other parameters should also be considered to ensure drug/excipients miscibility and thermodynamic stability of the final dosage form. Physico-chemical properties, such as solubility parameters, glass transition temperature, melting temperature, hygroscopicity, hydrogen-bonding donor or accepting groups, and mechanical properties are all key parameters that contribute to the achievement of the desired improvement in solubility, bioavailability and stability [15]. Numerous methodologies are available to characterize material properties in pre- and post-processing steps. The most commonly used methods are differential scanning calorimetry (DSC), thermogravimetric analysis (TGA), microscopic techniques, X-ray powder diffraction (XRPD), Fourier-transform infrared spectroscopy (FTIR), Raman spectroscopy, and dissolution tests.

In the case of highly crystalline and lipophilic APIs, already an initial assessment for the selection of suitable excipients can show clear limitations. As already mentioned, such compounds are particularly challenging and often require special formulation consideration. Thus, simple polymer systems might often not be suitable for the production of amorphous SDs [16,17] (c.f. sections 4, 6 and [18]). The use of lipid-based excipients can be a key for the formulation and stabilization of lipophilic compounds. It will be shown that the combination of lipid-based excipients with inorganic carriers enabled amorphous SDs of a low-dose crystalline lipophilic model compound, β -carotene (BC) [16] (c.f. sections 4, 6 and [18]).

Such multi-component formulations often exhibit a complex microstructure, which likely affect the final dosage form performance such as processability during downstream processing, mechanical properties, or dissolution behavior. Therefore a better characterization of this microstructure is crucial for a better understanding and tailoring of SDs quality attributes.

1.2. Objectives

The aims of this thesis address the aforementioned challenges to formulate a lipophilic as well as crystalline model compound with lipid-based amorphous SDs produced by HME. The formulation of such substances should overcome high crystal energy as well as limited water solvation. The use of conventional HME polymer systems is not sufficient to convert crystalline lipophilic compounds in an amorphous form and solid lipid excipients alone are not adapted for a melt extrusion process. Therefore, new kinds of formulations that involve specific excipient combinations are developed and new analytical tools are introduced. These formulations aim at taking advantage of polymer systems, lipid-based excipients and inorganic adsorbents to obtain amorphous SDs by HME. This thesis is subdivided into individual chapters, which study the formulation of lipid-based SDs and propose characterization tools for complex formulations.

The theoretical section presented in the second chapter aims at providing background information on the formulation of SDs and commonly used characterization methods.

A first objective of this PhD thesis is to compare sensitivity limits of commonly used methods to detect the presence of a low-dose crystalline compound in a lipid matrix. Based on the sensitivity

issues encountered with state-of-the-art methods, a new tool was introduced, which allowed detecting small amounts of crystalline substances.

Lipid-based excipients are particularly attractive for the formulation of lipophilic compounds. However, high amounts of lipid-based excipients cannot be used for the HME process due to their low melt viscosity. Therefore, a second aim was to develop new kinds of SDs by HME. The new approach is based on the combination of a polymer, a solid lipid, and a silica-based adsorbent. The target is to adsorb the lipid onto the inorganic carrier to design lipid microdomains that could further accommodate a poorly-water soluble compound.

The formulation of crystalline lipophilic compounds implies multiple excipient combinations. The third objective of this study is to introduce multifractal analysis to characterize complex hot-melt extrudates composed of a polymer, a liquid lipid and different types of inorganic silica-based adsorbents. The purpose is to study the influence of the concentration and the type of inorganic carrier as well as the screw speed on the formulation microstructure. This is complemented by the investigation of self-dispersion ability of extrudate pellets by optical imaging.

The final aim is to employ multifractal analysis to assess the influence of the adsorbent manufacturing process and the presence of an amorphous substance on the microstructure. Since changes in the microstructure can have an impact on final dosage form mechanical performances, mechanical properties of extrudates are also investigated.

Chapter 2

Theoretical section

2.1. Solid dispersions

Since the 1960's, solid dispersions (SDs) have become the most commonly used formulation technology to improve the solubility and bioavailability of highly crystalline and lipophilic drugs [13]. Their formulation involves an increase in surface area, the optimization of their wetting properties or the improvement of their apparent solubility. SD allows overcoming some limitations encountered with conventional solubilization techniques used for solubility enhancement, such as salt formation, co-solvent solubilization or particle size reduction. Salt formation cannot be applied to neutral compounds, solubilization leads primarily to liquid dosage forms, and finally very small particles obtained by particle size reduction can exhibit low mechanical properties and can therefore be difficult to handle. Further aspects of different formulation approaches for poorly-water soluble drugs can be inferred elsewhere [19]. According to Chiou and Riegelman [20] a SD is defined by a “dispersion of one or more active ingredients in an inert carrier at the solid state, prepared by the melting, solvent or melting solvent method”. Most of SD formulations contain organic excipients, with the principal component being a polymeric matrix. However, SD that contain inorganic additives have also been developed in recent years [21].

2.1.1. Solid dispersions containing organic excipients

2.1.1.1. Classification

Over the last decades four generations of SDs containing organic excipients were developed [4,6,22–24]. The first generation was initiated by Sekiguchi and Obi in 1961 [25]. Two types of

SDs were obtained by using crystalline carriers such as urea or mannitol, i.e. (i) eutectic mixtures, where both the drug and the carrier were in a crystalline state, and (ii) monotectic mixtures (or solid solutions), where the drug was in an amorphous form. Such first generation formulations with crystalline drug were suffering from little dissolution enhancement, while amorphous formulation in non-polymeric matrix were problematic from the perspective of physical stability. To overcome such issues, the second generation SD emerged in the 1970's for which crystalline matrices were replaced by natural or synthetic amorphous polymeric carriers. This generation includes three types of SDs depending on the physical state of the API in the matrix. The dispersion of the drug in an amorphous state corresponds to a glassy suspension, if the drug remains in the form of fine crystalline particles after the formulation process, a crystalline suspension is obtained and finally, a glassy solution corresponds to the molecular dispersion of the API in the matrix. Fig. 2.1 illustrates the three different types of amorphous SDs. In this generation of SDs, drug release in aqueous media is often limited by issues of poor dispersibility or short duration of drug supersaturation [4].

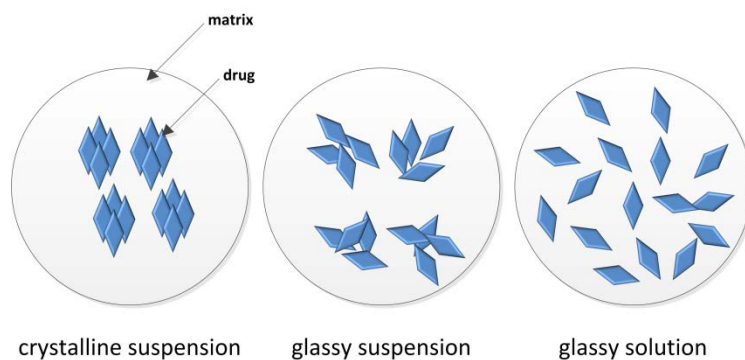


Fig. 2.1. Illustration of the different types of amorphous solid dispersions

This led to the development of the third generation of SD, which contains surface active agents or lipid-based excipients in combination with polymers to achieve improved drug precipitation inhibition upon aqueous dispersion, which is likely to result in enhanced oral absorption. Finally, a fourth SD generation was proposed to combine amorphous drug formulation technique with uses of insoluble or swellable polymers to control the release of drugs having short biological half-life [4]. Table 2.1 summarizes the properties of the four generation SDs.

Table 2.1. Classification and properties of solid dispersions [4,6,22,23,26]

	First generation	Second generation	Third generation	Fourth generation
Type of carrier	Urea Sugars (e.g. Mannitol or sorbitol)	Synthetic polymers (e.g. polyethylene glycol) Natural polymers (e.g. cellulose derivatives)	Surface active agents as carrier (e.g. Compritol 888 ATO, Soluplus®) Polymer + surface active agents (e.g. Tween 80)	Water insoluble or swellable polymers (e.g. Carbopol, Eudragit RS)
SD type	Nanocrystalline SD	Amorphous SD		Controlled release SD
Carrier-drug mixture	Eutectic or monotectic precipitates in crystalline matrix	Crystalline suspension	Glassy solution	Amorphous solid solution
Drug physical state	C	C	A	A or M
Carrier physical state	C	A	A	A
Number of phases (thermal event)	2 ($T_{m \text{ mixture}}$ Or $T_{m \text{ drug}} + T_{m \text{ carrier}}$)	2 ($T_{m \text{ drug}} + T_{g \text{ carrier}}$)	2 ($T_{g \text{ drug}} + T_{g \text{ carrier}}$)	2 or 1 ($T_{g \text{ drug}} + T_{g \text{ carrier}}$ Or $T_{g \text{ carrier}}$)
Physical drug stability	Stable	Risk of recrystallization	Stable	Risk of phase separation

A: Amorphous; C: Crystalline; M: Molecularly dispersed; T_m : melting temperature; T_g : glass transition temperature

2.1.1.2. Advantages and limitations

As already mentioned SD formulation is a way to formulate poorly water-soluble drugs in the form of solid dosage, which is the most preferred way of administration. General advantages of SDs compared to other formulation strategies can be highlighted [1,23]:

- For drug particle size reduction
- For drug wettability and porosity enhancement
- For the conversion of a crystalline drug into its amorphous state
- For homogeneous formulation preparation
- For stabilization of some chemically unstable drugs
- For apparent water solubility and drug absorption enhancement
- For taste masking
- For rapid disintegration oral tablet preparation
- For controlled release

Despite these numerous advantages, the commercialization of SD systems has been limited by some drawbacks [23,27]:

- Expensive and laborious methods of preparation
- Scale-up limitation of some manufacturing processes (other than HME)
- Physico-chemical stability of the drug and matrix
- Difficult incorporation of SD into solid dosage forms
- Limited drug:carrier ratio
- Solvent residue in a solvent method

However suitable carrier selection can overcome these limitations. Required properties for carriers are [1,5]:

- High water solubility for wettability and dissolution enhancement
- High glass transition temperature for stability enhancement
- Minimal water sorption
- Low melting point, thermostability and thermoplasticity for melting process
- Solubility in common solvents for a solvent process
- Solid solution formation with a drug (i.e. similar solubility parameter; cf. section 2.2.4)
- Inert and recognized as safe

2.1.1.3. *Manufacturing processes*

Different methods are used to produce SDs. Table 2.2 illustrates commonly used technologies in amorphous SD formulation. The goal is to mix a carrier with a drug to obtain a glassy suspension and preferably a glassy solution. The main challenge is to prevent phase separation due to recrystallization or formation of amorphous drug clusters. It can be prevented by targeting low molecular mobility of the components at the storage temperature and amorphous phase separation should be circumvented using an elevated process temperature for a sufficient time during preparation [1].

Table 2.2. Processing technologies used in amorphous solid dispersion manufacturing [28,29]

Solvent methods	Fusion methods
Spray drying	Melt granulation
Cryogenic	Hot-melt extrusion
Supercritical fluid	Milling
Fluid bed granulation	Ultrasonic assisted compaction
Solvent-controlled precipitation (e.g. microprecipitated bulk powder)	Kinetisol
Electrospinning	
Adsorption on mesoporous carrier	

In the solvent evaporation method, the drug and carrier are dissolved in an organic solvent [1,5]. The SD is then obtained by evaporation of the organic solvent, which requires low temperatures. Therefore, this technique is particularly interesting for drugs or carriers that are decomposing at high temperatures. However, since drug candidates used for SD formulations are generally hydrophobic and carriers are mostly hydrophilic, it can be difficult to select a suitable solvent that can solubilize both components. Moreover, large amounts of solvent are often required to achieve complete drug/excipient dissolution and a second drying step (e.g. vacuum, spray drying or lyophilization) is imperative to minimize residual solvent below acceptance levels [30].

A second technique for SD preparation is the supercritical fluid method (SCF) [1,24]. A fluid is in a supercritical state when its temperature and pressure are above its critical temperature and

pressure point. At this point, the liquid and vapor phases are in equilibrium and above this point the liquid and the gas have the same density and form a single phase. SCFs have the solvent properties of liquids but behave in many other respects like gases. Carbon dioxide is commonly used as SCF. It is able to solvate polymers and infuses small drug molecules into their swollen network for controlled release application. This method has the advantage to be fast and to give rise to high purity products and high yield due to ease of solvent removal. Moreover no aqueous solvent is needed, which prevents hydrolytic degradation of drugs [8,17].

Apart from the solvent-based methods, there is the possibility to produce SDs by means of different melting (or fusion) technologies (Table 2.2). These methods are used to the same extent as spray drying in SDs that are on the market [31]. The conventional laboratory-scale melting method is based on simple heating of the excipients and drug above their melting point or glass transition temperature before solidification in an ice-bath under vigorous stirring [1,5,24]. A first prerequisite for the use of this method is the drug-carrier miscibility in the molten state and their thermostability [18]. There is also a variant of the fusion method that makes of microwaves, mechanical or ultrasound energy [28,32]. While these different fusion methods are easy to apply at a laboratory scale, they are not equally suited for scale-up. Therefore, melt granulation and HME have become methods of choice as they are both scalable and can run in case of HME in a continuous operation mode. This process technology is on focus of the present thesis and further details can be inferred from section 2.2.

2.1.2. Solid dispersions containing inorganic carriers

Recently, another type of excipients (other than lipid or polymer) has been included in the list of materials that may improve formulation of poorly water-soluble compounds. Porous excipients or adsorbents having high pore volume and large surface area are particularly appealing as amorphous drug stabilizer and carrier. Large surface area materials have a high surface free energy. Upon adsorption of drug molecules, the system transfers to a lower free energy state and hence the drug is typically converted to a stable amorphous state. The drug physical stability results from the combination of decreased free energy and spatial constraints imposed by the pores. Indeed, the small pore size does not allow incorporation of enough drug molecules that could reach a critical nucleation size. Many studies reported that the use of porous materials

could improve poorly-water soluble substances dissolution. Indeed, the nano-confinement of drug molecules onto their surface and pores often leads to enhanced dissolution [21,33–35]. Most of the porous excipients used for the dissolution enhancement are silica-based materials. However, aluminum, titanium or carbon-based porous materials have also been developed for drug delivery [36]. Table 2.3 lists some ordered and non-ordered porous excipients that are used for the formulation of poorly water-soluble compounds. Porous media can be classified according to their average pore diameter. Microporous materials have pores smaller than 2 nm, mesoporous adsorbents have pore sizes between 2-50 nm and macroporous media display pores greater than 50 nm. The performance of formulations comprising such porous carriers is highly dependent on the inorganic material properties and the impact of pore volume/size/connectivity, which has been reviewed excellently [21,36,37]. Several methods have been introduced in the literature to incorporate porous drug carrier systems, such as organic solvent immersion, incipient wetness impregnation, or melt method [21,36,37]. Whereas, conventional methods for the preparation of adsorbed products are a batch process, Kinoshita et al. showed that HME can be used as an alternative continuous process for a melt-adsorbed product preparation [38]. The authors could successfully adsorb TAS 301 onto porous calcium silicate (Florite R) by batch melting method and also by a continuous method (HME). They observed similar improved dissolution rate and bioavailability of the drug in both amorphous melt-adsorbed products.

Table 2.3. List of inorganic excipients commonly used in pharmaceutical formulation

Adsorbent trade name (supplier)	Composition	Average particle size (µm)	Specific surface area (m ² /g)	Average pore diameter (nm)
Neusilin® US2 (Fuji Chemical Industry Co., LTD)[39,40]	Disordered aluminum magnesium silicate	44–177	300	15
Sylsilia® 350 (Fuji Chemical Industry Co., LTD) [40,41]	Disordered mesoporous silica	3.9	350	21
Florite® R (Tomita Pharmaceutical) [40,42]	Disordered porous calcium silicate	29	100	150

Adsorbent trade name (supplier)	Composition	Average particle size (μm)	Specific surface area (m^2/g)	Average pore diameter (nm)
Aeroperl® 300 Pharma (Evonik Industries) [43,44]	Disordered meso- and macroporous silica	33	300	30
Syloid® 244 FP (Grace) [40,45]	Disordered mesoporous silica	3.5	300	2.5-.5
Syloid® XDP 3050 (Grace) [45,46]	Disordered mesoporous silica	50	320	21
Upsalite [47]	Disordered mesoporous calcium carbonate	-	400-800	3-20
Parateck SLC (Merck) [48]	Disordered mesoporous silica	5–25	500	2–7
Sipernat® 50 (Evonik Industries) [49]	Disordered porous silica	40	500	-
NLAB Silica™ (Nanologica) [50]	Disordered mesoporous silica	0.3–50	up to 1300	2–50
MCM-41 [51]	Ordered mesoporous silica	-	800-1000	1.5–10
SBA-15 [52]	Ordered mesoporous silica	-	400-900	1–15

2.2. Hot-melt extrusion

HME has been primarily used in the plastic and the food industries since the 1930's. HME process consists in pumping raw materials with rotating screws under elevated temperature through a die to obtain a new material (the extrudate) having a desired shape [9]. Today, half of the plastic materials are produced by HME. It is used to give special shapes to tubes, pipes, plastic bags, etc. Cereals and pet food can also be produced by HME. It is an interesting way to mix the ingredients, to give special texture or to add nutritional ingredients like vitamins. Since the 1980's, there is a growing interest in using HME in the pharmaceutical field [53]. As

illustrated in Fig. 2.2, the number of issued patents and publications on HME in the pharmaceutical area has considerably increased the past two decades. Research and manufacturing propelled HME as an alternative method for bioavailability enhancement of poorly water-soluble drugs by producing SDs. During HME process of pharmaceutical excipients, the active compound is embedded in a carrier, usually composed at least of one thermoplastic polymer. Intense agitation and mixing caused by the rotating screws implies the de-aggregation of the suspended particles in the molten polymer and thus results in a uniform dispersion or a solid solution. HME is therefore an attractive alternative to traditional methods (e.g. spray drying, solvent method) to prepare pharmaceutical drug delivery systems such as granules, pellets or sustained release tablets [53,54].

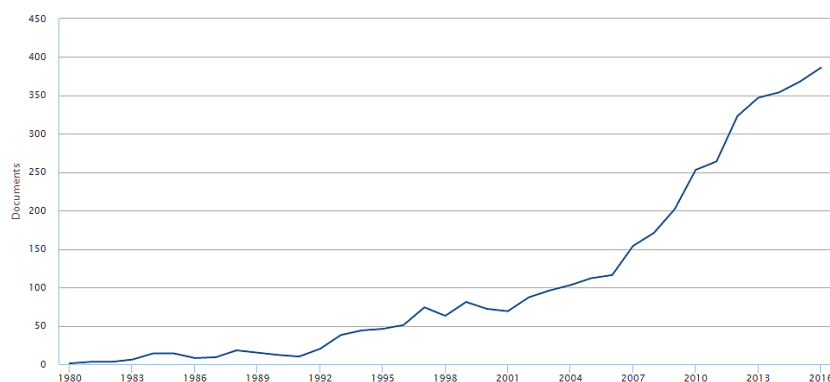


Fig. 2.2. Number of publications since 1980 to current on the topic of hot-melt extrusion (Source: Scopus, Search words: Hot-melt extrusion + Pharmaceuticals).

2.2.1. Equipment and process

The basic components of an extruder are: the hopper, barrel, control panel, torque sensors, heating/cooling system, and a die [53,55]. The hopper allows powder feed. The barrel, which contains the screws, can be segmented into individual heating zones and eventually comprises additional feed ports for heat sensitive or liquid materials. The screws, which represent the principal part of the extruder, can exhibit versatile configurations depending on the desired shear and mixing. Two types of screws are available: single- and twin-screws. The single-screw

extruder is commonly used in the plastic industry, while the twin-screw extruder is used in the pharmaceutical industry for its high mixing capability. Single-screw extruders have higher mechanical simplicity and a more reasonable investment cost compared to twin-screw extruder. However, twin-screw extruders have easier material feeding, higher kneading and dispersing capacities, less tendency to over-heat and shorter residence times (5 s to 10 min). Twin-screws can either rotate in the same (co-rotating) or opposite (counter-rotating) direction. Counter-rotating screws are used when high shear forces are needed since the molten material is squeezed between the screws when they come together. However, counter-rotating screws have some disadvantages such as air entrapment, high pressure generation, low maximum screw speed and low output. Co-rotating extruders are the most commonly used in the industry since high output and good mixing can be achieved thanks to high screw speed. The temperature of the barrel is controlled by electrical heating bands and monitored by thermocouples. Finally, a die is mounted at the end of the barrel and defines the physical shape of the extrudate. Additionally, downstream equipment can be attached to the die for the collection and shaping of extrudates (e.g. pelletization, granulation, tableting, film forming, calendaring, injection molding) [54,56]. The major difference between a plastic extruder and a pharmaceutical-class extruder is that metal parts in contact with the product must meet regulatory requirements, i.e. they must not be reactive, or absorptive with the product. Most screws are made from surface coated stainless steel with reduced friction. The equipment is configured for the cleaning and validation requirements associated with a pharmaceutical environment [57]. Fig. 2.3 shows a twin-screw extruder and different downstream processes, which can be combined with the extrusion process.

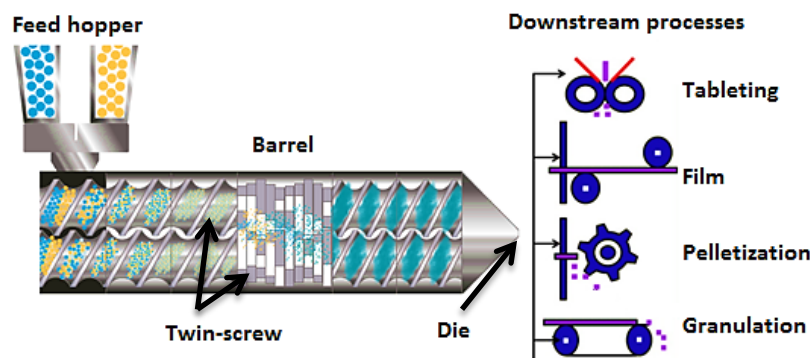


Fig. 2.3. Scheme of a twin-screw extruder and downstream processes. Adapted from [58,59]

The use of laboratory scale extruders (Fig. 2.4) for research and development of new materials can suffer from the costs of these materials since large sample sizes are needed. Therefore, scaled-down systems that use grams as opposed to kilograms can be a key for fast and low cost formulation screening. Such microscale compounder (or microcompounder) typically need small quantities from about 5 g of raw materials [60] and a conical design is the most commonly commercialized type. The operator can control the residence time thanks to a “backflow” channel (or recirculation channel) that can be opened or closed by a bypass valve. Fig. 2.5 illustrates an example of a microcompounder and the barrel design.

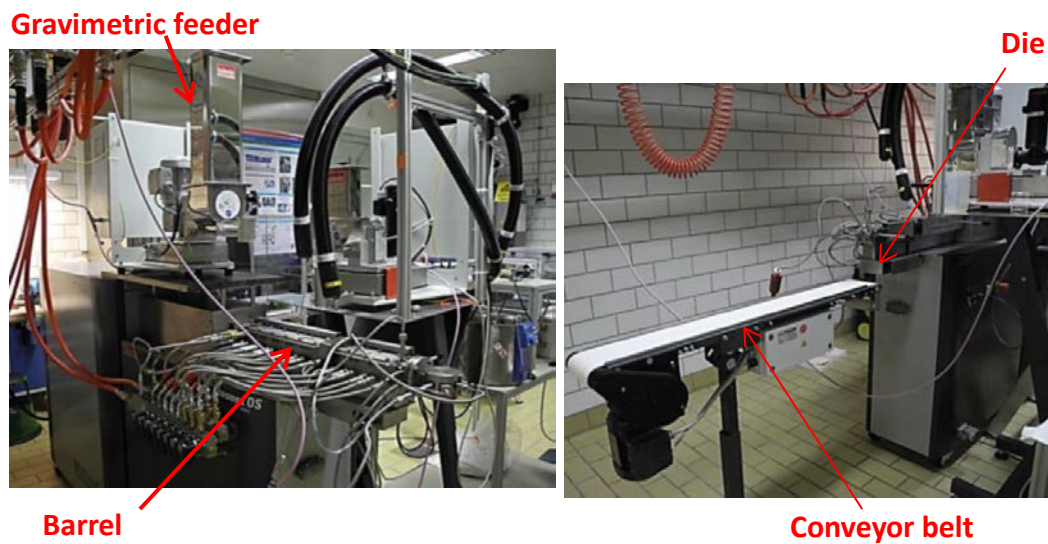


Fig. 2.4. Example of a Thermo Fisher laboratory scale twin-screw extruder

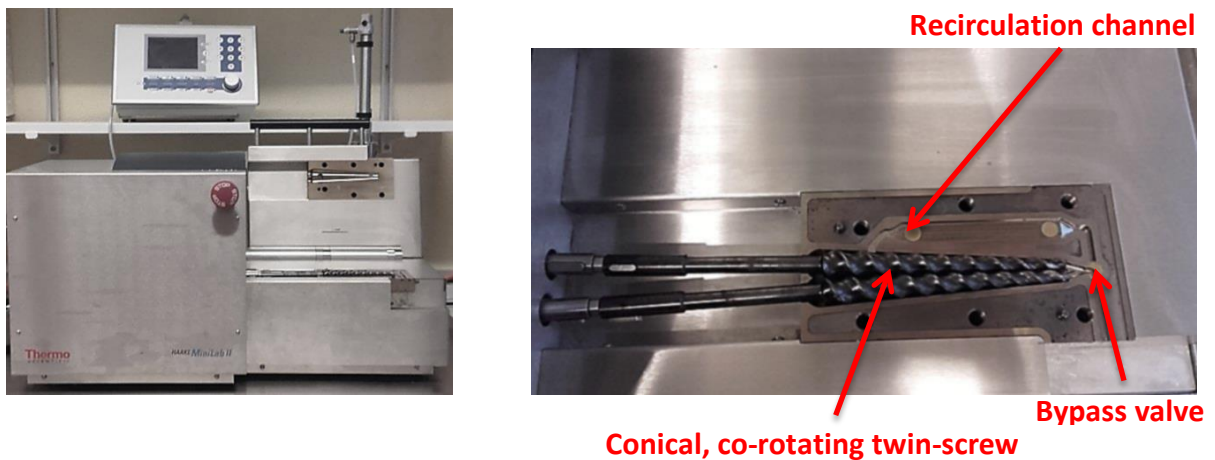


Fig. 2.5. Example of a Thermo Fisher microcompounder (left) and barrel design (right)

HME is a unit operation that can be subdivided into a series of subprocesses [57]. Fig. 2.6 illustrates the different consecutive barrel subsections. The first step of the HME process is the gravimetric or volumetric material feeding through a hopper. Heat sensitive or liquid materials can be added through additional feed ports along the side of the barrel. The feedstock reaches the conveying section in the barrel where conveying elements move the material to the die direction. Conveying efficiency can be tailored by adapting the geometry of the conveying elements. The material reaches then the melting section where softening and melting occurs by conductive thermal energy and mechanical energy input via the preheated barrel and the screws, respectively. Screw design can directly influence the residence time and the maximum shear stress. Screws that comprise only conveying elements would move the material towards the die direction via drag flow with minimal mixing. Therefore, kneading elements are essential for comparatively larger equipment to ensure sufficient mixing that can be a molecular dispersion of the miscible components. The use of plasticizers can also help to make this step easier by decreasing the melting point or the glass transition temperature of the polymer. Prior to extrusion of the material through the die, venting is applied to the melt. This step is essential to remove residual moisture or gas that might have been entrapped during intense mixing and melting. Finally, build-up pressure pushes the molten extrudate through the die, which defines the product shape (e.g. film, annular, circular). A conveyor belt is often employed for the cooling of the extrudate. As already mentioned, downstream processes can be used (e.g. injection molding, spheronization, tableting) [59].

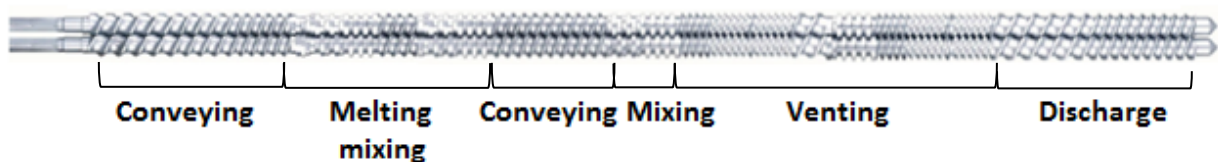


Fig. 2.6. Example of screw configuration showing the different subsections of twin-screw extrusion process. Adapted from [58].

HME screws are segmented and can be configured as desired to meet various application requirements [61]. The most common application of screw configurations is conveying, melting, mixing and shaping. Conveying elements are used in the feeding, conveying and venting

sections. They have a self-wiping lead geometry. Mixing elements are composed of a combination of single mixing elements with offsets of 30, 60 or 90°. High offset leads to low conveying but high mixing properties. Distributive flow elements are used to generate low-energy mixing when liquids are added to the melt in the barrel. The elements are composed of an outer grooved and inner plain diameter disk. Finally, discharge feed screws have a single lead geometry to generate the extrusion pressure to shape the final product at the die. Fig. 2.7 illustrates the different types of screw elements that are currently used in a HME process.

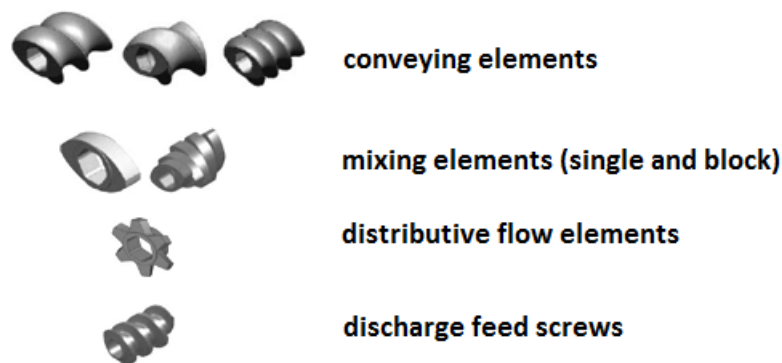


Fig. 2.7. Commonly used screw elements in pharmaceutical hot-melt extrusion process.
Adapted from [61]

Important is also the extrusion process itself, which can be adapted according to a desired final dosage form and performance [61]. The selection of an extruder type is the first choice that has to be made. As already mentioned, it can be single- or twin screw equipment. The screws may be designed individually with different elements (Fig. 2.7) and in the case of twin-screws, they can be configured either as co-rotating or as counter-rotating screws. The process temperature, the residence time and the screw speed also condition the final product quality and have to be carefully selected to avoid any drug or matrix degradation. The feed rate of the raw materials can have an influence on the throughput and the degree of fill can also affect the quality of mixing. As related before, the screw design is also a key parameter to achieve homogeneous dispersion, optimal residence time and low degradation. All the parameters are interconnected and a thorough understanding of their influence on the mixing quality, on the degradation, and on the viscosity of the materials is required to produce extrudates with desired quality attributes.

2.2.2. Advantages and limitations

The major advantage of HME is that it is a solvent free process and therefore no drying step is required in contrast to other methods used for the formulation of pharmaceutical compounds. HME also provides good mixing capability thanks to the use of the twin-screws, which implies a good agitation, de-aggregation of suspended particles in the molten polymer and thus a good content uniformity and dispersion. Moreover, it is an economical process with reduced production time, limited number of steps and a continuous operation. The residence time of the mixture in the extruder is low, which prevents degradation of heat-sensitive components, which makes HME preferred compared to other fusion methods. The dosage form can be adjusted by the numerous downstream processes (e.g. pelletizing, granulation, film forming, tableting) that can be combined with the extruder. Drug release profile can be adjusted according to the type of excipients [11,62].

Nevertheless, HME is a thermal process and therefore it cannot be used for the formulation of thermolabile compounds. The number of available polymers and excipients with good flow properties is rather limited. The cost of the equipment is relatively high and high energy input from the drive unit is needed. The use of excipients like plasticizer can have an influence on the stability of the final dosage form and may cause the recrystallization of the API in the matrix. However, most of these disadvantages can be controlled by appropriate adjustment of process parameters [14,53].

2.2.3. Excipients used in HME

The carrier is composed of one or several meltable substances (generally a polymer or low melting point wax) and other functional excipients. As previously mentioned, the number of available pharmaceutical grade polymers that can be used for preparing amorphous SDs is rather limited. Most commonly used polymeric carriers are listed in Table 2.4. A more extensive list of polymers and their properties can be found in the literature [9,63].

Table 2.4. Common pharmaceutical polymers used in hot-melt extrusion processes [53,54]

	Chemical name	Trade name	T_g or T_m (°C)	T_{degradation} (°C)
Immediate release	Polyvinylpyrrolidone	Kollidon [®] K12, K17, K30, K90, Plasdone [®] K25, K29/32, K90	90-170 (T _g)	175-250
	Polyvinylpyrrolidone vinylacetate	Kollidon [®] VA 64, Plasdone [®] S 630	101 (T _g)	230
	Polyvinyl caprolactam-polyvinyl acetate graft polyethylene glycol copolymer	Soluplus [®]	70 (T _g)	250
	Polyvinyl alcohol	Elvanol [®] Parteck [®] MXP	40 – 45 (T _g) 170 (T _m)	> 250
	Amino methacrylate copolymer	Eudragit [®] EPO	56 (T _g)	> 200
	Polyethylene glycol	Carbowax	20 (T _g) 37-63 (T _m) (M _w = 6000 g/mol)	≈ 250
	Hydroxypropylcellulose	Klucel [®]	130 (T _g)	260-275
	Hydroxypropylmethylcellulose	Methocel [®]	160-210 (T _g)	> 190
	Hydroxypropylcellulose acetate succinate	Aqoat [®]	120-135 (T _g)	>190
Sustained release	Polyvinylacetate	Sentry [®] plus	35-40 (T _g)	-
	Polymethacrylates	Eudragit [®] RL/RS	130 (T _g)	155
	Ethyl cellulose	Ethocel [®]	133 (T _g)	-
	Poly(ethylenvinylacetate)	Elvax [®]	65-70 (T _g)	
	Poly(ethylene oxide)	Polyox [®]	25-80 (T _m)	
	Polylactic-co-glycolide acid	Resomer [®]	40-60 (T _m)	
	Carnauba wax	-	81-86 (T _m)	> 250
	Chitosan		203 (T _g)	
	Xantan gum			
	Glyceryl palmitostearate	Precirol [®] ATO 5	52-55 (T _m)	-

T_g: glass transition temperature; T_m: melting temperature

Other additives can also be employed to improve processing conditions or final dosage performance. Table 2.5 summarizes common pharmaceutical functional additives used in HME. Plasticizers are used for lowering the glass transition temperature (T_g) and the melt viscosity of the polymer. This allows reducing drug and carrier degradation by lowering the shear force. Plasticizers are usually low molecular weight compounds. In some cases, the drug itself can function as a plasticizer [64]. The ability to decrease the T_g of the matrix, the physico-mechanical properties and the drug release of the final dosage form depend on the plasticizer type and concentration [9]. The physical and mechanical properties as well as the drug release of the dosage form are dependent on the nature and stability of the plasticizer. Ardwisson et al. [65] demonstrated that the volatilization of plasticizer during curing or storage can induce dramatic changes in drug release. Other additives can also be added to the formulation. The stability of the degradable polymers can be improved by the addition of preventive antioxidants or chain-breaking antioxidants, acid receptors or light absorbers. Thermal lubricants can also be used to facilitate the HME process.

Table 2.5. Common pharmaceutical functional additives used in hot-melt extrusion [9,11,28]

	Physical state	Molecular weight (g/mol) (T_m (°C) for solid additives) *
Plasticizers	Polyethylene glycol	L < 600
	Polyethylene oxide	S 800-20000 (30-60)
	Propylene glycol	L 76
	Triethyl/tributyl/acetyl triethyl citrate	L 276/360/318
	Diethyl/dibutyl phthalate	L 222/278
	Dioctyl phosphate	L 322
	Dibutyl sebacate	L 314
	Antioxidants	Butylated hydroxytoluene
Butylated hydroxyanisole		S 180 (48-55)
Citric acid		S 192 (153-159)
Ascorbic acid		S 176 (190-192)
Ethylenediamine tetraacetic acid		S 292 (245)

* Pubchem and Chemical Book; L: liquid; S: solid

As already mentioned, surfactants and lipid-based excipients have been introduced in amorphous SD formulations by Serrajuddin et al. in the 1990's to overcome limitations encountered in systems using polymeric carriers only [6]. Lipid-based excipients and surfactants can in some cases prevent drug recrystallization in the anhydrous matrix but the main benefits are of biopharmaceutical nature. Such additives can increase drug solubilization upon aqueous dispersion and may circumvent precipitation, while another mechanism is a possible enhancement of membrane permeability [66,67]. Table 2.6 summarizes commonly used lipid-based excipients used in HME.

Table 2.6. Commonly used lipid-based excipients [9,11,14,28]

Lipid-based excipients (surfactant/ plasticizers)	Physical state*	Molecular weight (g/mol) (T_m (°C) for solid compounds)*
Vitamin E TPGS	L	430
Triacetin	L	218
Polyoxyethylene of sorbitan esters (Tween)	L	Tween 20: 522
Sorbitan esters of long-chain fatty acids (Span)	S	Span 60: 430 (53)
Glyceryl behenate (Compritol® 888 ATO)	S	414 (69-74)
Castor oil	L	
Soybean oil	L	
Palmitic acid/stearic acid	S	256 (61-63)/284 (67-72)
Sodium lauryl sulfate	L	288
Polyoxyethylene hydrogenated castor oil (Kolliphor ®RH 40)	L	
Sucrose laurate	S	524
Glycerol monostearate/butyl stearate	S/L	358 (78-81)/340
Glyceryl palmitostearate (Precirol®ATO 5)	S	633 (50-60)
Lauroyl polyoxylglycerides (Gelucire® 44/14)	S	(42.5-47.5)
Stearoyl polyoxylglycerides (Gelucire® 50/13)	S	(46-51)
PEG-8 Caprylic-Capric Glycerides (Labrasol®)	L	

* Pubchem and Chemical Book; L: liquid; S: solid

Lipids in oral formulations such as HME extrudates have the ability to form different colloids in the process of dispersion and digestion. These colloids are enriched by endogenous bile salts and phospholipids and may foster drug solubilization thereby circumventing precipitation. Lipid-based excipients can affect drug absorption by different mechanisms and this has been summarized elsewhere [67]. The synergetic effect of a hydrophilic polymer, which increases the dissolution rate and of a lipid, which increases drug solubilization has proven advantages over traditional HME formulations [68]. Moreover, lipids have a low physiological toxicity, offer a wide range of physico-chemical properties and are inexpensive [69].

Lipids are also used in the so called solid lipid extrusion. Solid lipid extrusion also known as cold extrusion is performed below the lipid melting point or melting range. The plasticity is achieved by thermomechanical treatment of the lipid. This process is suitable for thermosensitive substances and is primarily used for controlled release. Since this study focused on HME, cold extrusion will not be further discussed. More details about solid lipid extrusion principle and applications can be found in the literature [69–73].

2.2.4. Selection of excipients

A critical requirement of any stable formulation is the miscibility between the drug and carrier. The selection of excipients for the formulation of poorly water-soluble APIs can be facilitated by using mathematical models that predict drug-polymer miscibility. Similarly to polymer-solvent chemistry these models calculate the interaction energies of a pharmaceutical polymer and an amorphous drug. Calculations usually consider a polymeric chain segment. *In silico* methods based on two-dimensional structure certainly have limitations with respect to conformational or supramolecular effects and also process factors are not considered regarding miscibility. Accordingly, the main application of such an *in silico* approach is early excipient screening for which high precision of estimates may not be needed. The most commonly used methods are the Flory-Huggins Theory and the solubility parameter concept [74,75]. The needed interaction parameters are not only estimated *in silico* but can alternatively come from experimental measurements such as inverse gas chromatography [76–79], melting point depression [80,81], energy of vaporization [77,78], solubility or swelling [82,83] methods. Table 2.7 summarizes computational and experimental methods that can be used to estimate drug-polymer miscibility.

Table 2.7. Commonly used computational and experimental methods for the estimation of drug-polymer miscibility

	Limitations	
Hildebrand	Suitable only for non-polar, non-associating systems [75]	
<i>In silico</i> methods	Group contribution	Only based on 2D structure, does not consider polymer-polymer and drug-drug self-association. Not suitable for salt-forming drugs [84]
	- Hansen	
	- Van Krevelen	
- Hoy		
Molecular dynamics simulation	Simplifications are made within models (e.g. selected force field, number of molecules and size of polymer fragments, duration of simulation)	
Energy of vaporization	Not suitable for non-volatile substances like polymers or thermolabile compounds [77,78]	
Swelling	Difficult prediction in the case of non-homopolymers [82]	
<i>Experimental</i> methods	Inverse gas chromatography	Influence of material surface properties. Selection of appropriate solvents is crucial [77,84]
	Solubility	Necessity to find the appropriate solvent [83]
	Melting point depression	Appropriate for polymers having a glass transition temperature significantly lower than drug melting point. Estimation of χ interaction parameter close to the melting point of the drug. Polymer-drug ratio limited to low polymer concentrations [81] Care is needed with experimental error propagation [85]

The Flory-Huggins theory can be applied to any binary mixture for example composed of a larger molecule (polymer) and a smaller molecule (amorphous drug). It takes into account interactions between the polymer and drug molecules and calculates the change in entropy according to the placement of the molecule units in a lattice model.

The Flory-Huggins theory uses the Gibbs free energy to predict miscibility of a drug and a polymer [75,86]:

$$\Delta G_M = RT \left[\underbrace{n_{drug} \ln \varphi_{drug} + n_{polymer} \ln \varphi_{polymer}}_{\text{Entropic contribution}} + \underbrace{n_{drug} \varphi_{polymer} \chi_{dp}}_{\text{Enthalpic contribution}} \right] \quad (2.1)$$

Where ΔG_M is the free energy of mixing, n_{drug} and φ_{drug} represent the number of moles and the volume fraction of the drug; $n_{polymer}$ and $\varphi_{polymer}$ are the number of moles and the volume fraction of the polymer, and χ_{dp} is the Flory-Huggins interaction parameter. A condition to ensure miscibility between the drug and the polymer is a negative ΔG_M . The entropic contribution is always negative ($\varphi < 1$ and thus $\ln \varphi < 0$) and depends on the size of the molecule. Small molecules have a large entropy term and thus are likely to be soluble in each other. On the contrary, high molecular weight compounds (e.g. polymers used in SDs) are likely to be poorly miscible due to low entropy term. The polymer-drug miscibility depends mostly on the enthalpy contribution, which can be computed using “Flory’s Chi” thermodynamic interaction parameter χ_{dp} [75]:

$$\chi_{dp} = V_m \frac{(\delta_{drug} - \delta_{polymer})^2}{RT} \quad (2.2)$$

where V_m is the molar volume of the solvent, R is gas constant, T is the temperature, and δ_{drug} and $\delta_{polymer}$ are the solubility parameters of the drug and polymer, respectively.

χ_{dp} can be obtained by using solubility parameters of the materials. The concept of solubility parameter was introduced by Hildebrand and Scott [74,75,87] to evaluate low molecular weight materials and polymers miscibility. Solubility parameters calculate the cohesive energy density (CED) per unit volume of materials, which corresponds to the attractive energy that holds atoms or molecules of two materials together. It is the amount of energy required to separate atoms or molecules constituting the materials to an infinite distance and it is mathematically defined as [83]:

$$\delta = (CED)^{0.5} = \left(\frac{E_v}{V_m} \right)^{0.5} \quad (2.3)$$

where E_v and V_m are the energy of vaporization and the molar volume of the compound at the temperature of vaporization, respectively. Since the first application of solubility parameters was

for liquid mixtures, several approximations were done to extend the theory to more complex systems. For example gases are described as hypothetical liquids and solids are treated as supercooled liquids. This allows using the theory of solubility parameters for ideal gases and organic solids having a low crystallinity. Since this theory is better suited for non-polar molecules interacting through weak forces, other methods have been suggested to calculate solubility parameters of pharmaceutical compounds. Hansen [88] subdivided the total solubility parameter (δ_i) into three components corresponding to the contribution of the different interactions between atoms or molecules, i.e. hydrogen bonds (δ_h), dispersion forces (δ_d), and polar interactions (δ_p). The total 3D Hansen solubility parameter is expressed as [76]:

$$\delta_i^2 = \delta_h^2 + \delta_d^2 + \delta_p^2 \quad (2.4)$$

Experimentally, partial and total solubility parameters can be determined by measuring the solubility of a material in liquids with known cohesive energy. This method assumes that the material of interest has the same solubility parameter as the one of the liquid in which it is completely and athermally dissolved [76]. Solution calorimetry can be used to ensure accurate heat of vaporization measurements. Inverse gas chromatography is an alternative method that allows the calculation of solubility parameters of pharmaceutical compounds by means of retention times of gases of known cohesive energies. Partial solubility parameters can also be estimated using molecular modelling or molecular dynamics calculations (Table 2.7).

One of the mostly used computational methods for the prediction of each solubility parameter component is the group contribution method, which requires knowledge of the chemical properties of the material that should be available for pharmaceutical compound. Each compound is broken into fragments with known parameters and the sum of the parts enables estimating the partial solubility parameters [76]:

$$\delta_{hi} = \sqrt{\frac{\sum E_{hi}}{V}}, \delta_{di} = \frac{\sum F_{di}}{V}, \delta_{pi} = \sqrt{\frac{\sum F_{pi}^2}{V}} \quad (2.5)$$

where E_{hi} , F_{di} and F_{pi} are the group contributions for different components of structural groups and V is the group contribution to molar volume. Examples of group contribution methods are those of Van Krevelen, Hoy and Hansen (Table 2.7). Lists of group contribution values are

available in the literature [89–91]. However, the group contribution method allows calculation of hydrogen bonds, it does not consider self-association between polymer-polymer and drug-drug molecules. Moreover, solubility parameters are calculated at room temperature and may rather apply for amorphous substances than crystalline structures that cannot be viewed as supercooled liquids. Nevertheless, solubility parameters have successfully been applied for prediction of drug-excipients miscibility [75]. Greenhalgh et al. [83] and Forster et al. [92] findings provided efficient prediction tools for drug-polymer miscibility. It is assumed that compounds having similar solubility parameters are likely to be miscible since the energy required for mixing is compensated by the energy released by the interactions between the compounds. According to Greenhalgh et al., the difference between two components solubility parameters ($\Delta\delta_t$) should be smaller than $7 \text{ MPa}^{1/2}$ to ensure good miscibility, whereas if $\Delta\delta_t > 10 \text{ MPa}^{1/2}$, the two substances are immiscible. Foster and al. also demonstrated that, when $\Delta\delta_t < 2 \text{ MPa}^{1/2}$, the two compounds form a glassy solution, whereas when $\Delta\delta_t > 10 \text{ MPa}^{1/2}$, they are immiscible.

Besides solubility parameters also other physico-chemical characteristics of polymers, additives and API have to be considered since the HME process imposes some restrictions due to the use of high temperature and mechanical energy. Table 2.8 shows the main properties of the excipients (polymers, additives) and API used in HME, which have to be taken into account before the processing. Basic requirements for polymers used in HME are a thermoplastic behavior, a suitable glass transition temperature, thermal stability, no toxicity, good dissolution properties. Additionally to polymeric carrier other additives can be used as processing aid. Besides compatibility with the drug and the polymer, they also require plasticizing or lubricant effect, thermal stability and no toxicity. Finally the drug itself should be stable at the processing temperature and its physico-chemical properties should be known to ensure efficient processing parameters and excipients selection. As shown by Friesen et al. [93], the drug melting point, glass transition temperature and partition coefficient (Log P), which measures the lipophilicity, can provide information on a suitable formulation strategy. The evolution of T_m/T_g as a function of Log P is shown in Fig. 2.8.

Table 2.8. Relevant characteristics of polymers, additives and API used in hot-melt extrusion [11]

Polymers	Additives	API
Water solubility	Plasticizing effect	Water solubility
Lipophilicity	Lubricant effect	Lipophilicity
Thermal stability	T_m	Thermal stability
T_g/T_m	Thermal stability	T_m
Chemical state	Physical state	Physical state
Melt viscosity	Compatibility with API & polymer	
Dissolution properties		
Interaction with API		

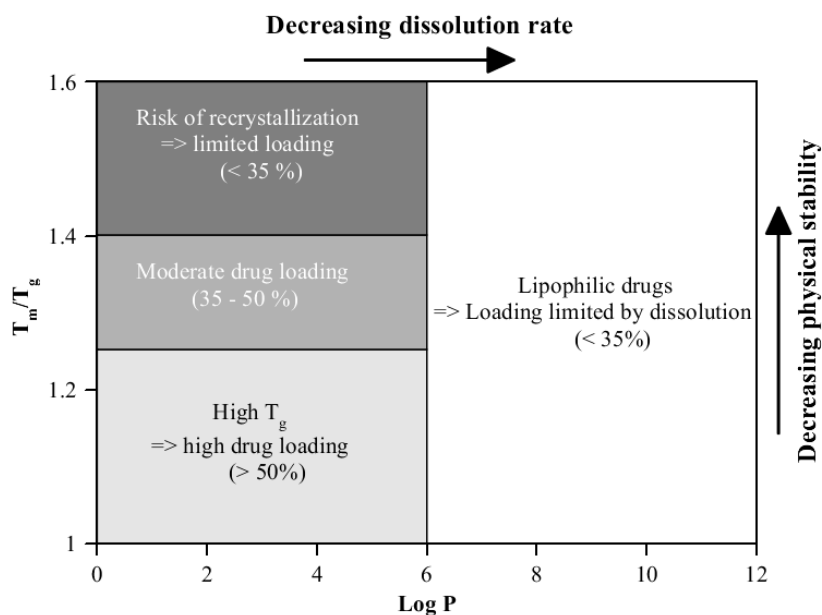


Fig. 2.8. T_m/T_g of drug as a function of $\text{Log } P$ and related drug loading range. Adapted from [93]

2.2.5. Solid-state characterization

The HME process generates extrudates that are generally intermediate products for final dosage forms. It is necessary to analyze the extrudates to confirm for example the formation of a SD and to monitor its stability during storage. Several methods can be employed to characterize raw

materials and the API physical state in the extrudates, as well as chemical stability and molecular interactions of drug and carrier. Table 2.9 summarizes the methods commonly used for SD characterization. Few comments will be given on selected aspects but not all of these methods are discussed in detail since a thorough discussion is beyond scope and there are already excellent reviews and book chapters [63,94,95].

Differential scanning calorimetry (DSC) is the most frequently used method to assess thermal properties of raw materials. Thermal events such as T_g and T_m can be detected by liberation or gain of energy (i.e. endothermic or exothermic phase transition). Prior to the extrusion process, it is essential to assess the polymer T_g since extrusion temperature should be 20-30°C above this temperature to ensure good flow properties [11]. Analysis of hot-melt extrudates allows evaluating drug-carrier miscibility. If a glassy solution has been obtained there is one T_g , which is characteristic for the miscibility between the drug and the carrier. If a glassy suspension has been obtained there are two T_g values (carrier and drug). For a crystalline suspension the T_g of the carrier and the T_m of the drug are visible. In the latter two, the drug and the carrier are not miscible [96]. Drug crystallinity can also be assessed by DSC analysis before and after processing as well as during storage under different conditions (e.g. temperature, humidity, light). However, DSC has clear limits of sensitivity and resolution for detection of weak thermal transitions or when overlapping thermal events occur. Modulated DSC (MDSC) can be used in such cases as an advanced thermoanalytical method [11,94]. In MDSC, sinusoidal wave modulation is superimposed onto the conventional linear heating rate. The DSC total heat flow is divided into reversing (e.g. glass transition, melting) and non-reversing (e.g. evaporation, crystallization, thermal decomposition) heat flow by Fourier transformation. MDSC is highly useful for amorphous SD studies since it allows differentiating T_g values from other interfering thermal events.

An alternative advancement in thermal analysis is fast-scanning DSC (or high-speed DSC). The heat is applied rapidly to avoid changes that might occur during slow measurements. It allows for a better understanding of polymer-drug compatibility since their miscibility is not affected during the high speed measurement [97,98].

DSC can be complemented with thermogravimetric analysis (TGA) that is based on the weight loss of a material as a function of time and temperature to determine, for example, the

degradation temperature. Moisture content, decomposition vaporization and sublimation temperatures can also be determined by TGA [4].

Spectroscopic techniques are non-destructive methods and allow for quantitative and qualitative analysis of HME formulations. X-ray powder diffraction (XRPD) is used to characterize the crystallinity of the extrudates by comparing the characteristic diffraction peaks of the crystalline form of the drug and the diffraction scattering signals of the extrudate [96]. Fourier-transform infrared spectroscopy (FTIR), Raman spectroscopy and solid state nuclear magnetic resonance are the most commonly used analyses to investigate intermolecular interactions and drug-carrier compatibility [4,94].

Microscopic techniques give information on surface morphology of SDs, phase separation or physical state of the drug [4]. Polarized light optical microscopy (PLM) can visualize crystals in the extrudates but it does not give quantitative information. The homogeneity of the extrudates, the presence of surface crystals, and the surface topography can be observed by scanning electron microscopy (SEM). SEM can be complemented by energy dispersive X-ray spectroscopy (EDS) to map the distribution and heterogeneity of components. Hot-stage microscopy can be used to investigate the presence of crystallites within a dispersion at high temperature as well as phase separation [11]. Finally, atomic force microscopy (AFM) is a surface analytical tool used to scan the surface morphology thanks to a tiny probe mounted on a cantilever [12]. It gives information on chemical nano-heterogeneity (phase imaging) and on the topography (amplitude imaging) of SDs.

Image analysis is a useful tool that provides qualitative information on SD. However, quantitative information is of interest for better characterization and understanding of pharmaceutical formulations. To achieve this, fractal and multifractal concepts can be used as complementary methods. Fractal geometry has been introduced in the 1960's by Mandelbrot to describe complex patterns that cannot be described by Euclidean geometry [99,100]. A fractal object is an object that is self-similar regardless of the scale of magnification and that can be described by a non-integer dimension or fractal dimension. Multifractal formalism applies for even more complex structures that can be viewed as the superposition of homogeneous fractal objects. It decomposes self-similar objects into intertwined fractal sets that have a singularity strength and fractal dimension. It combines a sequence of fractal dimensions that characterize the variability and heterogeneity of the object. By assigning a dimension (or a set of dimensions) to complex objects

fractal and multifractal theories provide a quantitative analysis. Fractal have been used in pharmaceuticals for example to study particle shape, surface morphology, crystal growth [100]. Only few studies using fractal geometry based on image analysis to characterize hot-melt extrudates have been published but such previous work was outside of pharmaceuticals [101–103]. Even less frequently has the multifractal formalism been used in applied sciences and the introduction to pharmaceuticals and hot-melt extrudates in particular is new (c.f. chapter 5; [104]).

Table 2.9. Common analytical methods used to investigate hot-melt extrusion formulations [63,94]

Property	Method
Drug-carrier miscibility	Hot-stage microscopy
	Differential scanning calorimetry
	X-ray powder diffraction
	Atomic force microscopy
	Fourier-Transform infrared imaging
Individual component distribution	Raman mapping
	Fluorescence microscopy
	Fourier-Transform infrared spectroscopy
Drug-carrier interaction	Raman spectroscopy
	Nuclear magnetic resonance spectroscopies (1-and 2-D methods)
	Fourier-Transform infrared spectroscopy
Surface morphology	Scanning electron microscopy
	Atomic force microscopy
Surface properties	Inverse gas chromatography
	BET
Mechanical properties	Dynamic mechanical analysis
Drug crystallinity	Polarized light microscopy
	Hot-stage microscopy
	Differential scanning calorimetry
	X-ray powder diffraction
	Atomic force microscopy
Stability	Differential scanning calorimetry
	Thermogravimetric analysis
	Dynamic vapor sorption
Microstructure Tomography	X-ray micro-or nano-tomography

2.2.6. Biopharmaceutical characterization

The aim of the present study was the design of novel type of formulations for poorly-water soluble compounds. The focus was more on material characterization, which entailed the introduction of new methods to address current needs for a better understanding of complex microstructures. The biopharmaceutical performances of the formulation were therefore not within the scope of this work. However, biopharmaceutical *in vitro* characterization is in general pivotal for the field of SDs because such formulation primarily target improved solubilization and absorption of poorly soluble compounds. Dissolution test is an efficient characterization method that allows selection of suitable excipients according to the targeted performances (e.g. enhanced dissolution, maintenance of supersaturated solution, amorphous state stability) [105]. Standardized tests and apparatus are described in the United State Pharmacopeia [106], European Pharmacopeia [107], and Japanese Pharmacopeia [108]. For the dissolution of amorphous SDs, it is important to characterize both the dissolution and the ability of the formulation to maintain a supersaturated state upon dissolution. Any of the dissolution apparatus used for solubility assessment can be selected. Usually, the basket and paddle apparatus are the most commonly used. When drug absorption is limited by the drug dissolution an *in vitro-in vivo* correlation may be established, provided that appropriate test conditions are used. Solubility and dissolution studies of amorphous SD is well reviewed in the literature [105,109–111]. A compilation of different *in vitro* methods for oral formulations can be inferred from Kostewicz et al [112]. Most notable are here novel chemical imaging methods that have been applied recently to study the drug release from solid dispersions [113–115].

2.3. β -carotene

In this study, β -carotene (BC) was chosen as a crystalline lipophilic model compound for the formulation of amorphous SDs by HME. BC belongs to the family of carotenoids.

More than 700 carotenoids have been identified in the nature and these natural chemicals are yellow, red, or orange pigments that can be found in plants, microorganisms or animals [116,117]. They are characterized by their conjugated double-bound chain that is responsible of their color and their antioxidant properties. Most abundant carotenoids in foods are BC, α -

carotene, β -cryptoxanthin, astaxanthin, lycopene, lutein, and zeaxanthin. Among these six principal carotenoids, the three first are the so-called provitamin A since they can be converted to retinol, an active form of vitamin A, in the human body. The non-provitamin A carotenoids are known to stimulate the immune system.

The best known carotenoid and most widely distributed carotenoid in foods and human blood and tissues is BC [118]. This carotenoid was isolated by Wackenroder in 1831 but its chemical structure (Fig. 2.9) was only elucidated later on, in 1930, by Karrer [119]. It was firstly fully synthesized in 1950 and commercialized by Roche in 1954.

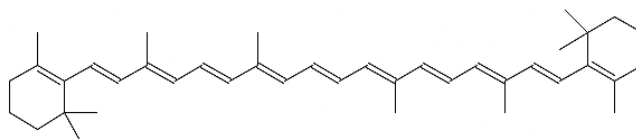


Fig. 2.9. Chemical structure of all-trans β -carotene

As previously mentioned, BC plays an important role in human health since it can be fragmented to vitamin A. Vitamin A is an essential nutrient, which plays a role in vision, reproduction, bone health, cell division, cell differentiation and immune system. The main sources of BC are dark orange fruits and vegetables (e.g. mango, apricot, carrots, sweet potatoes, pumpkins) and green vegetables (e.g. broccoli, chard). Alike the majority of carotenoids, BC is lipophilic and insoluble in water. Table 2.10 gives the principal physico-chemical properties of BC.

Table 2.10. Physico-chemical properties of β -carotene [120]

Molecular formula	$C_{40}H_{56}$
Molecular weight	536.9 g/mol
Color of crystalline powder	Red-orange
Melting point	176-182°C
clogP	11.12 *
Solubility in water	0.015 mg/L **
Solubility in fats and oils	0.05 mg/100mg
Solubility in cyclohexane	0.1 mg/100mg
Maximum absorption wavelength in cyclohexane	455-456 nm

* ChemAxon

** Experimental value measured by DSM

Due to its highly conjugated structure, BC is likely to isomerize. The most stable form in nature is the all-trans isomer, however thermal or mechanical treatment as well as exposure to light and oxygen can cause isomerization and degradation.

BC is mainly used as colorant in the food industry (e.g. beverages, margarine, milk) [121]. It is also available as individual supplements and in especially marketed supplements to promote visual health or for its provitamin A activity [122].

Pure crystalline BC commercialization is rather impractical due to its insolubility in water. The majority of marketed products are micronized oil suspensions, where BC is in microcrystalline form. Water-dispersible formulations containing pure crystalline BC are also commercialized. These products are colloidal suspensions, emulsions of oily solutions or dispersion in colloids containing surface active agents [123]. In the present study, BC served as a model compound that is both lipophilic as well as highly crystalline, so the compound was associated with particular biopharmaceutical challenges for which novel formulation approaches by HME were to be evaluated.

Chapter 3

Flow-through cross-polarized imaging as a new tool to overcome the analytical sensitivity challenges of a low-dose crystalline compound in a lipid matrix

Summary

Assessing the physical state of a low-dose active compound in a solid lipid or polymer matrix is analytically challenging, especially if the matrix exhibits some crystallinity. The aim of this study was first to compare the ability of current methods to detect the presence of a crystalline model compound in lipid matrices. Subsequently, a new technique was introduced and evaluated because of sensitivity issues that were encountered with current methods. The new technique is a flow-through version of cross-polarized imaging in transmission mode. The tested lipid-based solid dispersions (SDs) consisted of β -carotene (BC) as a model compound, and of Gelucire 50/13 or Geleol mono- and diglycerides as lipid matrices. The solid dispersions were analyzed by (hyper) differential scanning calorimetry (DSC), X-ray powder diffraction (XRPD), and microscopic techniques including atomic force microscopy (AFM). DSC and XRPD could analyze crystalline BC at concentrations as low as 3% (w/w) in the formulations. However, with microscopic techniques crystalline particles were detected at significantly lower concentrations of even 0.5% (w/w) BC. A flow-through cross-polarized imaging technique was introduced that combines the advantage of analyzing a larger sample size with high sensitivity of microscopy. Crystals were detected easily in samples containing even less than 0.2% (w/w) BC. Moreover, the new tool enabled approximation of the kinetic BC solubility in the crystalline lipid matrices. As a conclusion, the flow-through cross-polarized imaging technique has the potential to become

an indispensable tool for characterizing low-dose crystalline compounds in a lipid or polymer matrix of solid dispersions.

3.1. Introduction

Over 60% of the newly developed active compounds are poorly water-soluble [12]. Therefore, improving the solubility and oral bioavailability of such compounds has become a challenge in formulation development. Among the different formulation strategies, solid dispersions (SDs) represent one of the most efficient ways to overcome biopharmaceutical hurdles [4,6]. Over the last decades, four generations of SDs have emerged that are classified according to their composition [4]. The first generation, composed of a crystalline carrier (e.g. urea, fructose, mannitol), was developed in the 1960s. The second generation appeared in the 1970s and was based on amorphous polymeric carriers, such as cellulose derivatives, polyethylene glycol, or povidone. In the third generation SDs (1990s), surface active agents were used as additives (e.g. Tween 80, sodium lauryl sulfate, sucrose laurate) or as carriers (e.g. Compritol 888 ATO, Gelucire 44/1, poloxamer) to overcome the precipitation and recrystallization of the active compound that is otherwise often encountered with first or second generation SDs [4,124,125]. A fourth generation of SDs contains active compounds with short biological half-life, which require solubility enhancement as well as controlled release. For this purpose poorly-water soluble polymers such as ethyl cellulose, hydroxypropylcellulose, or polyethylenoxide are used [4].

Recently, the use of lipid matrices with or without surfactants in the field of the third generation SDs has generated great interest among pharmaceutical scientists because of the numerous advantages of lipid-based excipients (e.g. low physiological toxicity, high bioavailability, wide physico-chemical properties, as well as low costs) [69]. However, a drawback of lipid systems is a potentially low recrystallization rate and the issue of exhibiting different polymorphic forms (α , β , or β') [126]. Such polymorphic change can lead to altered release of an active substance or it may even cause compound expulsion from the lipid [127]. Important are the physical states of the active compound and of the matrix, which may change over time given their thermodynamic and kinetic properties. A well-known example of such physical changes is the conformational polymorphism that was observed with Ritonavir in the first marketed formulation (Norvir by

Abbott Laboratories) [124]. This emphasizes the importance of a thorough physical characterization of the active compound in the product to avoid such complications [125].

Chadha et al. [128] listed the most commonly used methods to study the compatibility between active compounds and excipients in solid dosage forms. They mentioned X-ray powder diffraction (XRPD), Fourier-transform infrared spectroscopy (FT-IR), hot stage microscopy (HSM) and differential scanning calorimetry (DSC). DSC has recently been complemented by the use of high speed or hyper-DSC (HDSC) for compound solubility studies in a semi-solid or solid matrix [97,129,130]. Besides the advantage of reducing analysis time with heating rates $>100^{\circ}\text{C}/\text{min}$, HDSC demonstrated higher sensitivity to detect small thermal events such as a glass transition of an amorphous sample [131]. It was also demonstrated that HDSC may be used to suppress undesirable thermal events like compound dissolution in the matrix that typically occurs during a slow heating rate [97]. Another very interesting application of HDSC is its use to assess solubility of the active compound in a complex matrix, for example in polymers [97] or in a wax [128]. The applied method in these studies was introduced by Theeuwes et al. [132] and is based on plotting the melting enthalpy of an active compound for different concentrations to extrapolate the solubility at the intersection with the X-axis. An alternative method has been suggested by Jannin et al. [133]. They concentrated on the melting enthalpy of the lipid matrix rather than that of the active compound. They assumed that the presence of an active substance would alter the lipid melting enthalpy. By analyzing the change in lipid enthalpy of fusion as a function of the active compound amount, they estimated the maximal amount of dissolved (or amorphous) compound in the matrix.

However, the applicability of the latter methods depends, a priori, on the compound amount and on the specific matrix used. It is a particularly challenging problem to detect a low amount of a crystalline substance in a crystalline matrix. Bikiaris et al. [134] highlighted the limitations of thermal methods in two cases, i.e. active compounds having a melting point higher than the glass transition temperature of the polymer or active compounds being dispersed in a low melting point crystalline matrix. To overcome such a challenge, the combination of several characterization methods was suggested. They emphasized the importance of combining DSC with XRPD, scanning electron microscopy, and hot stage microscopy to show the presence of active compound particles. Following the same idea, Vippagunta et al. [98] suggested to use XRPD and FTIR to overcome the limiting sensitivity of thermal analysis to determine the solid-state solubility of nifedipine in a polymeric matrix. Information about the physical state of the active

substance or of the excipients can also be provided by atomic force microscopy (AFM). Due to its high surface sensitivity, this method has a broad scope of different applications, e.g. crystal morphology characterization, polymorphs identification, homogeneity assessment, stability study, detection of compound-excipient interactions, or phase separations [135,136].

A particular hurdle analyzing the physical state of a dispersed substance in a solid matrix is sampling when dealing with low concentrations. Most of the mentioned analytical techniques rely on comparatively small sample volumes in which a low-dosed substance is present with only a few crystals. The analytical situation is further complicated by a lipid or polymer matrix that shows itself some crystallinity. The present study investigates such a case with a dispersed substance in a crystalline lipid matrix. Lipids can be processed below their melting point by (cold) solid lipid extrusion [69] or alternatively at least $\sim 20^{\circ}\text{C}$ above their melting point [98]. In this study, lipid SDs were prepared by melting them at 125°C (e.g. well above the melting points of the selected lipids) to simulate the temperature that could further be used in a melting process such as hot-melt extrusion. For the formulation of the SDs, a rather polar lipid, Gelucire 50/13 and a less polar lipid, Geleol mono- and diglycerides were selected as matrices. The first goal was to employ state-of-the-art methods to emphasize analytical sensitivity limits as well as sampling issues. The objective was to clarify the physical state of the model compound BC and it was further intended to determine its kinetic solubility. This kinetic value is the concentration of maximally dissolved (or amorphous) active compound in the matrix directly after manufacturing under the given conditions. The thermodynamic BC solubility and stability studies of the SDs were beyond the focus of the current research that focused on the analytical tools. A second aim was to explore flow-through cross-polarized imaging as a novel method to potentially overcome current analytical limitations.

3.2. Materials and methods

3.2.1. Materials

The lipids Gelucire 50/13 (Stearoyl macrogol-32-glycerides) and Geleol mono- and diglycerides (Glycerol monostearate 40-55, Type I) were kindly donated by Gatefossé (Luzern, Switzerland).

Crystalline BC was obtained from DSM Nutritional Products Ltd (Kaiseraugst, Switzerland). Titanium dioxide was purchased from Hänseler AG (Herisau, Switzerland). N-hexane, dichloromethane, cyclohexane, methanol, ethanol, and acetonitrile were obtained from Merck (Darmstadt, Germany). Butylated hydroxytoluene, tetrahydrofuran, N-ethyl-diisopropylamine, 2-propanol, and ammonium acetate were purchased from Sigma-Aldrich (Steinheim, Germany).

3.2.2. Preparation of the solid dispersions

Gelucire 50/13 and Geleol pellets were milled with a mortar and a pestle to obtain a fine powder. The physical mixtures (PMs) were prepared by weighing the lipid and BC (0.05–5%, w/w) in brown flacons and mixing them carefully with a spatula. SDs were obtained by melting the physical mixtures at 125°C in an oil bath during 5 min under stirring at 250 rpm. To avoid BC degradation, the samples were continuously flushed with nitrogen. The melts were cooled down to room temperature during 1 h before milling (with a mortar and a pestle) and analyzed.

3.2.3. Time-domain NMR

The solid fat content (SFC) of the raw lipids was measured by time-domain NMR (TD-NMR) using a minispec mq 20 (Bruker BioSpin GmbH, Rheinstetten, Germany). Since the samples were analyzed with the indirect method, olive oil was used as a reference. The as received lipid powders were molten at 125°C in an oil bath during 5 min before being transferred into 18 mm diameter test tubes (20 mm filling height). The melts were cooled to room temperature during 1 h. A serial tempering method was used for the SFC analysis. The tubes were placed at 0°C (ice-bath) during 60 min before the first measurement. The next measurements were carried out in the range of 10 to 80°C at 10°C intervals following an equilibration time of 30 min at each temperature. For each tube four scans were conducted with a frequency of 19.95 MHz and a pulse attenuation of 11 dB. The SFC was calculated from Eq. (1) [137]

$$\text{SFC (\%)} = \frac{\text{Sample}^{80^\circ\text{C}} \times \text{Oil}^T}{\text{Sample}^T \times \text{Oil}^{80^\circ\text{C}}} \times 100 \quad (3.1)$$

where *Sample* and *Oil* correspond to the signal intensity obtained for the sample and the olive oil, respectively. *T* is the temperature at which the measurement was carried out and 80°C is the final measurement temperature.

3.2.4. Differential scanning calorimetry

The thermal properties of the raw materials, the PMs, and the SDs were determined using a PerkinElmer DSC 8500 (Schelton, USA) under a dry nitrogen purge gas of 20 ml/min. The instrument was calibrated for heat flow and temperature with indium and water. Samples were accurately weighed (1.20 ± 0.05 mg) in 30 μ L aluminum pans and hermetically sealed. An empty pan was used as reference. Heating rates of either 5 or 150°C/min were used. The analyses were conducted in triplicates.

3.2.5. Statistical analysis

Analysis of the variance (ANOVA) was calculated using Statgraphics (v16.1.11, Statpoint Technologies, Inc., Warrenton, Virginia).

3.2.6. X-ray powder diffraction

XRPD patterns were obtained by using a D2 Phaser diffractometer (Bruker AXS GmbH, Karlsruhe, Germany) configured with a fast linear 1-D Lynxeye detector. The radiation was provided by a 1.8 kW Co KFL tube (wavelength = 1.79 Å) working with a Fe filter. The applied voltage and current were 30 kV and 10 mA, respectively. The powder samples were analyzed at room temperature over the 2θ range of 6–45°. The time per step was 0.6 s and the increment was 0.02° (2θ).

3.2.7. Polarized light microscopy in reflection-mode

To detect BC crystals in the molten lipid mixtures, the SDs were observed by polarized light microscopy in the reflection mode using an Olympus BX61 (Volketswil, Switzerland) equipped

with a U-PO3 polarizer and a U-AN360-3 analyzer. The melting procedure above the melting point of the lipids was based on a special Peltier-Element (Quick cool QC-32-0.6-1.2, Conrad, Emmenbrücke, Switzerland).

3.2.8. 3D-laser scanning microscopy

The surface of the SDs was observed with a Keyence VK-X200 Series 3D-laser scanning microscope (Mechelen, Belgium). SDs were prepared according to the method outlined in Section 3.2.2. A small droplet of each molten mixture was spread on a preheated glass slide. The samples were cooled to room temperature before analysis.

3.2.9. Atomic force microscopy

AFM images were acquired in the tapping mode using a Dimension 3100 with Nanoscope V (controller) from Bruker (Karlsruhe, Germany). A Budget Sensors Tap 190 Al-G cantilever with a resonance frequency of 190 kHz and a 48 N m^{-1} force constant was used. The samples were prepared as described in Section 3.2.2.

3.2.10. Reversed-phase high-performance liquid chromatography (RP-HPLC)

A chromatographic method was employed to evaluate BC degradation and cis-trans isomerization that could occur during the preparation process. The AOAC official method 2005.07 for analyzing BC in supplements and raw materials was used, which is based on RP-HPLC (method first action 2005) [138]. A sample containing 3% (w/w) BC was chosen as a reference for this analysis. The mobile phase consisted of butylated hydroxytoluene (50 mg/L)/2-propanol (2%, v/v)/N-ethyl-diisopropylamine (0.02%, v/v)/0.2% ammonium acetate solution (2.5%, v/v)/acetonitrile (45.5%, v/v)/methanol (45.0%, v/v). BC was extracted from the SDs with a butylated hydroxytoluene (100 mg/L)/ water (6%, v/v)/ethanol (40%, v/v)/dichloromethane (54%, v/v).

3.2.11. Flow-through cross-polarized imaging in transmission mode

A XPT-C particle analyzer (PS-Prozesstechnik, Basel, Switzerland) was employed for detection of BC crystals in low-concentrated samples (0.05–1%, w/w). A non-commercial instrument version was assembled with the intention to monitor samples in transmission mode by using cross-polarized light. For each concentration, five series of three hundred pictures were recorded with a Cosmimar Pentax TV lens extension tube (40 mm) attached to a cross-polarizer. The time interval between each picture was 100 ms. The molten mixtures were filled in a glass syringe heated with a heating pad (New Era Pump systems, Framingdale, USA). The melts were injected in the flow-through cell tempered at 15°C above the lipid melting point (65 and 72°C for Gelucire 50/13 and Geleol, respectively) with a Universal Thermostat 3680 Xavax. Each sample was collected in a beaker that was placed at the output of the flow-through cell. These samples were weighted to calculate the number of particles detected per gram of melt.

Shutter and light power were adjusted for each BC concentration to optimize the quality of the pictures. The number of crystals in each sample was detected by analyzing the pictures using the XenParTec software (v5.1, TechApp Switzerland).

Fig. 3.1 depicts a scheme of the method, which was centered on a dynamic image analysis particle analyzer (XPT-C). The measurement cell was connected to a flow-through cell that enabled analysis of relatively large sample sizes to cope with sampling. For the detection of crystalline particles, the instrument was equipped with a polarizer and an analyzer. This equipment allowed gentle heating thereby differentiating crystalline entities, which appeared white, from the dark molten lipid matrix. A CCD camera recorded pictures at defined time intervals. Analyzing the bright particles in each recorded image provided the number of crystalline BC particles in the molten SDs.

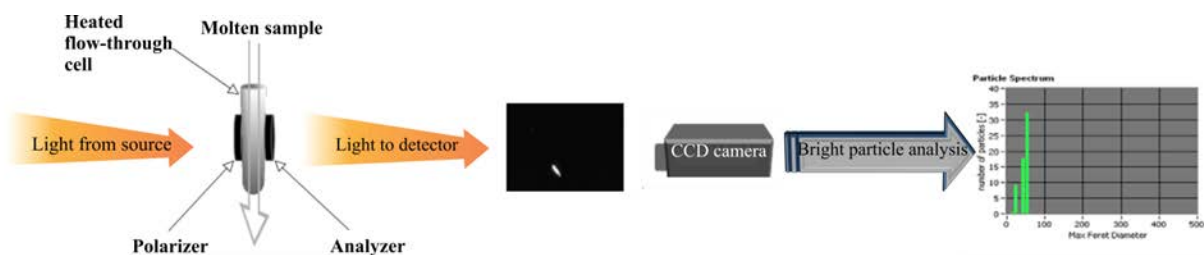


Fig. 3.1. Schematic of XPT-C cross-polarized particle analyzer

3.3. Results and discussion

3.3.1. Study of the raw materials

Prior to the study of the SDs, the crystalline properties of the raw materials were characterized as this can help understanding the solubility of the active compound in the excipients.

Previous studies have shown that an active substance preferentially occupies the amorphous regions of polymeric matrices [139]. This is comparable to lipid matrices where an active compound would be primarily solubilized in oily microdomains, while the active compound solubility in crystalline lipid is expected to be rather poor [140]. Therefore, the SFC of Gelucire 50/13 and Geleol was analyzed by means of TD-NMR. Geleol and Gelucire 50/13 are highly crystalline lipids with SFC values greater than 90% below 20°C (Fig. 3.2). Due to these high SFC values, it was assumed that the active compound solubility in these lipids would be rather limited. Gelucire 50/13 had a lower SFC and showed a broader melting range compared to Geleol. Both lipids are composed of long chain fatty acids but the presence of polyethylene glycol chains in Gelucire 50/13 and the broad lipid composition (mixture of mono-, di-, and triglycerides) [141] are likely to cause the comparatively lower SFC and wider melting range.

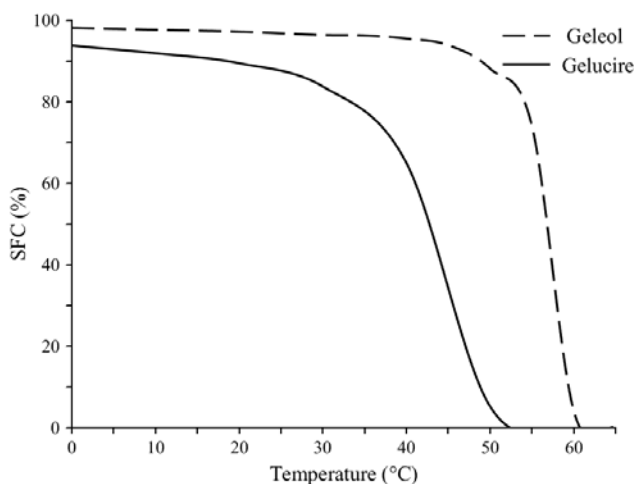


Fig. 3.2. Solid fat content profiles of pure Gelucire 50/13 (—) and Geleol (---) as a function of temperature obtained by TD-NMR.

Such compositional heterogeneity of Gelucire 50/13 was also reflected by the DSC analysis (Table 3.1). The scans at a heating rate of 5°C/min showed that Gelucire 50/13 melting was divided into three peaks: a major peak at 45.3°C accompanied by two smaller peaks. In contrast, Geleol exhibited only one narrow peak at 58.7°C. These results were in agreement with the SFC analysis (Fig. 3.2), which showed that Gelucire had a broader melting range and melted at a lower temperature compared to Geleol. The use of a high heating rate suppressed the small thermal events of Gelucire 50/13 (Table 3.1). Moreover, the fast heating rate broadened and shifted the melting peaks of the two lipids as well as of BC to higher temperatures (Table 3.1) as it was expected from literature [142].

Table 3.1. Melting peak and onset temperature of the raw materials obtained by DSC at heating rates of 5 C/min and 150°C/min. (1), (2), and (3) refer to the first, second and third peaks, respectively, that exhibited Gelucire 50/13 during melting.

	5°C/min		150°C/min	
	Onset (°C)	Peak (°C)	Onset (°C)	Peak (°C)
Gelucire 50/13	36.5 (1)	38.4	37.8	48.6
	42.5 (2)	45.3		
	48.0 (3)	50.9		
Geleol	55.6	58.7	60.8	65.8
Pure BC	177.0	180.2	185.8	192.7

Fig. 3.3 shows high resolution 3D-laser scanning images of the pure recrystallized lipids after melting. In the Geleol sample, spherulites were visible (Fig. 3.3b) whereas Gelucire 50/13 did not exhibit such a structure on the length scale studied (Fig. 3.3a). It was probably due to its compositional diversity that Gelucire 50/13 did not show distinct spherulites during crystallization, which resulted in a less ordered microstructure.

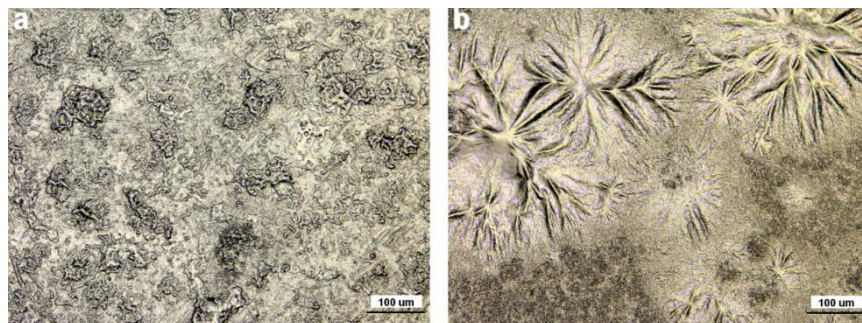


Fig. 3.3. 3D-laser scanning images of pure Gelucire 50/13 (a) and Geleol (b) (20x magnification).

3.3.2. Solid dispersion characterization with state-of-the-art methods

The BC formulations with Gelucire 50/13 and Geleol were studied using a series of different methods. The combination of these methods can be viewed as a state-of-the-art characterization. DSC is one of the most abundantly used methods to characterize pharmaceutical SDs. A heating rate of 5°C/min was first selected to analyze physical mixtures of crystalline BC (1–5%, w/w) with the given lipids. No melting peak of BC could be detected at 185°C in these reference samples (data not shown). The absence of a melting endotherm could result from BC dissolution during analysis, therefore significantly faster heating rates were evaluated. A (hyper) heating rate of 150°C/min was chosen because even higher heating rates resulted in limited analytical resolution since the lipid melting peak broadened and overlapped with the melting peak of BC. In contrast to low heating rates, the HDSC traces at 150°C/min (Fig. 3.4) revealed some endothermic events between 120 and 180°C in SDs containing at least 5 or 3% (w/w) BC in Gelucire 50/13 (Fig. 3.4a) and Geleol (Fig. 3.4c), respectively. These events can be attributed to the melting of BC as they were also observed with the physical mixtures of lipid and crystalline BC (Fig. 3.4b, d). However, Fig. 3.4 indicates that the melt enthalpies were very small and appeared not always exactly at the same temperature. The reproducibility was poor and some individual DSC traces did not exhibit any recorded endotherm. Sampling issues due to an inhomogeneous dispersion of the small amount of crystalline active compound were accounting for these inconsistent thermograms. Moreover, the absence of a BC melting peak in SDs could be

due to an amorphous state of BC or to the fact that BC dissolved in the liquefied lipid during the DSC measurement.

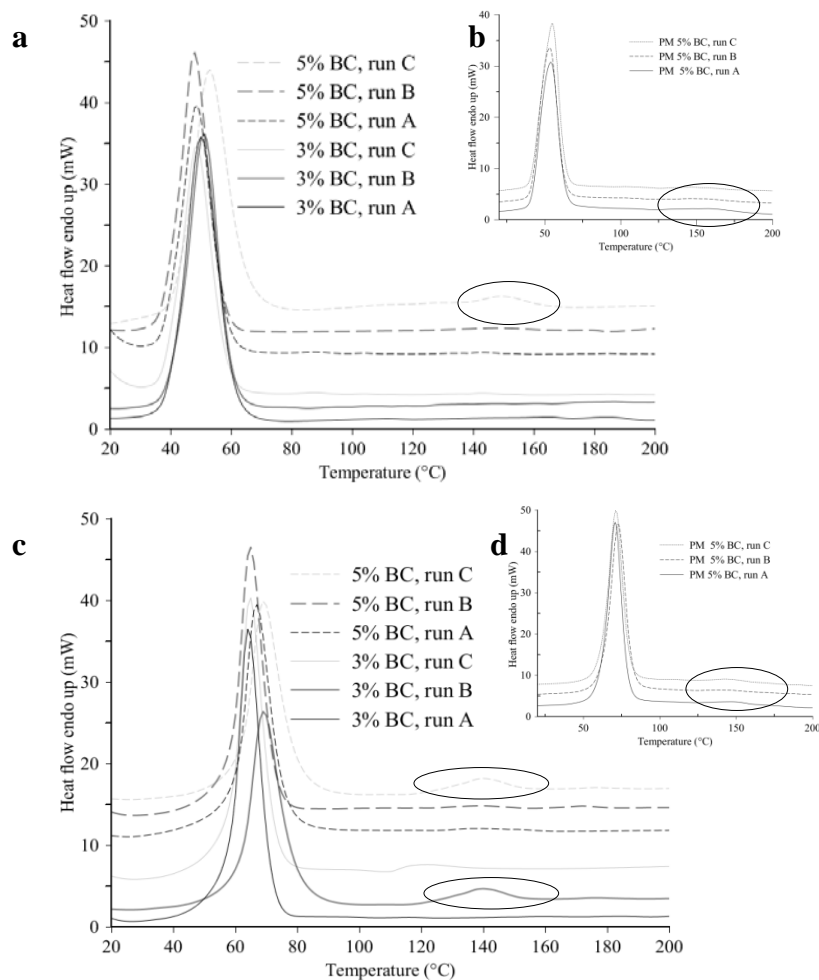


Fig. 3.4. DSC thermograms of Gelucire 50/13 (a, b) and Geleol (c, d): solid dispersions containing 3 and 5% (w/w) BC (a, c) and physical mixtures containing 5% (w/w) BC (b, d). The circles indicate BC endotherms (heating rate of 150°C/min).

To assess the sensitivity limit of the DSC instrument, physical mixtures (PMs) of BC with an inert carrier (titanium dioxide) were analyzed. A BC melting endotherm was clearly visible at ~185°C in PMs at 3% (w/w) BC, whereas in the physical mixtures with 1% (w/w) BC the melting endotherm was not visible in all thermograms (data not shown). Such poor reproducibility was explained again by the aforementioned sampling issues when low active

compound concentrations are analyzed. However, these experiments in an inert matrix indicated a sensitivity limit of the DSC instrument between 1 and 3% (w/w) BC. While these experiments used titanium dioxide as an inert matrix, the lipid formulations with active compound may have exhibited a BC interaction with the lipid either as part of manufacturing or during the measurement. Bikiaris et al. [134] showed that active compound went completely into solution during the heating even though HDSC and rather high active compound concentrations (20%, w/w) were used. Consequently, PMs composed of the lipids and crystalline BC were analyzed to validate this assumption. As a result, only PMs containing 5% (w/w) BC showed a poorly reproducible minor melting endotherm of the active compound at $\sim 150^{\circ}\text{C}$ (Fig. 3.4.b, d). Therefore, most of the active substance could have also dissolved in the SD at 1 to 5% (w/w) BC. Moreover, it cannot be ruled out based on the thermoanalytical data that a fraction of amorphous compound was present even though a clear glass transition temperature was not detected. Such differentiation of different physical compound states was not possible at these low concentrations close to the sensitivity limit of the method.

Theeuwes et al. [132] proposed a method that employed active compound melting enthalpies at different concentrations (0.8–25%, w/w) to extrapolate a solubility value. However, in our study it was not possible to directly assess the kinetic BC solubility in the matrix due to the erratic observation of the BC melting peak in the thermograms. Another indirect method was proposed by Jannin et al. [133] based on the fact that a dissolved active compound in lipid can affect the lipid melting. Thus, lipid enthalpy can be plotted against different active compound concentrations to possibly reveal a change in excipient enthalpy with increasing compound concentrations. The highest active substance concentration for which a change in lipid enthalpy is recorded should correspond to the active compound solubility. Table 3.2 summarizes the lipid melting enthalpies obtained for the different BC loads using the HDSC heating rate of $150^{\circ}\text{C}/\text{min}$. The comparison of the values obtained and the associated standard deviations showed that the active compound concentration had apparently no effect on the lipid melting enthalpy. To test this assumption a one-way ANOVA was calculated for BC-containing formulations. The p-values obtained were 0.3 and 0.09 for Gelucire 50/13 and Geleol formulations, respectively. These results confirmed that the comparison of different active compound loads did not have a significant effect on the lipid enthalpy of fusion in the concentration range studied. These results were confirmed by complementary experiments using

TD-NMR. Mixtures of Gelucire 50/13 or Geleol and different concentrations of BC (1–5%, w/w) were analyzed according to the method outlined in Section 3.2.3. The aim was to compare the SFC of the pure lipids with BC loaded formulations. The TD-NMR profiles of the BC loaded samples (data not shown) could not be clearly differentiated from those of the pure lipids (Fig. 3.2). The crystalline lipid was hence rather unperturbed by the presence of compound. In light of these HDSC and TD-NMR results, it was likely that the kinetic BC solubility was rather low so that a significant effect was not detected for the concentration range studied.

Table 3.2. Enthalpy of melting of the lipid-based solid dispersions containing different concentrations of β -carotene (BC) (150°C/min heating rate).

	BC concentration (% , w/w)	Lipid melting enthalpy (J/g)
BC/Gelucire 50/13	0	126.66 ± 0.81
	0.5	122.98 ± 1.72
	1	117.73 ± 3.73
	3	120.66 ± 5.61
	5	117.69 ± 3.10
BC/ Geleol	0	110.45 ± 3.57
	0.5	116.56 ± 4.00
	1	113.84 ± 4.76
	3	107.99 ± 6.02
	5	106.86 ± 3.25

Given the different issues of sampling and sensitivity, it was important to complement the HDSC analysis with further physical methods. The sensitivity of the XRPD was first assessed by analyzing the PMs of the individual lipids and BC. For both excipients, even though the signal was very low, BC crystalline peaks could still be detected at an active substance load of ~1% (w/w) (data not shown). Fig. 3.5 shows XRPD patterns of the SDs together with that of the pure active compound. Pure Gelucire 50/13 exhibited three main broad crystalline peaks at 22.4, 25.1, and 27.2° (2 θ) and Geleol showed only one broad crystalline peak at 25.1° (2 θ). The broadness of these peaks can be explained by heterogeneity in crystallite sizes that is likely caused by the aforementioned chemical heterogeneity of the lipids. Gelucire 50/13 SDs comprising 3 and 5%

(w/w) of BC showed characteristic BC peaks in the scattering ranges of $17.0\text{--}20.6^\circ$ (2θ) and $28.6\text{--}29.3^\circ$ (2θ) (Fig. 3.5a). The presence of these peaks confirmed existence of crystalline compound in the SD. Therefore, disappearance of the active compound endotherm in the DSC thermograms was at least partially due to its dissolution during heating. In the diffractogram corresponding to a 1% (w/w) BC content, the presence of these peaks was not so evident given the signal to noise ratio. This was in line with the sensitivity limit as observed with the physical mixtures. In Geleol SDs, BC crystalline peaks were only clearly visible for an active substance load of 5% (w/w) in the scattering range of $16.7\text{--}22.1^\circ$ (2θ) and $28.6\text{--}29.2^\circ$ (2θ) (Fig. 3.5b). The absence of BC crystalline peaks at for example 3% (w/w) was interesting given the sensitivity limit of around 1% (w/w) BC that was estimated from the XRPD experiments of the PMs. The SD could have exhibited less crystalline material than the reference PM due to some amorphous BC. This assumption can also be confirmed by the shift observed in the peak positions of both lipids in SDs containing BC. Indeed, the presence of BC likely affected the crystalline structure of the lipids. Another parameter that could also limit the detection of crystalline BC is the broadening of the compound crystalline peaks observed in the lipid SDs (Fig. 3.5a, b). In line with literature, a decrease in crystallite size is corresponding to widening of crystalline peaks [143,144]. Therefore, it is possible that during manufacturing, besides partial BC amorphization, some decrease in crystallites size could also have occurred. Based on the XRPD and HDSC data, it was obviously not possible to determine how much of crystalline or amorphous material was present in the 3% (w/w) SD using Geleol. This low BC concentration was certainly problematic regarding sampling in HDSC. However, since one run of the 3% (w/w) BC in Geleol SD displayed a clear endothermic peak, there was evidently some crystalline material present. A better understanding of the physical state of BC at low concentrations obviously required further analytical methods apart from HDSC and XRPD.

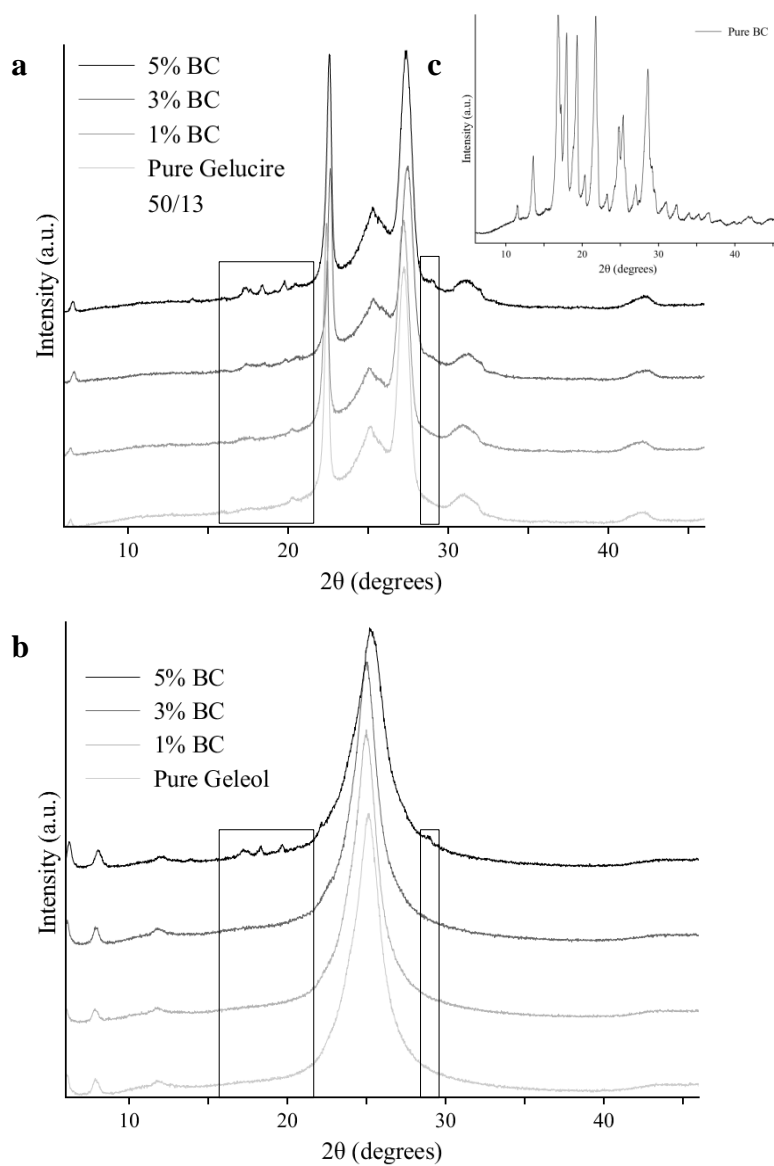


Fig. 3.5. XRPD diffractograms of Gelucire 50/13 (a) and Geleol (b) solid dispersions containing 0 to 5% (w/w) BC, as well as of pure BC (c). The rectangles mark BC main crystalline peaks for differentiation from the lipid matrix.

Detection of BC crystals in the molten or solid state SDs was investigated by microscopic techniques. The focus was on low-dose formulations with a BC content of up to 1% (w/w) because this was here a barely accessible range for the experimental techniques of HDSC and XRPD. Polarized light microscopy in reflection mode showed that molten lipids were completely

transparent, whereas all the molten samples containing BC presented the characteristic orange color of the active compound and contained aggregated particles (Fig. 3.6). It is however important to stress that particle detection was more difficult in samples having a low active compound load. That was for example the case with a BC concentration of 0.5% (w/w) (Fig. 3.6a, c) for which the analysis of a higher sample amount was necessary to detect the presence of BC particles. This confirmed again that sampling issues due to low BC concentration made it difficult to identify the physical state of BC.

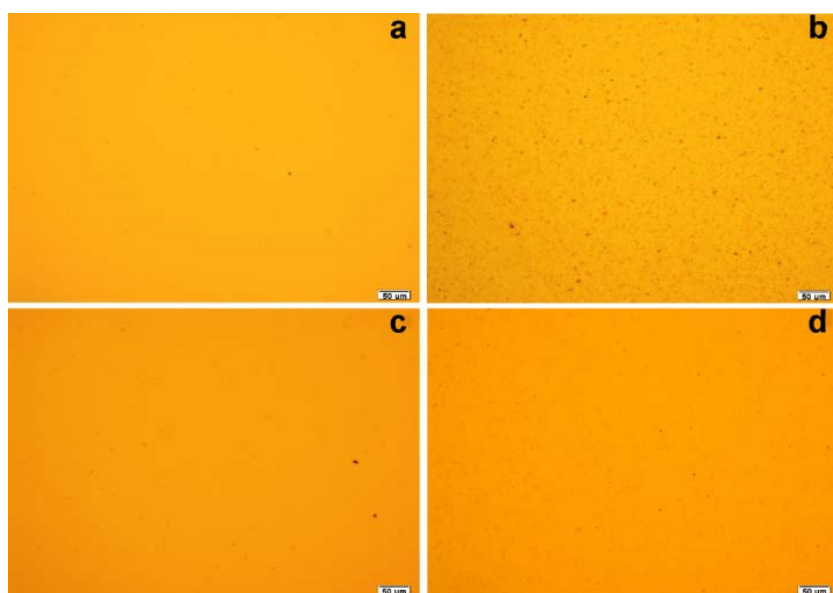


Fig. 3.6. Polarized light micrographs of molten Gelucire 50/13 solid dispersions containing 0.5% (a) and 1% (b) (w/w) BC, as well as Geleol solid dispersions containing 0.5% (c) and 1% (d) (w/w) BC.

Polarized light microscopy could detect BC particles in the molten SDs, therefore it appeared interesting to investigate the surfaces of the SDs by 3D-laser scanning microscopy and AFM. 3D-laser scanning microscopy provided information about the topography and the color of a sample. As a result, inspection of the SDs containing BC indicated the presence of shiny particles (Fig. 3.7b, d). These shiny particles were absent in the pure lipids (Fig. 3.7a, c) as well as in the SDs containing 0.5% (w/w) BC (data not shown), so they most likely corresponded to BC

crystals. In Geleol SDs, the particles were mostly located in the interstitial spaces between the spherulites.

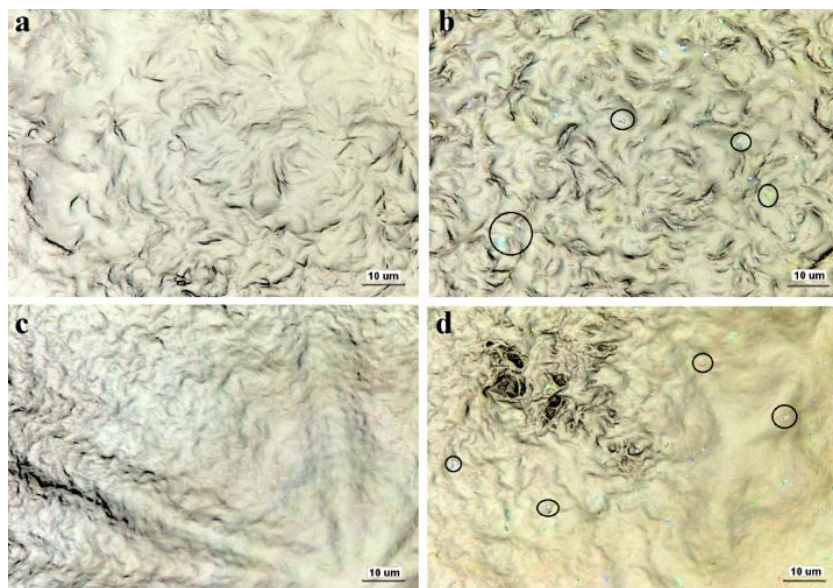


Fig. 3.7. 3D-laser scanning images of Gelucire 50/13 (a, b) and Geleol (c, d) solid dispersions containing 0% (a, c) and 1% (b, d) (w/w) BC (150x magnification). The circles highlight shiny particles present on the surface of the samples.

The last microscopic technique used to analyze the BC samples was AFM. Usually, AFM is employed to investigate amorphous SDs where for example crystalline compound can be detected in an amorphous carrier. Phase image can be constructed from the results of the tapping mode and different areas tell about differences in local viscoelastic properties and adhesion forces of the materials. Materials having different mechanical characteristics give a different response to the applied force and thus exhibit different color contrasts. Soft materials appear dark in the phase image whereas hard materials appear light [136,145]. We used phase image AFM analysis to identify the presence of BC crystals within the lipid matrices. The superposed AFM topography and phase images are displayed in Fig. 3.8. The comparison of the surface of pure lipids (Fig. 3.8a, c) and BC loaded formulations (Fig. 3.8b, d) did not reveal clear differences since the phase as well as the topography appeared similar. The different tints observed could result from the heterogeneous crystallization of the lipids. Interestingly, the particles detected by

3D-laser scanning microscopy were not detected by the AFM method. Laser light can scan a surface while penetrating slightly, whereas the AFM tip could only give information directly of the sample surface. The lack of AFM sensitivity may therefore arise from particles that are covered with a thin lipid layer. Another possibility is that the low amount of BC crystals dispersed in the crystalline lipid matrix did not result in sufficient mechanical differentiation for the AFM tip.

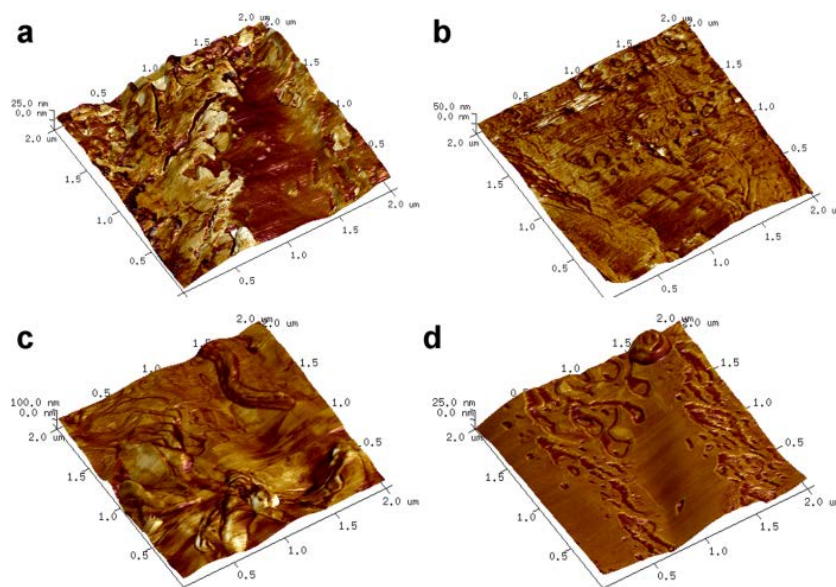


Fig. 3.8. Atomic force microscopy superposed topography and phase images of Gelucire 50/13 (a, b) and Geleol (c, d) solid dispersions containing 0% (a, c) and 1% (w/w) BC (b, d) with an x, y-scale of 2 μm .

As mentioned earlier, it could not be ruled out that a small BC fraction was in an amorphous state. Therefore, SDs containing 5% (w/w) BC were analyzed by 3D-laser scanning microscopy and AFM. 3D-laser scanning images (Fig. 3.9a, b) showed that besides the shiny crystalline particles (already detected in low-dose SDs) additional red colored areas were visible. These areas covered a higher surface in Gelucire 50/13 SD ($>20 \times 20 \mu\text{m}$) than in Geleol SD ($\sim 20 \times 20 \mu\text{m}$). The different appearance compared to typical crystalline particles could indicate the presence of some amorphous BC.

Moreover, the absence of such red areas in samples at a low-dose could be explained by sampling issues. Interestingly, AFM did not identify amorphous regions even at 5% (w/w) BC concentration. As in SDs containing less BC, no clear differentiation could be made between the pure lipids (Fig. 3.9c, d) and their SDs containing 5% (w/w) BC (Fig. 3.9e, f). These different findings may be attributed to differing fields of view. Indeed, the size of the samples analyzed by AFM ($30 \times 30 \mu\text{m}$) was in the range of the surface covered by the red areas ($> 20 \times 20 \mu\text{m}$). The 3D-laser scanning microscopy enabled, on the other hand, to observe a much larger sample size ($> 80 \times 80 \mu\text{m}$). Given these findings, amorphous BC may have occurred to a rather limited extent and appeared probably in the form of surface amorphization of BC particles. A considerable amorphous phase would have likely been identified (at 5% (w/w) BC) at length scales analyzed by AFM.

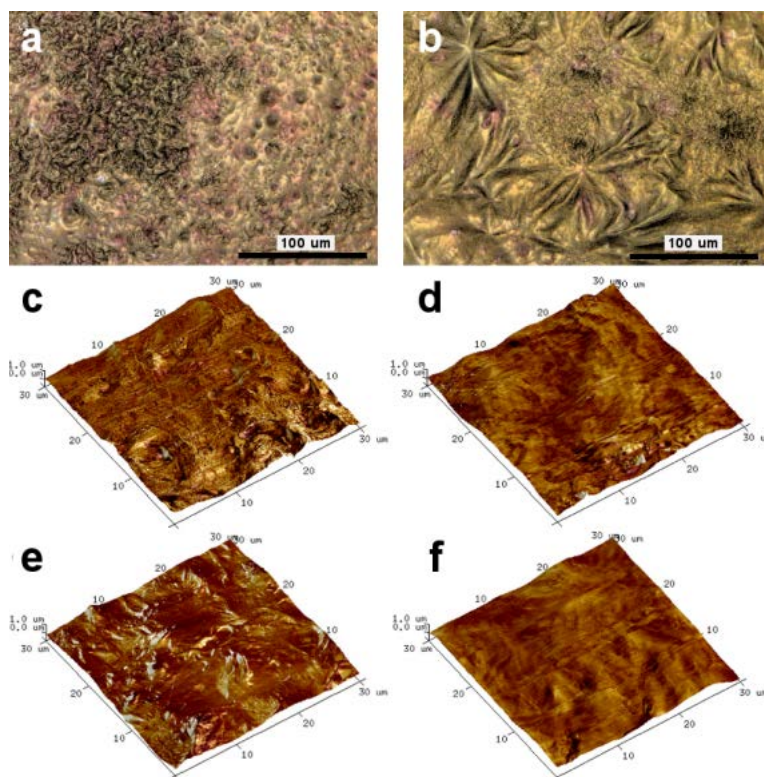


Fig. 3.9. 3D-laser scanning images (a, b) and atomic force microscopy superposed topography and phase images (c-f) of Gelucire 50/13 (a, c, e) and Geleol (b, d, f) solid dispersions containing 0% (c, d) and 5% (w/w) BC (a, b, e, f).

It can be concluded from the obtained experimental results that different state-of-the-arts methods showed sensitivity issues to detect crystalline BC in a mostly crystalline lipid matrix. The main problem was obviously the sampling at such low concentrations studied. While in microscopy analysis the increase in sample size could substantially lower the detection limit, this was different compared with DSC or XRPD. In the latter methods, the detection limits observed were depending on the measuring conditions and on the given detector technology. In this study, the limits were reflecting screening conditions on standard equipment. Moreover, rather short X-ray radiation was deemed as beneficial to avoid optional BC degradation. Such degradation of the labile BC can in principle occur under different stress conditions, which also involves heat treatment.

Even though the chemical stability was not within the primary scope of this study, it would be relevant to know, whether a major fraction of BC degraded during sample preparation. Reversed phase HPLC analysis of SDs (3% (w/w) BC) demonstrated that a majority of the active compound remained chemically stable after the heating process. Indeed, BC recovery was 90% and 77% in Gelucire 50/13 and Geleol SDs, respectively. Moreover, the assessment of trans- to cis-isomerization also provided acceptable results. The transformation from trans- to cis-isomer was ~23% in Gelucire 50/13 SDs and ~25% in Geleol SDs. Such an extent of isomerization is rather common in BC formulations [146]. These results confirmed that the obtained physical findings in this study were not greatly influenced by chemical degradation of BC.

3.3.3. Study of the solid dispersions using flow-through cross-polarized imaging

The different state-of-the-art methods showed limits of sensitivity and particularly issues of sampling were critical for analyzing low concentrations of BC in crystalline lipids. There is the risk to draw erroneous conclusions about the physical state of BC especially when only one or two standard methods are used. The microscopic techniques were as expected best suited to analyze low concentrations but considering a typical field of view in polarized light microscopy or a conventional scanning range in AFM, sampling is again the most critical factor. It seems unpractical to analyze a sufficiently large sample size to study the selected model systems

appropriately. Therefore, a new method was needed. This work introduces flow-through cross-polarized imaging as a new analytical tool. Fig. 3.10 represents the number of particles per gram of molten sample as a function of the BC concentration. Raw molten lipids were analyzed first to investigate the possible presence of crystalline particles remaining after gentle melting of the lipid. The number of particles identified in the pure lipids was used as a reference for analyzing the SDs containing BC. Fig. 3.10a displays the number of detected particles for different BC concentrations in Gelucire 50/13, which may provide a first estimate of the kinetic solubility of BC. Since the number of particles counted at 0.05–0.1% (w/w) BC was in the range of counts obtained for pure lipid, this threshold can indeed be viewed as a measure of kinetic solubility (Fig. 3.10a). The Geleol SDs were similar to the Gelucire 50/13 SDs in that the number of crystalline entities was for most concentrations above the reference (Fig. 3.10b). However, the BC concentration of 0.05% (w/w) displayed an overlapping standard deviation with that of the pure lipid. This suggested that the limit of detection was reached and that the solubility was estimated to be in vicinity of this threshold concentration. Moreover, in both lipid systems, increasing BC concentration until 0.8% (w/w) was leading to a moderate increase in the detected particles. Then an increase of BC amount to 1% (w/w) resulted in a sharp increase of both the number of particles and the standard deviations. Such higher standard deviations could be explained by an increase in the opacity of the samples with rising BC content and thus by an increased difficulty to detect crystalline particles in a quantitative way. Moreover, aggregation of crystalline particles could further lead to increased standard deviations for the particle numbers. Results from flow-through cross-polarized imaging confirmed that BC kinetic solubility was indeed below the sensitivity limit of DSC and XRPD, which thereby explained why these methods were critical to use for the selected model systems.

The analysis of the recorded pictures would in principle also allow quantitative analysis of particle size greater than one micrometer. However, due to shadow effects of the cross-polarized light there was some halo that integrated into the particle size analysis. Moreover, aggregates were leading to a systematic bias so that the novel tool may be less adequate for quantitative particle sizing. Compared to state-of-the-art methods, the new flow-through cell cross-polarized imaging technique demonstrated highest sensitivity to detect crystalline BC. It was successfully used to overcome the sampling issues encountered with the other techniques, since the flow-through cell allowed analyzing higher sample amounts.

Sample sizes of the introduced method were typically thousand times larger than those investigated by DSC or microscopic techniques. As demonstrated, it provided qualitative and quantitative information concerning BC crystals and enabled an approximation of BC kinetic solubility. There is certainly a limitation of the new method when another compound would melt close to the analysis temperature. Solubilization of compound during heating is likely to become problematic for the novel flow through technique. In contrast to DSC, where the melting temperature of the compound has to be reached to detect crystalline substance, the samples only required gentle heating to enable the matrix to flow. Since the melting point of BC is rather high ($\sim 180^{\circ}\text{C}$), such gentle heating is not expected to cause relevant compound solubilization during analysis.

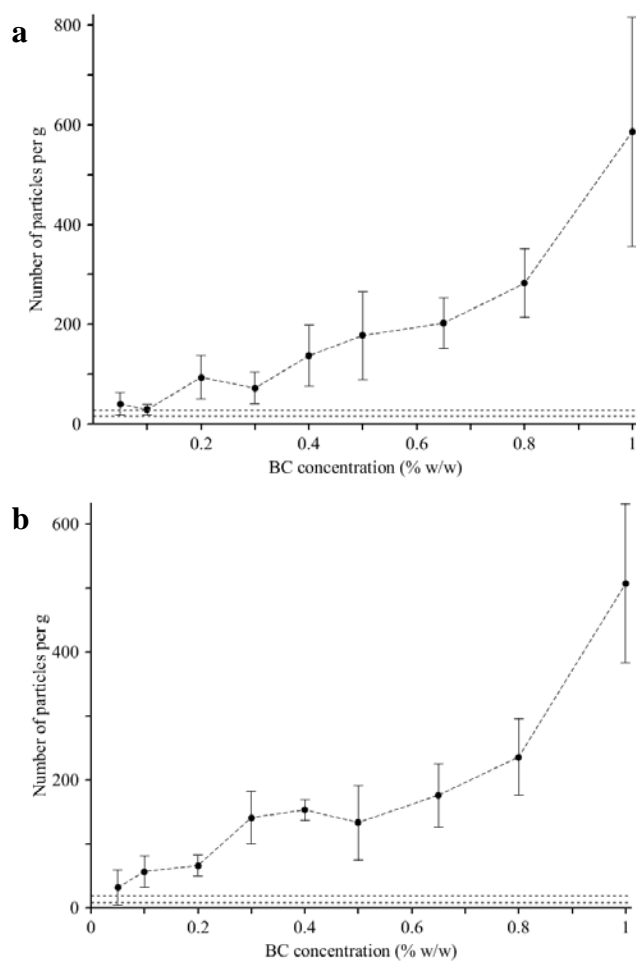


Fig. 3.10. Number of particles per gram of molten Gelucire 50/13 (a) and Geleol (b) samples as a function of BC concentration detected by cross-polarized light in transmission mode. The dashed lines represent the variability of the pure (BC-free) samples.

3.4. Conclusion

State-of-the-art methods exhibited clear sensitivity limits for the characterization of the physical state of low amounts of BC in crystalline lipids. It was shown that DSC and XRPD could identify the presence of BC crystals in samples containing at least 3% (w/w) BC. However, use of conventional polarized light microscopy in transmission mode as well as 3D-laser scanning microscopy revealed BC particles in samples having much lower BC concentrations. The drawback of classical microscopy and in particular of AFM is the small sample size. Introduction of a flow-through cell attached to cross-polarized dynamic imaging provided the means to cope with such sampling issues. It was found suitable not only to qualitatively assess the samples but also to estimate the kinetic solubility of BC in the different matrices. It may even be used to study quantitatively the degree of drug crystallinity provided that the particle density is known apart from the particle size. Particle aggregation or opacity of a sample could, however, make such analysis troublesome. The new technique has further potential for other applications. In several delivery systems the first appearance of a few crystalline substance particles is an indicator of physical instability. This is for example true for amorphous SDs. Depending on the physical state of the studied system, there would be further technical development needed for the current version of the flow-through cell. A further technical development could address advancement in the heating of the measurement chamber. Moreover, detection of a few crystalline particles in a matrix is interesting also for other applications in pharmaceuticals, for example regarding lipid-based formulations filled in capsules. The lipids are here often partially crystalline and the active compound is generally dissolved in the matrix. Changes in the matrix during aging, which could be due to polymorphism or because of an increased SFC may alter the active compound solubility in the matrix. First active compound precipitation can occur long before such a quality issue is for example detected in the dissolution tests. Therefore, flow-through cross-polarized imaging bears for different delivery systems a high potential to early anticipate quality failures that are due to physical instability.

Chapter 4

Molecularly designed lipid microdomains for solid dispersions using a polymer/inorganic carrier matrix produced by hot-melt extrusion

Summary

Amorphous solid dispersions have for many years been a focus in oral formulations, especially in combination with a hot-melt extrusion process. The present work targets a novel approach with a system based on a fatty acid, a polymer and an inorganic carrier. It was intended to adsorb the acidic lipid by specific molecular interactions onto the solid carrier to design disorder in the alkyl chains of the lipid. Such designed lipid microdomains (DLM) were created as a new microstructure to accommodate a compound in a solid dispersion. Vibrational spectroscopy, X-ray powder diffraction, atomic force microscopy as well as electron microscopic imaging were employed to study a system of stearic acid, hydroxypropylcellulose and aluminum magnesium silicate. β -carotene was used as a poorly water-soluble model substance that is difficult to formulate with conventional solid dispersion formulations. The results indicated that the targeted molecular excipient interactions indeed led to DLMs for specific compositions. The different methods provided complementary aspects and important insights into the created microstructure. The novel delivery system appeared to be especially promising for the formulation of oral compounds that exhibit both high crystal energy and lipophilicity.

4.2. Introduction

Solid dispersions (SDs) represent one of the most successful strategies to improve the solubility and bioavailability of poorly water-soluble compounds [5]. The first generation of SDs comprised crystalline carriers (e.g., urea or mannitol) and was developed in the 1960s. The second generation of SDs emerged in the 1970s with the replacement of crystalline excipients by amorphous matrices (e.g., polymers or sugar glasses) to overcome the low release rate of crystalline SDs. However, the supersaturated state of the compound in the polymeric carrier led to its precipitation and crystallization, which negatively affected the release rate and drug absorption [4,24]. Another problem of several formulations was their rather poor dispersibility in aqueous media such as gastrointestinal fluids, and therefore a third generation of SDs was developed in the 1980s. Serajuddin [6] proposed that the use of surface active agents (e.g., lipid excipients) as carriers or in combination with polymers can be beneficial in several formulations with respect to anhydrous SDs and was deemed as particularly advantageous for the dispersion behavior in aqueous media.

Among the different SD preparation techniques such as spray drying, solvent evaporation or melt agglomeration methods, hot-melt extrusion (HME) has become a common manufacturing process over the last two decades [4]. HME has several advantages such as being a solvent free and continuous process with high applicability and scalability [53]. The most commonly used matrices are thermoplastic polymers like cellulose derivatives, polyethylene oxides, or polyvinylpyrrolidone [54]. In addition to polymers, other excipients can also be used as carriers for HME, and a few reports showed that, as with the melt-adsorption method, stable melt-extruded amorphous SDs could be produced by adsorbing an active compound onto an inorganic carrier [147,148]. There are hence different ways to molecularly disperse a compound in a matrix or to convert it into small amorphous domains.

To explore the full potential of amorphous systems, the development of new microstructures would be of high interest. The aim of this study was within this scope to target designed lipid microdomains (DLMs) for delivery systems by HME. This new approach is based on a combination of a lipid, a polymer and an adsorbent. The lipid was here meant to adsorb onto the carrier surface to obtain disordered microdomains of lipid alkyl chains to accommodate an active compound. In contrast, previous studies by Gupta et al. [33] and Maclean et al. [147] intended the amorphization of an acidic drug by direct adsorption onto an inorganic carrier like aluminum

magnesium silicate (AMS). They showed that the acidic moiety of the compounds interacted with silicate silanol groups through H-bonds and with magnesium and aluminum ions present on the adsorbent surface through ion-dipole interactions. These interactions drove the amorphization and stabilization of the acidic drugs. Our novel approach was to employ a fatty acid to adsorb onto the AMS inorganic carrier to achieve the aforementioned DLMs for amorphous drug delivery.

The DLM formulations were prepared by HME. Hydroxypropylcellulose (HPC) was used as an immediate or controlled release polymer, and stearic acid (SA) was employed as plasticizer and acidic lipid to interact with AMS (Neusilin US2). The first aim was a proof-of-concept regarding the technical feasibility of DLM formulations. The influence of AMS on SA crystallinity was studied in the melt extrudates by X-ray powder diffraction (XRPD), atomic force microscopy (AFM), and scanning electron microscopy (SEM). Interactions between the lipid and the inert material were investigated by attenuated total reflectance Fourier-transform infrared (ATR-FTIR) spectroscopy. The second aim was then to use the DLM delivery system to formulate a model compound, i.e., β -carotene (BC).

4.3. Materials and methods

4.3.1. Materials

HPC (Klucel EF Pharm) was kindly donated by Ashland (Schaffhausen, Switzerland). N-hexane (purity 99%), dichloromethane (purity 99.5%), cyclohexane (purity 99.5%), methanol (purity 99.8%), ethanol (purity 99.5%), and acetonitrile (purity 99.9%) were obtained from Merck (Darmstadt, Germany). Butylated hydroxytoluene (purity 99%), tetrahydrofuran (purity 99.5%), N-ethyl-diisopropylamine (purity 98%), 2-propanol (purity 98%), ammonium acetate (purity 98%) and stearic acid were purchased from Sigma-Aldrich (Steinheim, Germany). AMS (Neusilin US2) was obtained from Fuji Chemical Industry Co., Ltd. (Toyama, Japan). Crystalline β -carotene (BC) was supplied by DSM Nutritional Products Ltd. (Basel, Switzerland).

4.3.2. Hot-melt extrusion

HPC, SA and AMS were weighed and premixed with a spatula at different ratios. Table 4.1 summarizes the different compositions of the extrudates that were prepared by the HME process using a Thermo Scientific Haake MiniLab II conical, co-rotating, twin-screw microcompounder (Thermo Electron, Karlsruhe, Germany). The premix was manually fed into the extruder hopper and the temperature of the barrel was set to 160°C. The screw speed during the feeding step was 50 rpm, followed by one minute mixing at 250 rpm. Subsequently, the extrudate strand was allowed to exit from the flat die by opening the bypass valve. The strands were stored in the fridge until analysis. Extrusion with BC (3%, w/w) was performed using the same conditions. The BC strands were stored in sealed aluminum bags purged with nitrogen until analysis. The placebo samples and BC formulations will be denoted HPC/SA/AMS and HPC/SA/AMS/BC, respectively. The most promising formulation containing 70/10/20% (w/w) HPC/SA/AMS, will be named designed lipid microdomain (DLM) system.

Table 4.1. Formulation composition of extrudate strands produced by HME.

HPC (% <i>, w/w</i>)	SA (% <i>, w/w</i>)	AMS (% <i>, w/w</i>)	BC (% <i>,w/w</i>)
100	0	0	0
90	10	0	0
85	10	5	0
80	10	10	0
75	10	15	0
70	10	20	0*
80	0	20	0
97	0	0	3
87	10	0	3
77	0	20	3
67	10	20	3**

HME = hot-melt extrusion

HPC = hydroxypropylcellulose

SA = stearic acid

AMS = aluminum magnesium silicate

BC = β -carotene

* Designed lipid microdomain (DLM) formulation

** DLM formulation containing 3% (w/w) BC

4.3.3. Time-domain nuclear magnetic resonance

The solid fat content (SFC) of raw SA was measured by time-domain NMR (TD-NMR) using a minispec mq 20 (Bruker BioSpin GmbH, Rheinstetten, Germany). Since the samples were analyzed with an indirect method, olive oil was used as a reference. The lipid powder and the olive oil were filled into separate 18 mm diameter test tubes (20 mm filling height) and heated at 100°C in an oven for 45 min. A serial tempering method was used for the SFC analysis. The tubes were placed at 0°C (ice-bath) for 60 min before the first measurement. The subsequent measurements were carried out over a range of 10–80°C, following an equilibration time of 30 min at each temperature. For each tube, the samples were scanned four times with a frequency of 19.95 MHz and a pulse attenuation of 11 dB. The SFC was calculated from Eq. (1) [137]:

$$\text{SFC (\%)} = \frac{\text{Sample}^{80^\circ\text{C}} \times \text{Oil}^T}{\text{Sample}^T \times \text{Oil}^{80^\circ\text{C}}} \times 100 \quad (4.1)$$

where *Sample* and *Oil* correspond to the signal intensities obtained for the sample and the olive oil, respectively. T is the temperature at which the measurement was carried out, and 80°C is the final measurement temperature.

4.3.4. X-ray powder diffraction

XRPD patterns were obtained using a D2 Phaser diffractometer (Bruker AXS GmbH, Karlsruhe, Germany) configured with a fast linear 1-D Lynxeye detector. The radiation was provided by a 1.8 kW Co KFL tube (wavelength = 1.79 Å) working with a Fe filter. The applied voltage and current were 30 kV and 10 mA, respectively. Instead of being milled, the extrudate strands were cut into 2–2.5 cm long pieces to avoid the potential recrystallization of the lipid. Four of these pieces were positioned in parallel in a sample holder and analyzed at room temperature over the 2θ range of 6–37°. The time per step was 3 s, and the increment was 0.02° (2θ). SA crystallite size was estimated using the Diffrac.Eva v4.0 software (Bruker AXS GmbH, Karlsruhe, Germany). Sizes were evaluated by means of Scherrer equation from the full width at half maximum of selected peaks.

4.3.5. Attenuated total reflectance Fourier-transform infrared spectroscopy

ATR-FTIR spectra of pure compounds and extrudates were acquired in the 4000–600 cm^{-1} range using a Varian 670 IR spectrometer (Varian Inc., Palo Alto, CA, USA) equipped with a golden gate high temperature heated diamond ATR top plate (Specac Ltd., Swedesboro, NJ, USA). The spectral resolution was 4 cm^{-1} . Temperature-variable ATR-FTIR analysis of pure SA was performed from ambient temperature to 95°C using a Specac 4000 series high stability controller (Specac Ltd., Swedesboro, NJ, USA). The temperature ramp was set to 5°C/min, and the sample scan number was 16. Spectra were processed using the Agilent ResolutionsPro v5.3.0.1694 software (Agilent Technologies, Santa Clara, CA, USA).

4.3.6. Atomic force microscopy

The extrudates were cut with a razor blade. AFM images of extrudate cross sections were acquired in tapping mode with a Dimension 3100 with Nanoscope V (controller) from Bruker (Karlsruhe, Germany). A Bruker RFESP rectangular cantilever with a resonance frequency of 75 kHz and a 3 $\text{N}\cdot\text{m}^{-1}$ spring constant was used.

4.3.7. Scanning electron microscopy and energy dispersive X-ray spectroscopy

Cross sections of extrudates were analyzed using a tabletop SEM TM3030 Plus (Hitachi, Tokyo, Japan). Pictures were taken with an acceleration voltage of 15 kV. Multiple elemental analysis was assessed by energy dispersive X-ray spectroscopy (EDS) with a Quantax 70 system (Bruker Nano GmbH, Berlin, Germany), which consists of an X Flash Min SVE signal processing unit, a scan generator and Megalink interface, and an X Flash silicon drift detector 410/30H (Bruker Nano GmbH, Berlin, Germany).

4.3.8. Reversed phase high-performance liquid chromatography

A chromatographic method was employed to evaluate BC degradation and cis-trans isomerization that could occur during the HME process. The AOAC official method 2005.07 for analyzing BC

in supplements and raw materials was used, which is based on reversed phase high-performance liquid chromatography, RP-HPLC (Szpylka and DeVries, 2005). The mobile phase consisted of butylated hydroxytoluene (50 mg/L)/2-propanol (2%, v/v)/N-ethyl-diisopropylamine (0.02%, v/v)/0.2% ammonium acetate solution (2.5%, v/v)/acetonitrile (45.5%, v/v)/methanol (45.0%, v/v). BC was extracted from the SDs using butylated hydroxytoluene (100 mg/L)/water (6%, v/v)/ethanol (40%, v/v)/dichloromethane (54%, v/v).

4.4. Results

4.4.1. Study of raw materials

Since the objective was to design lipid microdomains, the crystallinity of pure SA was first characterized to better understand the changes induced by the presence of AMS. The SFC of pure SA was assessed by TD-NMR at different temperatures (Fig. 4.1a). SA exhibited a SFC greater than 99% at room temperature and a melting range between 65°C and 75°C. The main SA crystalline peaks in the XRPD spectrum were at 7.8, 13.0, 23.8, 25.1, and 27.9° (2 θ) (Fig. 4.1b). In contrast, both HPC and AMS showed amorphous XRPD halos (data not shown). Crystallite size analysis showed that SA crystallites had sizes between 25 and 53 nm.

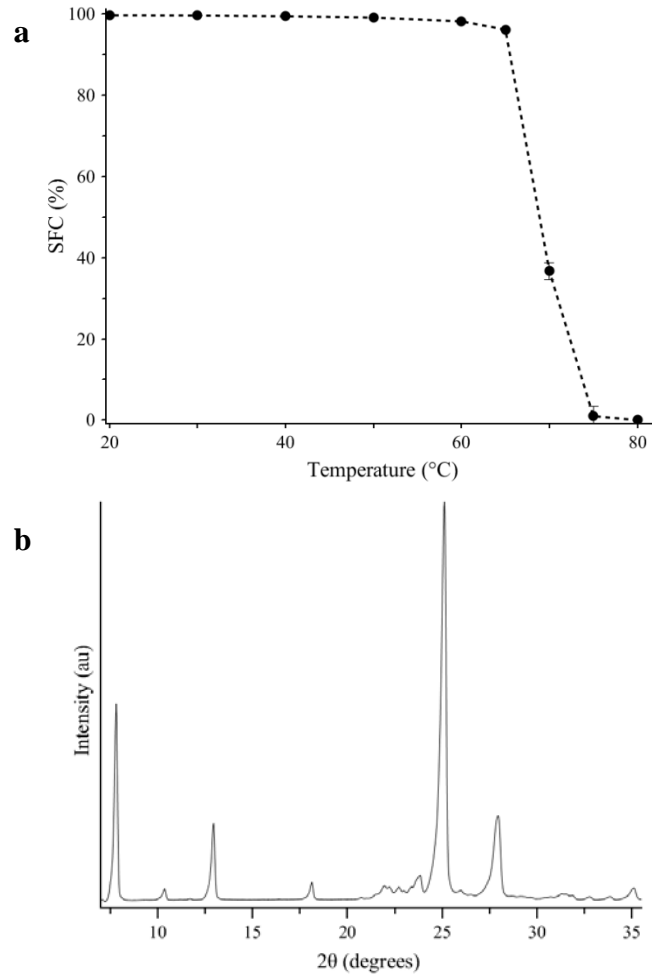


Fig. 4.1. Solid fat content (SFC) profile as a function of temperature measured by TD-NMR (a), and XRPD diffractogram (b) of pure stearic acid (SA).

4.4.2. Characterization of extrudate strands

4.4.2.1. Evaluation of SA crystallinity by XRPD

HPC hot-melt extrudates containing 10% (w/w) SA were produced at 160°C with increasing amounts of AMS (Table 4.1). XRPD analyses showed that the presence of AMS led to a complete disappearance of SA peaks at 7.8 and 13.0° (2θ) (Fig. 4.2). Interestingly, an increase in AMS concentration from 5 to 15% (w/w) resulted in a gradual decrease in SA peak height around

23, 25 and 28° (2 θ). Crystallite size analysis showed that SA crystallites were smaller in presence of AMS than in pure SA. Indeed, the crystallite sizes were between 22 and 36 nm in extrudates containing AMS. This showed that the crystallization of the lipid was influenced by the presence of the adsorbent. Shifts in the peak positions could also be observed. Shifts are usually attributed to changes in the crystalline structure or to the presence of impurities [149]. However, since the samples were not analyzed in powder form but rather in the form of strand pieces, such shifts were likely due to the positioning and not perfectly flat surfaces of the extrudates. In the formulation containing 20% (w/w) AMS, no SA crystalline peak was visible, showing that the lipid did not recrystallize after HME. This confirmed the hypothesis that the adsorbent interacted with SA acidic moiety to induce disorder in the alkyl chain configuration, leading to a lack of lipid crystallinity. This reference system was referred to as designed lipid microdomain (DLM) formulation throughout the article.

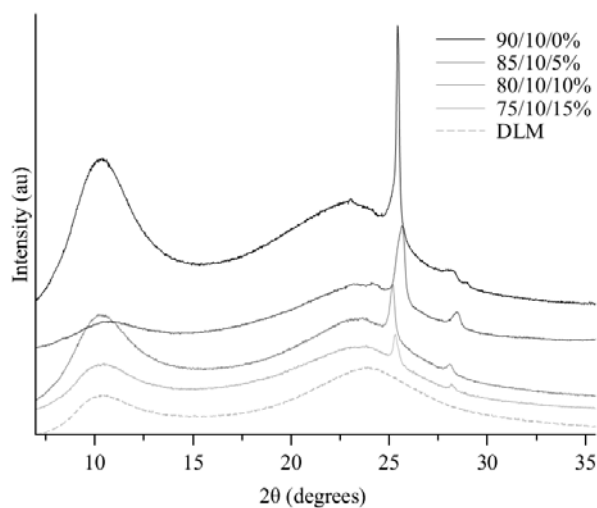


Fig. 4.2. XRPD diffractogram of extrudates containing different ratios of hydroxypropylcellulose (HPC), stearic acid (SA) and aluminum magnesium silicate (AMS). The ratios are denoted HPC/SA/AMS in the figure. The designed lipid microdomains (DLM) formulation is composed of 70/10/20% (w/w) HPC/SA/AMS.

4.4.2.2. Interaction of SA with AMS

ATR-FTIR spectroscopy was used to study the interactions between SA and the groups present on the AMS surface (i.e., silanol, aluminum and magnesium ions). Changes in the absorbance spectra were observed in four different regions in presence of the adsorbent. The first region was the high-frequency region (3100–2400 cm^{-1}), related to OH and CH stretching vibrations (Fig. 4.4a). The second region between 1750 and 1550 cm^{-1} was characteristic of C=O and COO⁻ stretching vibrations (Fig. 4.3a), and the third vibration region (1500–1180 cm^{-1}) was assigned to dimer ring, C--O--H bending and CH wagging (Appendix A: Fig. 4.14). Finally, the last region (750–700 cm^{-1}) displayed changes of methylene rocking vibrations (Fig. 4.4b). The 1180–800 cm^{-1} absorption range could not be interpreted because of overlapping bands corresponding to HPC ethereal (C--O--C) and Si--O vibrations.

SA head group vibrations

In the pure SA and 90/10% (w/w) HPC/SA extrudate spectra, a broad band corresponding to SA dimer H-bonded hydroxyl groups was visible in the 3100–2400 cm^{-1} region. The absence of this band in extrudates containing AMS (data not shown) indicated a modification in SA intermolecular interactions.

The characteristic C=O stretching band of SA dimers was observed at 1699 cm^{-1} with a small shoulder at 1685 cm^{-1} (Fig. 4.3a). A shift to a higher frequency (1703 cm^{-1}) was observed in all extrudates. Moreover, an increasing amount of AMS led to the vanishing of this band, while a new band appeared at 1587 cm^{-1} , indicating carboxylate formation. Fig. 4.3b shows the evolution of the area under the curve corresponding to the dimer and the carboxylate vibration bands. Since both bands are isolated, the integral band can be used for quantification providing more robust results than a single absorbance value. The intensity of the dimer band gradually decreased with an increasing AMS content, while the carboxylate band intensity increased to reach a maximum for the DLM formulation. It could also be observed that the intensity of the C--O--H vibrations at 1429, 1410 (in-plane bending), and 1297 cm^{-1} (stretching) decreased with AMS concentration until they practically disappeared in the DLM formulation (Appendix A: Fig. 4.13). The observed changes in SA head group vibrations with increasing amount of adsorbent showed a modification

in the lipid intermolecular interactions and suggested the creation of new interactions between SA and the inorganic carrier, as was targeted for the DLM.

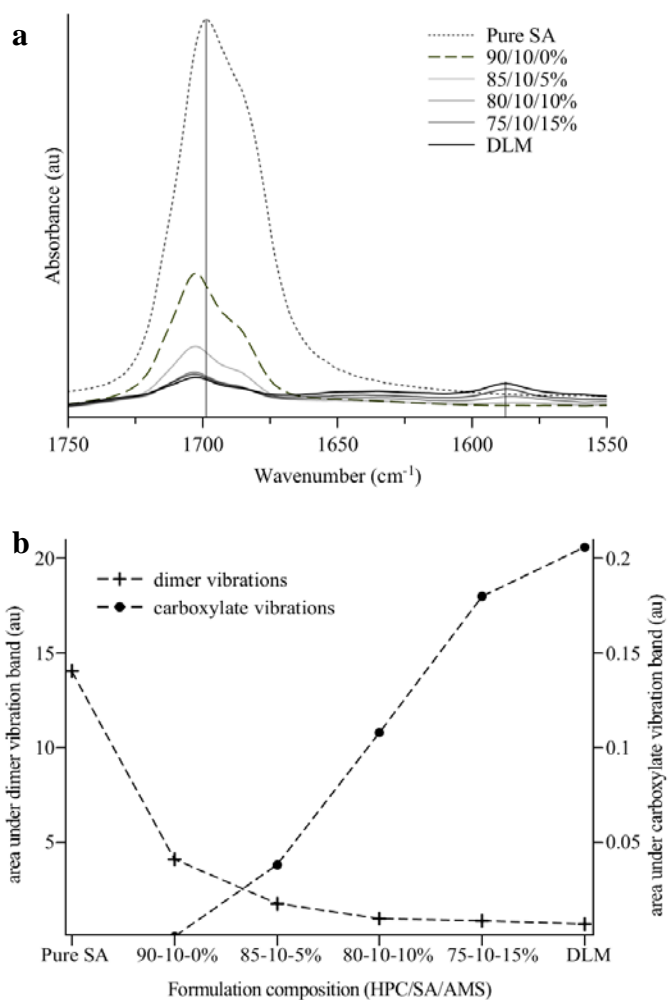


Fig. 4.3. Room temperature ATR-FTIR absorption spectra of pure SA, and HPC/SA/AMS extrudates in the regions of C=O and COO⁻ stretching (a), and area under the curve corresponding to dimer band (- - + - -) and carboxylate band (- -●- -) as a function of formulation composition (b).

SA alkyl chain vibrations

Changes showing disruption in the alkyl chains conformation were observed in the region 3000-2800 cm⁻¹, corresponding to CH stretching vibrations (Fig. 4.4a). A significant decrease in the

intensity of the two bands characteristic of asymmetric (2914 cm^{-1}) and symmetric (2847 cm^{-1}) CH_2 stretching vibrations was noted with increasing amount of AMS. Moreover, the weak asymmetric CH_3 vibration band (with a maximum at 2954 cm^{-1} and a shoulder at 2964 cm^{-1}) was only visible clearly in the 90/10% HPC/SA and 85/10/5% HPC/SA/AMS extrudates. In the other formulations, the two asymmetric vibrations as well as the symmetric vibration at 2871 cm^{-1} could not be detected. In the region $1500\text{--}1180\text{ cm}^{-1}$ (Appendix A: Fig. 4.13), the CH_2 scissoring vibrations appeared as a doublet (1471 and 1462 cm^{-1}) in pure SA.

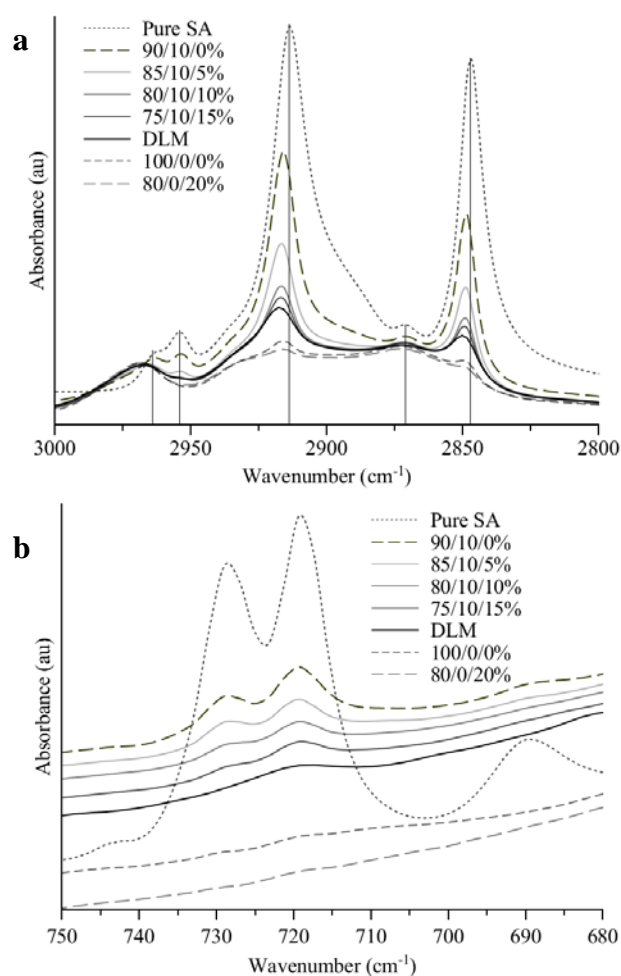


Fig. 4.4. Room temperature ATR-FTIR absorption spectra of pure SA, and HPC/SA/AMS extrudates in the regions of CH stretching (a), and CH rocking (b) vibrations.

The intensity of the two peaks decreased when AMS amounts increased and were even not visible at all in the DLM formulation. Additionally, the intensity of the methylene wagging bands between 1350 and 1150 cm^{-1} (Appendix A: Fig. 4.13) started to vanish with increasing AMS concentration until practical disappearance in the DLM system. In the region 750–700 cm^{-1} (Fig. 4.4b), the CH_2 rocking vibration band appeared as a doublet (729/719 cm^{-1}) in pure SA. It was again observed that the band started to vanish with an increasing amount of adsorbent. In the DLM system, only a shoulder could be detected at approximately 719 cm^{-1} . In conjunction with the changes in head group vibrations, the aforementioned CH vibration modifications indicated that the alkyl chain conformation of the pure lipid was strongly disrupted by the presence of the adsorbent.

4.4.2.3. Temperature-variable ATR-FTIR analysis of SA

SA head group vibrations.

In the DLM delivery system, it seemed that SA exhibited disorder of the alkyl groups due to molecularly designed interactions with AMS. To better understand the observed changes in the DLM formulation, the comparison with SA FTIR bands upon melting appeared to be of great interest. Indeed, the melting that corresponds to a progressive loss of crystallinity also leads to an increased disorder and could be related to the non-crystallinity of SA in the DLM system. As shown in Fig. 4.5 and Fig. 4.6, variations were observed in the same regions as described above for the extrudates. The most important changes occurred between 72 and 73°C, corresponding to SA melting. Above 75°C, the spectra did not show any further changes. In the region 1750–1550 cm^{-1} the carboxylic acid band started to shift to higher frequencies between 72 and 72.5°C and showed a maximum shift of 13 cm^{-1} at 73°C (Fig. 4.5). As expected, no band corresponding to carboxylate formation (1630–1550 cm^{-1}) was observed, in contrast to the DLM formulation. Changes could also be detected in the region 1500–1150 cm^{-1} (Appendix A: Fig. 4.14). From room temperature to 73°C, the intensity of C--O--H bending and stretching vibrations (1429, 1410 and 1297 cm^{-1}) strongly decreased. Finally, above 75°C, they only appeared in the form of broad bands corresponding to a high disruption in dimer intermolecular interactions when SA was in a molten state.

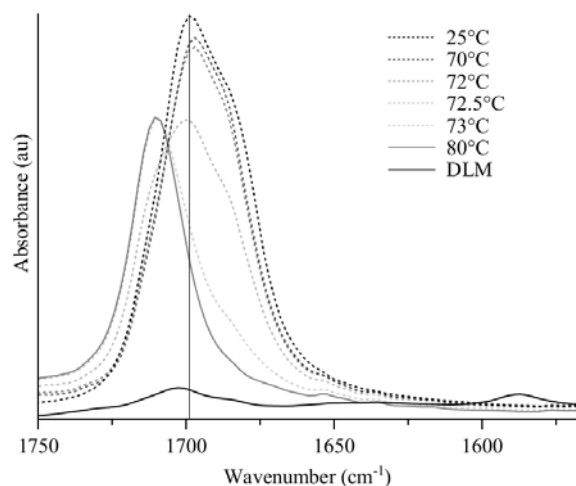


Fig. 4.5. ATR-FTIR absorption spectra of SA as a function of temperature, and of the DLM formulation extrudate at room temperature in the regions of C=O and COO⁻ stretching vibrations.

SA alkyl chain vibrations

Fig. 4.6a shows that the band intensity in the region 3000–2800 cm⁻¹ of pure SA (corresponding to CH₂ and CH₃ stretching vibrations) decreased with increasing temperature. The two CH₂ stretching vibrations started to shift to higher frequencies between 72 and 72.5°C and showed a maximum shift of 7 cm⁻¹ at 73°C and above. Temperature had the same effect on the CH₃ stretching vibrations of SA. The intensity of the doublet at 2964 (asymmetric stretching) and 2954 cm⁻¹ (symmetric stretching) decreased with increasing temperature until it only appeared as a shoulder at 2954 cm⁻¹ when SA was in the molten state. Additionally, SA CH₂ scissoring vibration doublet (1471 and 1461 cm⁻¹) exhibited an intensity decrease with increasing temperature (Appendix A: Fig. 4.14). Above a temperature of 65°C, the two peaks merged and only a single band was visible at 1463 cm⁻¹. The same phenomenon was observed for the CH₂ rocking vibration (Fig. 4.6b). The two peaks of the doublet that were visible at 25°C (728/719 cm⁻¹) progressively merged until they appeared as a singlet at 721 cm⁻¹ above 55°C. It was also observed that the wagging bands between 1350 and 1150 cm⁻¹ changed on heating. The intensity of the successive band decreased upon SA melting until its complete disappearance above 75°C.

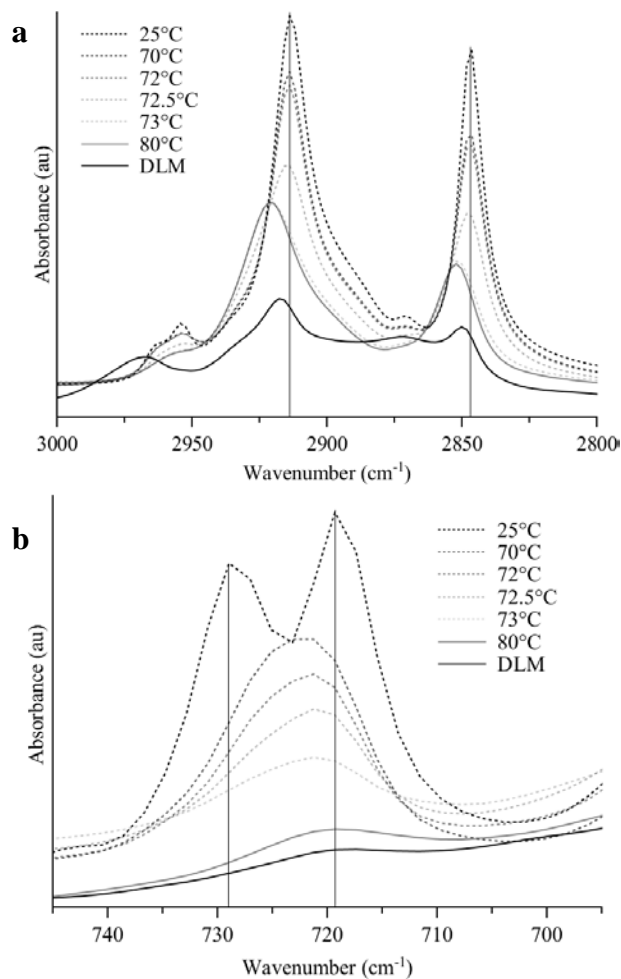


Fig. 4.6. ATR-FTIR absorption spectra of SA as a function of the temperature, and of the DLM formulation extrudate at room temperature in the regions of CH stretching (a), and CH rocking vibrations (b).

4.4.2.4. AFM and SEM/EDS analyses of the extrudates

Since XRPD and FTIR analyses showed a disruption in SA crystallinity due to AMS, it was of great interest to examine the presence of SA crystals in the extrudate strands. AFM analysis was chosen since it allows differentiating crystalline areas from an amorphous phase by assessing the mechanical properties of a sample surface. Fig. 4.7 shows the 3D height images of extrudate cross sections. The pure HPC extrudate appeared smooth (Fig. 4.7a), whereas the 90/10% (w/w) HPC/SA sample (Fig. 4.7b) displayed large sharp structures (~ 100 – 800 nm) protruding from the

surface that probably corresponded to SA crystals. In presence of 5% AMS (Fig. 4.7c), these structures were still visible but appeared to be smaller (100–400 nm). By increasing the AMS amount to 15% (w/w), their number decreased (data not shown). Finally, in the DLM sample, no SA crystalline structure could be detected, suggesting that the lipid did not recrystallize following HME (Fig. 4.7d).

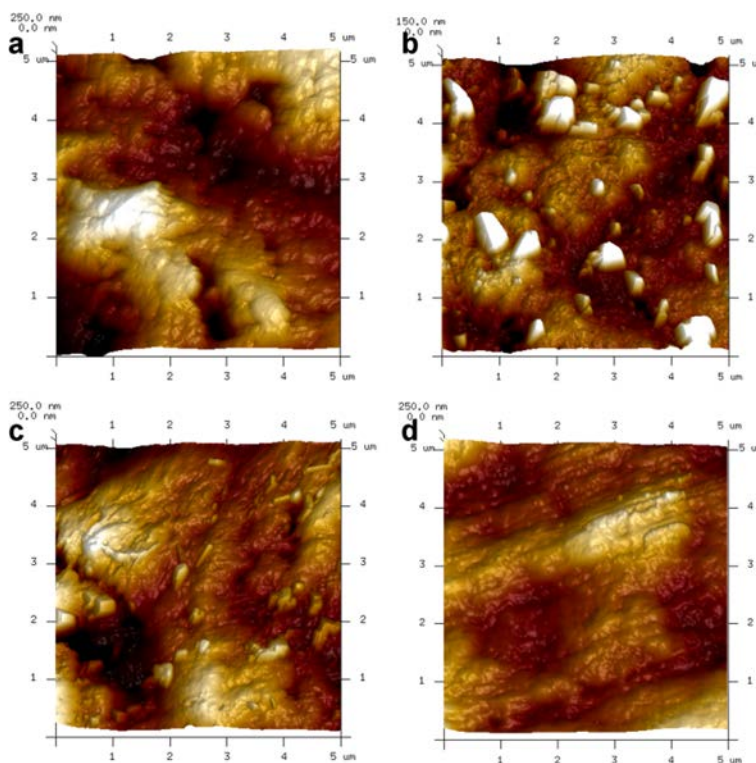


Fig. 4.7. AFM 3D height images of extrudates composed of 100% HPC (a), 90/10/0% (b), 85/10/5% (c) (w/w) HPC/SA/AMS, and DLM system (d) with x, y scale of 5 μm . Protruding white structures in (b, c) correspond to SA crystals.

SEM and EDS analyses were conducted to elucidate the distribution of the components in the extrudates (Fig. 4.8). The extrudate composed of pure HPC had a smooth surface (data not shown). In contrast, the extrudate without SA, composed of 80/20% (w/w) HPC/AMS was rather porous (Fig. 4.8a). Moreover, structures of approximately 34–40 μm were protruding from the surface. As shown in the EDS picture (Fig. 4.8b), these structures were composed of Si, Al, Mg,

and O, which corresponded to the adsorbent composition. Regions of porosity as well as others that were rich of Si, Al, Mg, and O were also observed in the samples containing up to 15% (w/w) AMS (data not shown). In the DLM formulation (Fig. 4.8c), some structures were also visible. However, in contrast to the samples containing lower amounts of AMS, they did not correspond to Si, Al, Mg, and O rich areas in the EDS image (Fig. 4.8d). The EDS colors corresponding to the different atoms were homogeneously distributed.

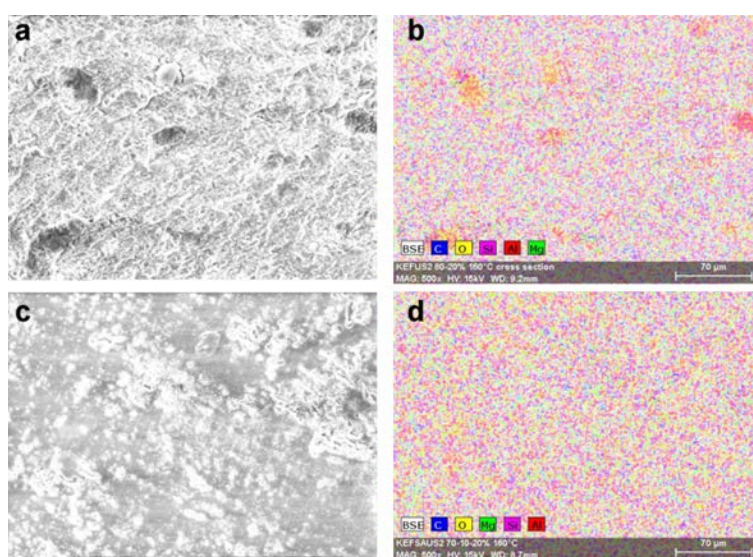


Fig. 4.8. SEM (a, c) and corresponding EDS (b, d) pictures of 80/20% (w/w) HPC/AMS (a, b) and DLM system (c, d).

4.4.3. Extrudates containing β -carotene as model compound

The DLM formulation was extruded with 3% (w/w) BC. For comparison, BC was also extruded with HPC alone, HPC/SA, as well as HPC/AMS. Table 4.1 summarizes the different formulation compositions of the BC extrudates. XRPD diffraction patterns were analyzed to assess the presence of BC crystalline peaks in the extrudates and to determine if the presence of BC had an effect on SA crystallinity. Fig. 4.9a shows that in pure BC the main peaks appeared at 13.6, 16.9, 18.0, 19.4, 21.8, 24.8, 25.4 and 28.7° (2 θ). In the extrudate composed of 97/3% (w/w) HPC/BC

(Fig. 4.9b), the BC peaks were still visible around 17.0, 19.7 and 22.0° (2 θ). In the 77/ 20/3% (w/w) HPC/AMS/BC sample, only two small BC crystalline peaks could be detected around 19.8 and 22.2° (2 θ). Finally, in the DLM system containing BC, no crystalline peaks were detected. As mentioned previously, the peak shifts could be again interpreted as an effect of the strand positioning in the sample holder.

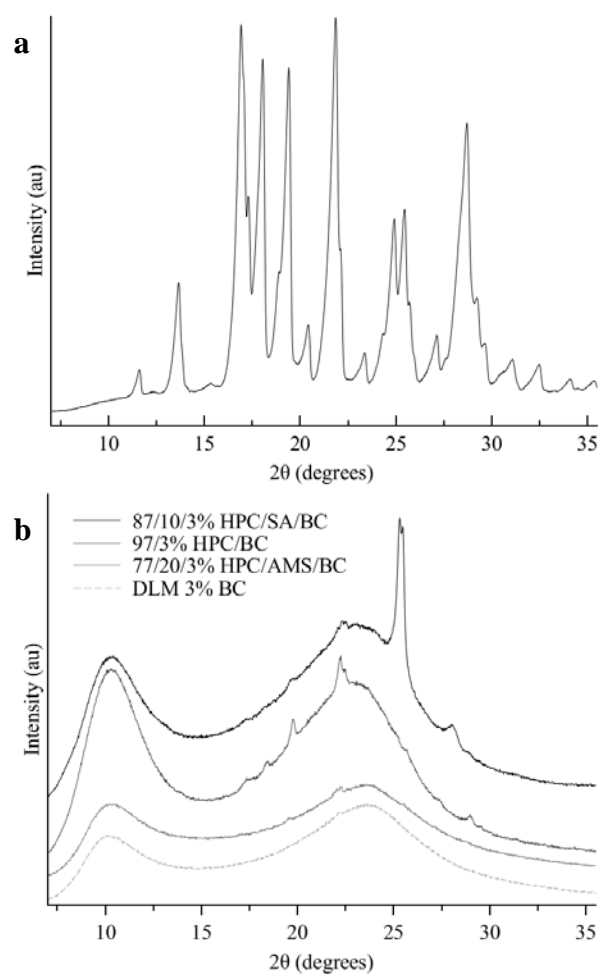


Fig. 4.9. XRPD diffractograms of pure β -carotene (BC) (a) and of extrudates containing 3% (w/w) BC (b).

We also analyzed ATR-FTIR spectra to verify that BC did not disturb the interactions between AMS and SA and to identify potential further interactions that were caused by BC. In presence of

BC, changes could only be detected in the carbonyl region (Fig. 4.10). Compared to the DLM formulation, the intensity of the C=O stretching band was lower in presence of BC, whereas the carboxylate band looked similar.

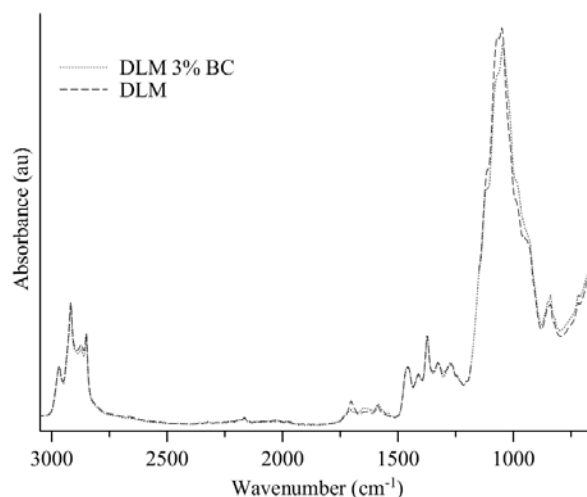


Fig. 4.10. Room temperature ATR-FTIR spectra of placebo DLM formulation and DLM formulation containing 3% (w/w) BC.

In a next step, AFM images of BC extrudates were analyzed to potentially identify the presence of any crystalline BC in the matrix. The comparison between BC formulations was based on phase pictures (Fig. 4.11) in which crystals were more easily detected compared to in height images. As shown in Fig. 4.11a, small structures were clearly visible in the 97/3% (w/w) HPC/BC extrudate. Thus, numerous dark entities were present on the surface and could be assigned to BC crystals. In the 87/10/3% (w/w) HPC/SA/BC extrudate (Fig. 4.11b), it was difficult to differentiate BC crystalline structures from other large entities that corresponded to SA crystals. However, since the number of small entities was greater in the BC formulation than in the placebo system, it was suggested that they corresponded to BC crystals.

In the sample composed of 77/20/3% HPC/AMS/BC, small BC structures could again be hardly differentiated from other large protruding structures (Fig. 4.11c). These entities could most likely be assigned to AMS since they were also visible in the 80/20% (w/w) HPC/AMS sample (data not shown). However, small structures in the BC containing sample seemed to be more

numerous, which could be assumed to be due to the presence of crystalline BC. Finally, in the BC loaded DLM sample (Fig. 4.11d), there was no protruding structure detected, which entails that neither SA nor BC were in a crystalline form.

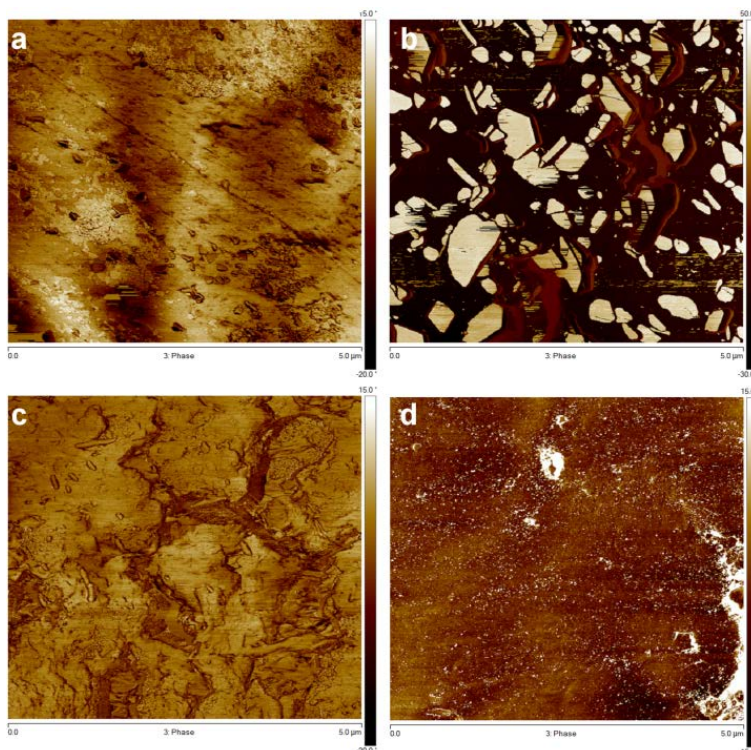


Fig. 4.11. AFM phase images of extrudates composed of 97/3% (w/w) HPC/BC (a), 87/10/3% (w/w) HPC/SA/BC (b), 77/20/3% (w/w) HPC/AMS/BC (c), and DLM formulation containing 3% (w/w) BC (d). Large white structures visible in (b) correspond to SA crystals already identified in the height images (Fig. 4.8).

To complement the physical studies of the formulations, we also conducted a chemical analysis of BC in the products. Even though BC stability was not within the primary scope of the study, it appeared important to verify that BC degradation was acceptable for a thermal manufacturing process. It was found that BC degradation was less than 20% in all formulations (data not shown). BC was primarily a model compound but the results of the chemical analysis were rather promising with respect to using HME as processing technique.

4.5. Discussion

4.5.1. Molecular design of lipid microdomains

The present study aimed at a new microstructure for SDs using HME. Fig. 4.12 displays the targeted molecular interactions between the lipid acid SA and the inorganic carrier to reduce the lipid crystallinity, thereby creating DLMs for inclusion of molecularly dispersed or amorphous compounds. In this study, AMS was chosen as an inorganic excipient because of its potential to interact with an acidic moiety. Unlike previous studies where the acidic compound was a drug [33,147,150], we adsorbed a lipid excipient to design microdomains for amorphous compound formulation. The acidic lipid excipient, SA, had a further role as HPC plasticizer in the HME process. TD-NMR analysis of pure SA showed that it is a highly crystalline fatty acid at room temperature, having a melting range between 65 and 75°C. Fig. 4.12 shows that pure crystalline SA exists as H-bonded dimers with an orthorhombic packing of methylene chains [151,152].

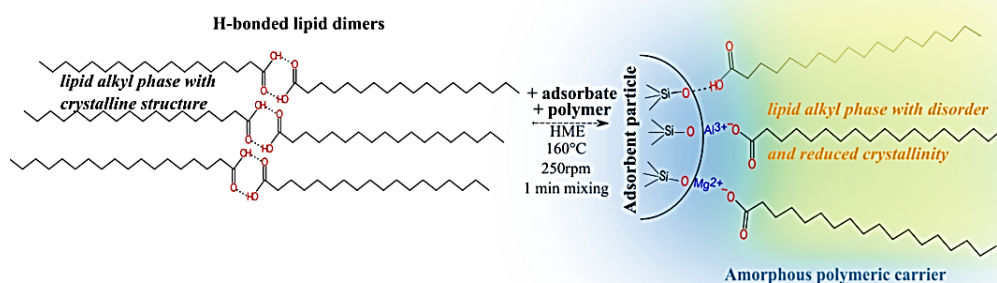


Fig. 4.12. Schematic of H-bond and ion-dipole interactions between stearic acid (SA) and aluminum magnesium silicate (AMS) in the designed lipid microdomains (DLM) system.

According to previous studies, a perfect crystalline structure leaves only little space for accommodation of an active compound [139,140,153]. In a classical lipid SD, any active compound is hence mainly located between the lipid chains, in amorphous microdomains, or

between the lipid layers [153]. Therefore, designing microdomains, where the fatty acid would be in a non-crystalline state, could be of great interest to accommodate an active compound in the final formulation. Moreover, it could also limit stability issues such as compound expulsion over time due to polymorphic changes of crystalline lipid [127]. XRPD diffractograms (Fig. 4.2) demonstrated a lower SA recrystallization using increasing amounts of AMS. Comparison of SA crystallite size with the size of the protruding entities visible in AFM pictures showed that SA was multicrystalline. Indeed, it was found that SA crystallites had sizes between 22 and 36 nm by XRPD in the extrudates, whereas SA crystals in AFM images had sizes between 100 and 800 nm. XRPD analysis allowed measuring the size of the single crystallites that composed the protruding structures visible by AFM. Finally, it was even feasible to completely inhibit SA recrystallization following the HME process, as was achieved with the DLM formulation. The disappearance of SA crystals with an increase in AMS concentration was confirmed by AFM analysis (Fig. 4.7). The AFM images suggested that the DLM system did not contain any SA crystals, whereas they could clearly be detected in the other extrudates. These results further supported the illustration given in Fig. 4.12 with respect to the DLM microstructure. The molecular interactions between the two excipients were also supported by ATR-FTIR spectroscopy. Several changes were observed in the vibrations of the SA head groups and alkyl chains that depended on the AMS content (Fig. 4.3 and Fig. 4.4). Interestingly, the same bands were affected upon SA melting (Fig. 4.5 and Fig. 4.6). The heating experiments started with SA in the form of H-bonded dimers, which could be identified by the presence of a large band between 3100 and 2400 cm^{-1} , a C=O stretching band at 1699 cm^{-1} , and C--O--H stretching and bending vibrations at 1429, 1410 and 1297 cm^{-1} . The orthorhombic packing of the alkyl chains was identified by the splitting (known as Davydov splitting) of methylene scissoring (1461 and 1471 cm^{-1}) and rocking (728 and 719 cm^{-1}) bands [151]. Upon SA melting, it was observed that the dimer and alkyl chain vibrations bands showed important transitions (Fig. 4.5 and Fig. 4.6). Namely, all head group vibrations vanished, and the C=O stretching vibration band (1699 cm^{-1}) shifted to higher frequencies with the temperature. These changes proved that as SA was heated, the dimer associations became less ordered. Additionally, all alkyl chain vibration bands vanished with temperature, methylene stretching bands shifted to higher frequencies, and Davydov splitting of scissoring and rocking vibrations decreased. It is known that peak position and intensity are related to the degree of conformational order of the methylene chains [152]. Therefore, the peak shifts and their intensity reduction can be explained by an increasing disorder in the lipid methylene chain conformation

upon melting. This was also supported by the decrease in Davydov splitting, which is observed when a modification in the alkyl chain packing occurs [151].

As mentioned previously, the observed spectral modifications of extrudates containing AMS were similar to those observed upon SA melting. Indeed, the same vibration bands vanished and shifted with increasing amount of adsorbent as with rising temperature. The highest band modifications were observed with the DLM system. The band shift was similar to that observed in SA spectrum at 72.5°C. The peak vanishing was similar to that of molten SA above 80°C. Thus, it can be concluded that in the extrudates, the presence of AMS provided a relevant degree of disorder in SA conformation (Fig. 4.12). Upon cooling, it seemed that SA did not return to its initial crystalline structure but was mostly in a highly disordered form. Another important observation was also the appearance of a new band at 1587 cm⁻¹ that corresponded to carboxylate formation. The appearance of the carboxylate band showed that other interactions were involved. As reported by Bahl and Bogner, and Gupta et al. [33,150], Al³⁺ and Mg²⁺ ions present on the AMS surface can interact with an acidic compound via ion-dipole interactions. As illustrated in Fig. 4.12, it could be assumed that the interactions between AMS and SA were of a double nature: (1) H-bonds between SA carboxylic groups and AMS silanol groups and (2) ion-dipole interactions between carboxylate groups and the adsorbent cations. The results found by XRPD and AFM analyses were in agreement with the ATR-FTIR spectral changes. The gradual decrease in FTIR vibration band intensity (head group and alkyl chain vibrations) with an increased adsorbent amount was in correlation with a decrease in SA XRPD crystalline peak intensity. In the case of the DLM formulation, no SA crystalline peak was visible at all, which could be linked to the nearly complete vanishing of ATR-FTIR vibration band intensity, corresponding to a higher disruption in SA crystalline lattice. However, it could not be ruled out that a very small fraction of SA was still in crystalline form. Indeed, the dimer peaks did not completely disappear, and the band shifts were less pronounced than for molten SA. However, since they could not be detected by XRPD or AFM analyses, it can be assumed that potentially remaining dimers would not affect the capacity of the system to accommodate a poorly water-soluble compound. Long-term stability studies were beyond the scope of the present study but they could reveal the thermodynamically most stable structure. It is possible that the SA adsorption on the inorganic carrier is only the kinetically favored structure, so that residual SA nuclei would give rise to further growth and crystallization. Residual crystals of SA would, on the other hand, barely have relevance for a DLM formulation when the SA interaction with the

carrier is thermodynamically stable. It is interesting to compare the current strategy of the DLM system for HME with nanostructured lipid carrier (NLC) formulations. In NLC systems, imperfections are created by the incorporation of a liquid lipid into a crystalline lipid carrier. This avoids the expulsion of the active compound [140,153]. NLC systems are primarily used in non-oral formulations but this is not the main difference from the DLMs. The latter novel systems were designed by a targeted molecular interaction between excipients. In contrast, NLC formulations are based on the inclusion of an excipient that disturbs the lipid crystallization.

A further aspect to consider in the novel SDs is macroscopic homogeneity. From SEM and EDS analyses, it was concluded that the DLM system displayed a homogenous distribution of all components. The lipid domains were obviously quite evenly distributed in the systems, and the absence of larger aggregates of any kind might be advantageous from a stability viewpoint.

4.5.2. Formulation of a lipophilic, highly crystalline compound using DLM

As already mentioned, BC is a lipophilic compound having a high crystalline energy. Therefore, the use of conventional HME polymeric formulations can be a challenge to obtain an amorphous solid dispersion. Indeed, there are only few polymers with a solubility parameter that is reasonably close to the estimated solubility parameter (δ) of our model compound BC ($\delta_{BC} = 17.5 \text{ MPa}^{1/2}$, as estimated by Molecular Modeling Pro, v6.2.6.; Norgwyn Montgomery Software, USA). Thus, a suitable polymer should be selected so that the solubility parameter difference between polymer and compound is minimal to achieve good miscibility, i.e., $\delta_{\text{polymer}} - \delta_{\text{compound}} < 7 \text{ MPa}^{1/2}$ [83,92]. According to this rule, lipids, which usually have a solubility parameter between $10.5\text{--}24.5 \text{ MPa}^{1/2}$ [83], are good candidates for BC formulation. However, it was reported in a previous study that BC solubility was essentially low in simple lipid-based SDs [154]. The present work therefore used the novel DLM delivery system to assess its ability to accommodate BC in an amorphous form. The temperature (160°C) was deliberately set below the BC melting point ($\sim 180^\circ\text{C}$) to limit thermal degradation. Even though HPC has a Hansen solubility parameter of $20.8\text{--}22.1 \text{ MPa}^{1/2}$ [155], it was expected that a formulation composed of the polymer alone would not enable converting BC in an amorphous state (Fig. 4.9b). This probably resulted from the extrusion temperature being below BC melting point. The formulations composed of 77/20/3% (w/w) HPC/AMS/BC and 87/10/3% (w/w) HPC/SA/BC

exhibited small BC crystalline peaks, which indicated that neither system could entirely accommodate 3% amorphous BC. In contrast, the DLM system allowed total disappearance of BC crystallinity because of the lipid microdomains. XRPD results were supported by AFM analysis. No BC or SA crystals could be detected in the DLM formulation. In the polymer/BC extrudate, however, BC crystals were clearly visible. In the HPC/SA/BC and HPC/AMS/BC samples, BC crystals could not easily be detected, but the presence of numerous small particles compared to the placebo samples was assigned to BC crystallinity. Since BC is sensitive to temperature, it was important to verify that the lack of BC crystalline XRPD peaks or structures in the DLM system were not the result of a high degradation during HME. HPLC stability data showed that even though BC was exposed to a high processing temperature its degradation was comparatively low. It was also observed that all-trans BC was lower in the formulations containing AMS. Even though BC was primarily used as model compound, the novel DLM formulations could not only be meaningful from a physical viewpoint but also with respect to minimal chemical degradation following manufacture.

4.6. Conclusion

The aim of the current work was to design lipid microdomains on an inorganic carrier by HME in a polymeric matrix. The classical SD formulation approach usually involves the selection of excipients and analyzing the structure and stability of the SD and the potential resulting interactions. In this study, an entirely new approach was to molecularly design excipient interaction to obtain a desired microstructure to host amorphous drugs. This new way of thinking could be employed in future formulations to specifically design also other microstructures to tailor SD formulation properties such as stability, release rate, or drug loading capacity. This could also be assisted by molecular modeling for the prediction of compatibility and interactions between different excipients. The advantage of the DLM delivery system was the absence of solid lipid recrystallization after HME. It is certainly an advantage that the HME processing technology is a single-step, solvent free process that can run in a continuous way. It is interesting to mention that the use of AMS facilitated the cleaning of the extruder barrel, which could increase the production efficiency. DLM is a newly introduced delivery system that has a high potential in the field of SD formulation. It would be of great interest to conduct long term

stability studies. Such future studies may also test the performance of the DLM SDs with respect to drug release and behavior upon *in vitro* digestion, and finally pharmacokinetic studies *in vivo* would be next steps in the further development of this pertinent novel delivery principle.

Appendix A

Spectra corresponding to C--O--H bending and stretching as well as CH scissoring and wagging vibrations of extrudates and of pure SA upon melting are presented in this Appendix A to support information given in sections 4.4.2 and 4.4.3.

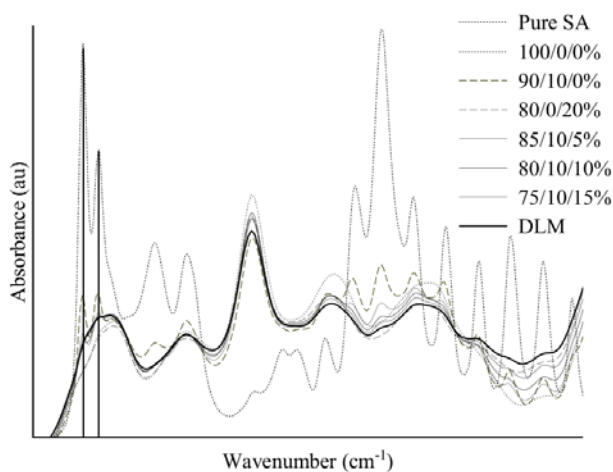


Fig. 4.13. Room temperature ATR-FTIR absorption spectra of SA, and HPC/AMS/SA extrudates in the region of C-O-H bending and stretching as well as CH scissoring and wagging vibrations.

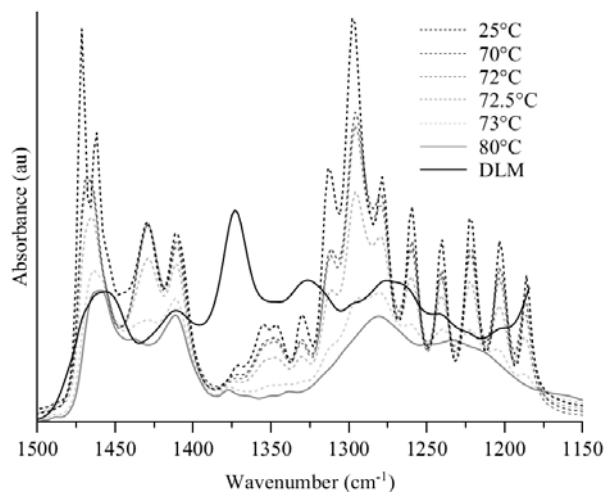


Fig. 4.14. ATR-FTIR absorption spectra of pure SA and of the DLM formulation as a function of the temperature in the region of C-O-H bending and stretching as well as CH scissoring and wagging vibrations.

Chapter 5

Multifractal characterization of pharmaceutical hot-melt extrudates

Summary

Multifractal geometry has become a powerful tool to describe complex structures in many fields. Our first aim was to combine imaging and multifractal analysis to better understand the microstructure of pharmaceutical extrudates. A second objective was to study erosion/dispersion behavior of the formulations because it would condition release of any drug. Different formulations containing a lipid, a polymer and different silica-based inorganic carriers were produced by hot-melt extrusion at various screw speeds. Multifractal analysis was based on scanning electron microscopy/energy dispersive X-ray spectroscopy images. This microstructural analysis was complemented with dynamic optical imaging of formulation erosion/dispersion behavior. Multifractal analysis indicated that inorganic carrier type and concentration as well as the screw speed affected the microstructure of the extrudates. The aqueous erosion/dispersion study showed that only the type and concentration of inorganic carrier were important. The use of microstructural and dispersion analysis appeared to be complementary to better characterize and understand complex formulations obtained by hot-melt extrusion.

5.2. Introduction

Fractals revolutionized the geometric description of real objects and they have been applied in various fields like geophysics, material sciences, ecology, agronomy, medical sciences, or more recently, pharmaceutical sciences [99,100]. The concept of fractals enables description of

Adler C. *et al.* Multifractal characterization of pharmaceutical hot-melt extrudates. *Pharmaceutical Research* 34 (2017) 321-332.

complex physical objects that have irregular shapes or fragmented structures and that can therefore be assigned to non-integer dimensions. Fractals are characterized by their self-similarity or invariance under scale of magnification [99,156]. Even more complex are multifractals that can be viewed as a superposition of homogeneous monofractal objects, i.e. objects that are invariant by translation. Although multifractals provide a powerful mathematical model for complex structures, applied sciences were more often using a single fractal dimension to describe non-Euclidean objects [156]. Applications of fractal geometry have largely profited from modern tools of image analysis [157–160]. Evolution and advances in imaging techniques over the last decades have enabled better characterization and understanding of objects structure and morphology. While optical microscopy is the simplest method but limited to micrometer range, electron microscopy enables observation of systems in the nanoscale range [161]. Other useful methods are for example atomic force microscopy for topographic measurements or confocal Raman spectroscopy, which provides information on molecular composition [162]. Fractal analysis of such imaging data is particularly of interest when it is possible to link a mathematical dimension (or set of dimensions) to object microstructure. In geoscience, for example, multifractal analysis of images was used to quantify clusters of calcium silicate hydrate from Portland cement [160]. Another example in food sciences emphasized discrimination of apple microstructures by multifractal analysis [159]. In pharmaceutical technology, Thibert et al. [163] found a link between surface geometry of granules in solid dosage forms and physical behavior (i.e., bulk density, compressibility, and angle of repose) using fractal geometry. There are other further promising applications of classical fractal analysis in pharmaceutical technology [100] but the multifractal formalism has to our knowledge not been used to investigate pharmaceutical excipients or drug products.

In this study, multifractal analysis was applied to characterize solid pharmaceutical formulations produced by hot-melt extrusion (HME). These extrudates contain silica-based adsorbents, which can be advantageous regarding a direct interaction with drug or with lipids. Indeed, as shown by Gupta et al., interactions between an inorganic carrier and a drug can imply the formation of a physically stable amorphous formulation [33]. In another study, Adler et al. targeted interactions between an adsorbent and a fatty acid to thereby design microdomains of non-crystalline lipid, which facilitated inclusion of a poorly soluble compound [16]. Such rather complex drug delivery systems are needed to formulate new drug candidates because they often exhibit poor aqueous solubility that typically leads to erratic oral drug absorption [10,13,26]. The formulation of such

challenging compounds relies on specific combinations of excipients and process parameters and HME has become one of the preferred manufacturing technologies. Besides being a solvent-free, continuous process with wide application in the pharmaceutical industry, HME also provides high mixing quality [57,164]. Indeed, the shear forces generated by the rotating screws ensure good mixing and hence dispersion of components in the formulation. Typical pharmaceutical studies focus on the physical state of the drug in such extrudates but regarding dosage form performance, it seems that a better structural understanding of such components should be achieved in general. The purpose of the current work was to analyze images of produced extrudates by multifractal geometry using scanning electron microscopy (SEM)/energy dispersive X-ray spectroscopy (EDS). Different silica-based adsorbents (granulated, fumed, hydrophobic, hydrophilic, crystalline) were selected. The formulation microstructure is at least to some extent defining the product attributes. It can later in development be tested how changes of the microstructure affect given quality attributes such as mechanical properties, drug release, or stability. Therefore, the influence of the concentration as well as the type of inorganic material were studied with a general interest in effects on the obtained microstructure. Since screw speed is an important parameter in the HME process, this factor was also considered in the multifractal analysis. The structural analysis was complemented with optical imaging of aqueous erosion/dispersion behavior because the type of erosion and dispersion is expected to be critical for oral dosage form performance. Previous use of optical imaging for self-dispersion testing has primarily focused on matrix systems intended for controlled release [165]. Only a few studies reported the use of optical imaging for the assessment of erosion/swelling behavior of solid dispersions (e.g. Harmon et al. and Bialleck et al. [166,167]). Our approach was to study self-dispersibility as an early check and de-risking method in solid dispersion development. A typical prerequisite of biopharmaceutical performance is that solid dispersions exhibit some degree of self-dispersion ability [6]. A good self-dispersibility may likely facilitate good drug release. However, one should bear in mind that good dispersibility of placebo extrudates cannot guarantee suitable release kinetics. As described by Pudlas et al. and Bravo-Osuna et al. [113,168], strong drug/excipient interactions can still lead to poor or even absence of drug release. On the other hand, poorly self-dispersing formulations have a high risk of inadequate drug release. In our study, interactions between excipients or strong adsorption to the inorganic carrier bear indeed the risk of inadequate dispersibility so that an early screening of self-dispersibility was

conducted. Thus, combination of microstructural and dispersion analysis was aiming at a better understanding of complex extrudates.

5.3. Essentials of multifractal analysis

Fractal objects are characterized by their self-similarity regardless of the observation scale. Mathematically, this property can be translated by the scaling law:

$$N(\varepsilon) \sim \varepsilon^{-D_0} \quad (5.1)$$

where N is the number of features having a certain linear dimension ε , and D_0 is the fractal dimension of the object [99,157,159]. The box-counting method is one of the existing methods that allow calculation of the fractal dimension from binary two-dimensional images. The approach consists in covering a 2-D image with boxes of sizes ε . The number N of boxes containing at least one pixel of the observed object is recorded and this procedure is repeated with a range of different box sizes. The fractal dimension D_0 is calculated from the equation:

$$D_0 = \lim_{\varepsilon \rightarrow 0} \frac{\log N(\varepsilon)}{\log \frac{1}{\varepsilon}} \quad (5.2)$$

However, more complex structures cannot entirely be described by monofractal analysis. Multifractal is an extension of fractal analysis, which decomposes self-similar measures into intertwined fractal sets that are characterized by their singularity strength and fractal dimension [157,159,169]. Multifractals can therefore be described as a superposition of homogeneous fractal objects and are characterized by a sequence of generalized fractal dimensions [99,159]. In multifractal analysis the probability P_i of finding the object pixel in the i^{th} box is determined by:

$$P_i(\varepsilon) \sim \varepsilon^{\alpha_i} \quad (5.3)$$

with α_i Lipschitz-Hölder exponent corresponding to the density in the i^{th} box [157,159].

The number of boxes $N(\alpha)$ where P_i has singularity strengths between α and $\alpha + d\alpha$ is found to scale as:

$$N(\alpha) \sim \varepsilon^{-f(\alpha)} \quad (5.4)$$

where $f(\alpha)$ is the Hausdorff fractal dimension of the set of boxes with singularities α [169,170].

The box counting method determines the partition function $X(q, \varepsilon)$, which can be considered as the probability to find the object in the i^{th} box for different moments q varying in the $[-\infty; +\infty]$ interval. The partition function is expressed as follows:

$$X(q, \varepsilon) = \sum_{i=1}^{N(\varepsilon)} p_i^q(\varepsilon) \sim \varepsilon^{(q-1)D_q} \quad (5.5)$$

with D_q the generalized dimensions corresponding to the scaling exponents for the q^{th} moment of the measure. D_q is finally defined as:

$$D_q = \frac{1}{1-q} \lim_{\varepsilon \rightarrow 0} \frac{\log \sum_{i=1}^{N(\varepsilon)} p_i^q(\varepsilon)}{\log \varepsilon} \quad (5.6)$$

In the present work, three generalized dimensions were of particular interest. Firstly, D_0 , the capacity dimension, which describes how a multifractal system covers the observed domain.

Secondly, D_1 , the information dimension (or Shannon entropy) that characterizes the degree of disorder in a distribution. And finally, D_2 , the correlation dimension that indicates the degree of clustering. Higher D_0 values indicate higher degree of space coverage, while higher D_1 values correspond to higher disorder, and lower D_2 values, suggest a higher clustering level [171]. Fig. 5.1 depicts the general shape of a multifractal system for which $D_2 < D_1 < D_0$. More precisely, a multifractal curve is initially concave downwards before an inflexion point around $q = 0$ is reached and finally, it becomes concave upwards as q increases. The particular case $D_2 = D_1 = D_0$ suggests a simpler structure that is monofractal [172].

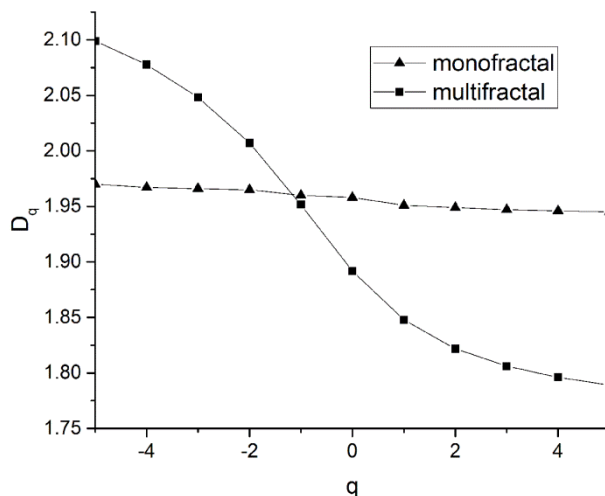


Fig. 5.1. Generalized dimensions D_q versus moment q for a multifractal (■) and a monofractal (▲) object.

5.4. Materials and methods

5.4.1. Materials

Vinylpyrrolidone-vinyl acetate copolymer (PVPVA; Kollidon VA 64) was purchased from BASF (Ludwigshafen, Germany). Propylene glycol dicaprylocaprate (Labrafac PG) was kindly donated by Gattefossé (Saint-Priest, France). Hydrophilic colloidal silicon dioxide (Aerosil 300), hydrophobic colloidal silicon dioxide (Aerosil R 972), granulated form of colloidal silicon dioxide (Aeroperl 300 Pharma) were supplied by Evonik Industries (Hanau, Germany). Aluminum magnesium silicate (Neusilin US2) was obtained from Fuji Chemical Industry Co., Ltd. (Toyama, Japan). Calcium silicate (Florite R) was supplied by Kobo Products SAS (Labège, France).

5.4.2. BET powder specific surface area

The specific surface area was determined for a basic characterization of inorganic carriers by physical adsorption of nitrogen gas using a Micromeritics Gemini V surface area and pore size

analyzer (Norcross, USA). Powders were conditioned over night at 105°C in nitrogen prior to analysis. BET values were calculated by the software Gemini v2.00 (Table 5.1).

Table 5.1. Adsorbents used in the extrudate formulations

Adsorbent	Chemical name	BET surface area (m²/g)
Aeroperl 300 [44]	granulated silicon dioxide	263 ± 1
Aerosil 300 [173]	hydrophilic fumed silicon dioxide	274 ± 5
Aerosil R 972 [173]	hydrophobic fumed silicon dioxide	126 ± 13
Neusilin US2 [39]	aluminum magnesium silicate	340 ± 1
Florite R [42]	porous calcium silicate	145 ± 1

5.4.3. Hot-melt extrusion

Prior to HME, physical mixtures were prepared by weighing and mixing different ratios of PVPVA, Labrafac PG and adsorbent with a spatula. Table I describes the different adsorbents used. Formulation compositions and process parameters used in the study are presented in Table 5.2.

Table 5.2. Composition of the extrudates and screw speeds used during HME process

Adsorbent	Formulation composition PVPVA/Labrafac PG/adsorbent (%, w/w)	Screw speed (rpm)
Aeroperl 300	85/10/5	150
	82/10/8	150, 250, 350
	80/10/10	150
Aerosil 300	82/10/8	150
Aerosil R972	82/10/8	150
Neusilin US2	82/10/8	150
Florite R	82/10/8	150

Premixes were manually fed into the hopper of a DSM Xplore MC 5 conical, co-rotating twin-screw microcompounder (Geleen, Netherlands). After 1 min mixing time at 150°C, the extrudate strand was allowed to exit from a 2 mm diameter die by opening the bypass valve. The extrudates were collected after cooling at ambient temperature and pelletized using a Thermo Scientific Process 11 Variable length pelletizer (Karlsruhe, Germany). Extrudates pellets were stored in the fridge until analysis.

5.4.4. Scanning electron microscopy and energy X-ray dispersive spectroscopy

Extrudate pellets were observed with a Hitachi SEM TM3030 PLUS (Tokyo, Japan). A voltage of 15 kV and 1000 × magnification were used. EDS analysis was based on a Quantax 70 system (Bruker Nano GmbH, Berlin, Germany) consisting of an X Flash Min SVE signal processing unit, a scan generator and Megalink interface, and an X Flash silicon drift detector 410/30H Bruker Nano GmbH, Berlin, Germany). Samples were scanned during 6 min to map silicon (Si) atoms present in the inorganic materials.

5.4.5. Image processing and multifractal analysis

Prior to multifractal analysis, EDS pictures were converted to 1020 × 760 pixels binary pictures using the image manipulation program GIMP (v2.8.14). Fig. 5.2 illustrates the conversion from a SEM/EDS picture (a) to a binary picture (b). The Image J plugin image analysis FracLac was employed to perform the box counting multifractal analysis. The black and white pictures were used and black color was set as background. The number of grid orientations, the maximum box size as % of pixels, and the moment q range were set to 4, 60, and $[-5; 5]$, respectively. Power series of box sizes was selected and box sizes were 2, 4, 16, 64 and 256 pixels. Fig. 5.2c, d show examples of grid sizes used in the box-counting method. For each formulation five extrudate pellets were analyzed.

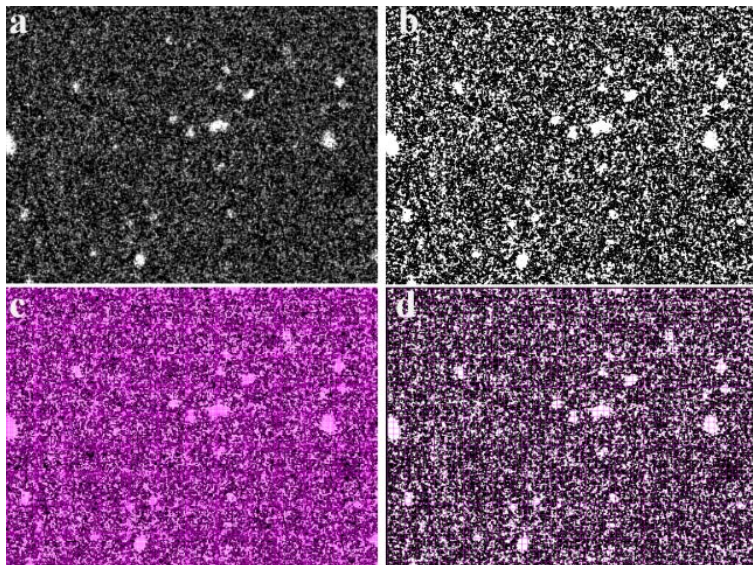


Fig. 5.2. Illustration of the conversion of a SEM/EDS 2D-picture (a) to a binary picture (b) and examples of box sizes used in the box-counting method (c, d). Only boxes containing at least one pixel of the object are counted.

5.4.6. Dispersion and erosion of pellets in water

Aqueous dispersion and erosion of pelletized extrudates was investigated by dynamic optical imaging using a Malvern Instruments Morphology G3S microscope (Instrumat AG, Renens, Switzerland). A pellet was placed in a beaker, 50 μL water was added and without stirring, images were taken every 5 s with the microscope using the Morphologi software v8.11. In each image, the pellet diameter was measured using Image J software v1.49 and the normalized diameters, X/X_0 were calculated as a function of time, where X_0 is the diameter of the dried pellet and X is the pellet diameter at the time of analysis. The experiment was repeated five times for each formulation.

5.4.7. Statistical analysis

Analysis of the variance (ANOVA) was calculated using OriginPro 2016 (vB9.3.226 Academic, OriginLab Corporation, Northampton, USA). Tukey's honest significance difference test was used for means comparison of generalized multifractal dimensions D_0 , D_1 and D_2 .

5.5. Results and discussion

5.5.1. Understanding the microstructure of pharmaceutical extrudates

5.5.1.1. Multifractal analysis of extrudate pellets containing Aeroperl 300

A twin-screw microcompounder was used to produce a series of extrudate formulations containing increasing amounts of the silica-based carrier Aeroperl 300 (5, 8 and 10% (w/w)) at 150 rpm screw speed. Samples of the extrudates were then studied by electron microscopy and EDS for subsequent image analysis using multifractals. Si distribution in the extrudate pellets is shown in Fig. 5.3a-c and the complex structure of the inorganic clusters provided a challenge for a quantitative differentiation. Therefore multifractal analysis was conducted to reveal the likely influence of increasing concentration of the inorganic carrier on the extrudate microstructure.

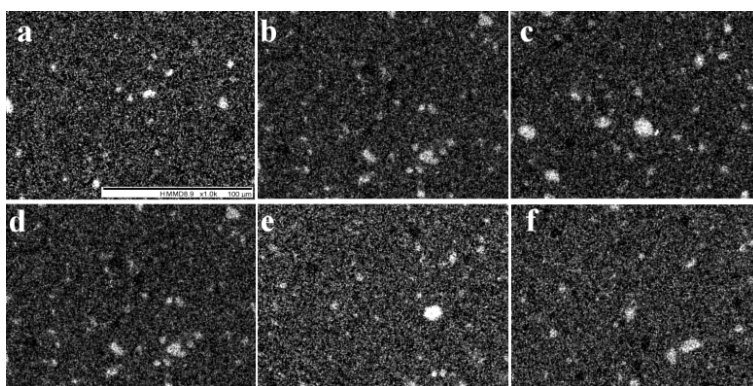


Fig. 5.3. SEM/EDS 2D-pictures of Si distribution in 85/10/5 (a), 82/10/8 (b), and 80/10/10% (w/w) (c) PVPVA/Labrafac PG/Aeroperl 300 extrudates and in 82/10/8 % (w/w) PVPVA/Labrafac PG/Aeroperl 300 extrudates produced using 150 (d), 250 (e), and 350 rpm (f) screw speeds.

From Fig. 5.4, which presents the generalized dimension D_q versus the moment q , it can be inferred that the three formulations were best described as multifractals since they all exhibited a similar decreasing D_q with increasing q . These differences were pronounced so that multifractal

modeling was required and an alternative consideration as monofractals would not have been adequate. In order to compare the three formulation microstructures, D_0 , D_1 and D_2 were taken into account. It could be seen that increasing the silica adsorbent concentration implied an increase in all three dimensions. However, while comparing the samples containing 5 and 8% (w/w) Aeroperl 300 and taking standard errors into account, the difference appeared to be rather small. In contrast, the extrudate containing 10% (w/w) inorganic carrier exhibited significantly higher D_0 , D_1 , and D_2 values. It was also interesting to note that the standard errors decreased with increasing adsorbent amount. As already reported by Bumm [174], an increase in silica concentration resulted in an increasing particle breakage. This was likely to result in higher apparent space coverage of the adsorbent in the images, which was reflected by a higher D_0 value. Higher D_1 value meant that the degree of disorder increased as well and finally, a higher D_2 value corresponded to lower clustering level.

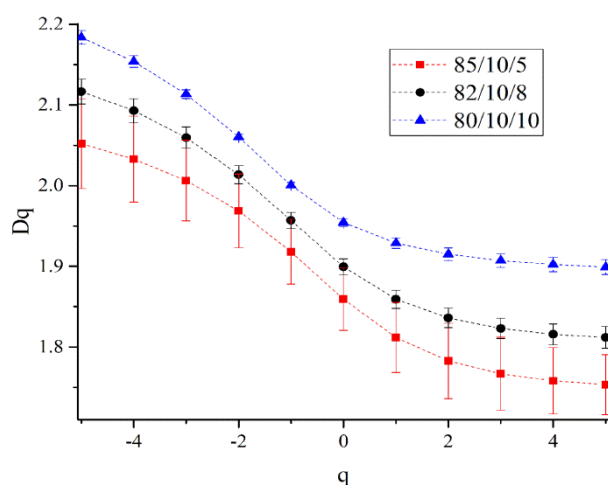


Fig. 5.4. Generalized dimension spectrum over the $[-5;5]$ moment q range of formulations containing 85/10/5, 82/10/8, and 80/10/10% (w/w) PVPVA/Labrafac PG/Aeroperl 300 prepared at 150 rpm.

Apart from the concentration of inorganic carrier, it was also of interest to study screw speed that is a most important HME process parameter. As reported by Bumm [174], the screw speed can have an influence on particle breakage and most probably on the microstructure. The formulation

composed of 82/10/8% (w/w) PVPVA/Labrafac PG/Aeroperl 300 was produced with three different screw speeds (150, 250, and 350 rpm) to assess the influence on the silica microstructure. SEM/EDS pictures of the produced extrudates are presented in Fig. 5.3d–f. No relevant difference could be again observed by the naked eye. However, as shown in Fig. 5.5, differences could be revealed in the generalized fractal dimensions for the different screw speeds. It was observed that an increase in the screw speed resulted in an increase in the generalized fractal dimensions. In the present case, Aeroperl 300 is a granulated form of colloidal silicon dioxide that is composed of spherical particles with a porous structure [44]. While exposed to high screw speeds during the HME process, the silica granules can be partly destroyed and particles may have returned to their primary aggregated form [175]. This result is interesting to compare with Bumm's report [174] who studied silica filler into thermoplastics in HME process and found an increase in silica agglomerates breakage as screw speed increased. During extrusion, the breakage of Aeroperl 300 granules may not only have caused higher apparent space coverage in the images. Also higher heterogeneity and lower degree of clustering make sense in line with our finding of increased values of the capacity dimension D_0 , the entropy dimension D_1 , and the correlation dimension D_2 . Fig. 5.5 further suggests that the 150 rpm screw speed exhibited significantly lower generalized dimensions compared to the higher speeds at 250 and 350 rpm, which had partly overlapping standard errors. This can be interpreted in that maximum particle breakage at high screw speed would lead to levelled off values in fractal dimensions. Such effects are important to know from a process development perspective to make sure that selected process conditions provide a reproducible microstructure. Process robustness would be desirable to achieve reproducibility in the quality attributes of pharmaceutical excipients and final end products. Indeed, identifying a robust operating space for process engineering is of great importance since the gained insights into how to achieve a desired microstructure in a highly reproducible way is attractive for pharmaceutical process development as well as production.

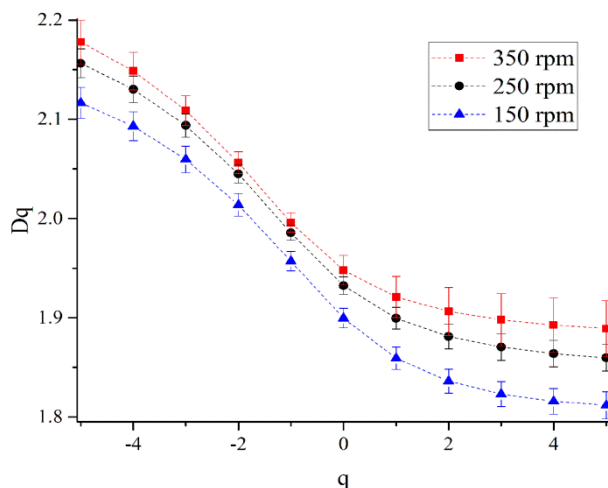


Fig. 5.5. Generalized dimension spectrum over the $[-5;5]$ moment q range of 82/10/8 % (w/w) PVPVA/Labrafac PG/Aeroperl 300 formulations prepared using 150, 250, and 350 rpm screw speeds.

5.5.1.2. Multifractal Analysis of extrudates containing different adsorbents

Different kinds of adsorbents were selected in a next research step to study the influence of physico-chemical properties on the microstructure by multifractal analysis. Aerosil adsorbents are fumed silicon dioxide with high density and small primary particle size (< 50 nm; Appendix B: Fig. 5.10). Aeroperl 300 is a granulated silicate (Appendix B: Fig. 5.11a, d) and Florite R is a calcium silicate with petaloid crystal structure (Appendix B: Fig. 5.11b, e). Finally, Neusilin US2 was selected as a granulated magnesium aluminum silicate (Appendix B: Fig. 5.11c, f).

SEM/EDS 2D-pictures are shown in Fig. 5.6. The presence of clusters can be readily seen in the extrudates containing Florite R (c) and Neusilin US2 (d), which may have been due to the original high particle size of the raw materials. Multifractal analysis was performed to understand their microstructure.

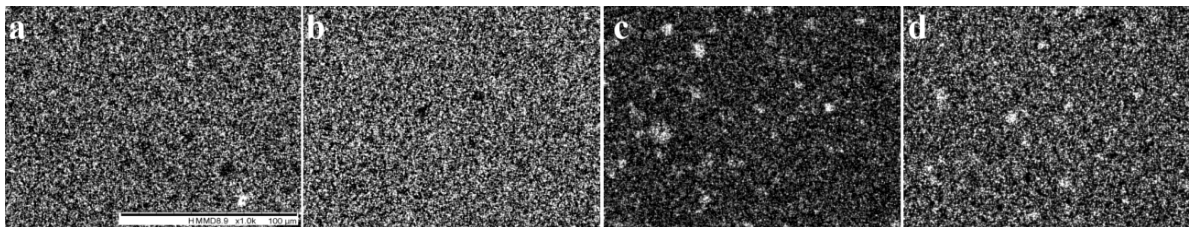


Fig. 5.6. SEM/EDS 2D-pictures of Si distribution in extrudates containing 82/10/8 % (w/w) PVPVA/Labrafac PG/adsorbent extrudates, where the adsorbents are Aerosil 300 (a), Aerosil R 972 (b), Florite R (c), and Neusilin US2 (d).

As shown in Fig. 5.7, a difference was evidenced between the different inorganic carriers of rather high granulated particle size as opposed to the fumed silica material (i.e. Aerosil). The one-way ANOVA using Tukey's method for comparison of mean D_0 , D_1 and D_2 values showed that Aerosil resulted in significantly different values from Neusilin US2, Florite R, and Aeroperl 300. Indeed, as shown in Fig. 5.7, Aerosil 300 and Aerosil R 972 exhibited higher generalized dimensions than the other adsorbents. This was due to small primary particle size of Aerosil materials, which led to better apparent space coverage (higher D_0) than granulated particles. An intuitive expectation would have been that the presence of granulated particles of different size in Neusilin US2, Florite R and Aeroperl 300 and their partial breakage during HME would result in higher heterogeneity. However, the D_1 values of the latter three inorganic carriers were lower than those of Aerosil excipients. This might be due to the short mixing time (1 min) and low screw speed (150 rpm) that did probably not lead to sufficient breakage of the granulated ingredients. For a comparison, Aeroperl 300 was also extruded at 250 rpm (Fig. 5.5, black curve) and the generalized dimension spectrum superposed perfectly with the one of Aerosil 300. This confirmed that a sufficiently high screw speed was necessary using Aeroperl 300 to break granules and to reveal the typical aggregates of primary silica particles. The lower D_2 value observed for the granulated materials confirmed a rather high level of clustering that could also be seen in the SEM/EDS pictures (Fig. 5.3b and Fig. 5.6c, d). The multifractal analysis provided a tool to gain better understanding of the microstructure caused by the adsorbent. We studied the influence of concentration, screw speed, and adsorbent type on Si microstructure in the extrudates. The comparison of the generalized multifractal dimensions provided information on coverage (or capacity), homogeneity, and cluster level. All this information is of great interest to

scientists in pharmaceutical product development or quality control to tailor drug delivery systems of desired attributes and to make sure that their structure and hence properties are obtained in a reliable way throughout manufacturing.

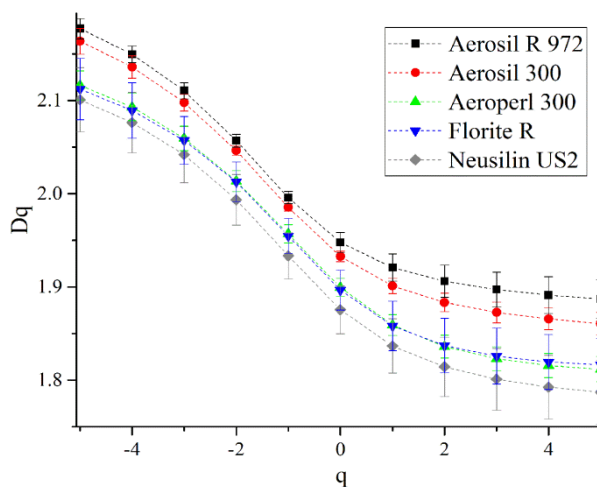


Fig. 5.7. Generalized dimension spectrum over the $[-5;5]$ moment q range of 82/10/8 % (w/w) PVPVA/Labrafac PG/adsorbent formulations. The adsorbents were Aerosil 300, Aerosil R 972, Florite R, and Neusilin US2.

5.5.2. Automated static imaging of pellets self-dispersion

Self-dispersion in aqueous media is an important characteristic of pharmaceutical extrudates. It was not expected to find a correlation with the results of multifractal analysis but since pharmaceutical formulations would have to release an active substance, it was important to study also the ability of the extruded pellets to self-disperse and erode in aqueous environment. In absence of any stirring, this ability is named as self-dispersion, which should exhibit a reasonable short duration with respect to the intended gastrointestinal release. This method was used as an early check for drug formulation development using complex matrices. Indeed, poor self-dispersion is likely to result in poor drug dissolution. Therefore, a self-dispersion study can be considered as a de-risking method for selecting matrices that could further be used for drug formulations. Extrudates dispersion and erosion was observed by

automated optical microscopy. PVPVA is a water soluble polymer that is used to improve the dissolution of poorly water-soluble drugs and thus their bioavailability [176]. Such hydrophilic polymeric matrices are erodible and dissolve after a more or less pronounced swelling step [165]. When a solid dosage form comes into contact with an aqueous medium, a rapid water uptake occurs. The polymer becomes hydrated and forms a gel layer with expansion or swelling of the matrix that gradually erodes and completely dissolves. According to Colombo et al. [177,178], the release of a drug is controlled by both its diffusion from the solid core through the gel layer and by the erosion of this gel. The dispersion of swellable solid dosage forms is characterized by a growth of the gel layer in parallel to the reduction of the dry core size and finally by an increase in matrix diameter over time. According to the rate of matrix erosion and gel layer formation, the drug release can be tailored, i.e. it may provide controlled or immediate release. Since different kinds of adsorbents were used in this work, it was critical to study their influence on the self-dispersion behavior of the pellets. Thus, evolution of erosion and swelling fronts of extrudate pellets was monitored over time, where the erosion front corresponds to the frontier between the medium and the gel layer, and the swelling front separates the still dried matrix from the gel layer. Erosion and swelling fronts are highlighted in Fig. 5.8a that illustrates pellet self-dispersion and erosion over time. Fig. 5.9 shows the evolution of the erosion (a, c, e) and swelling (b, d, f) fronts for the different formulations. Fig. 5.9a displays the erosion front of pellets containing different Aeroperl 300 amounts and during the first 40 s, the erosion front moved outwards ($X/X_0 > 1$). This was because of matrix expansion that occurred before the front moved inwards, which reflects matrix self-dispersion or erosion. In parallel, the swelling front decreased owing to water penetration. A first observation was that, even though the standards errors were rather high, pellets containing Aeroperl 300/Labrafac PG showed a tendency to differ from pure polymer pellet regarding a more important matrix expansion phenomenon (first 40 s) and a slower erosion. The high standard errors are partially due to the difficulty of selecting identical pellets. Indeed, some notable variation in dimension and weight was observed among the produced pellets. Although pellets were selected according to their mass, the dissolution behavior also depended on the diameter and height, which may have caused variation even though measured diameters were normalized by initial values in Fig. 5.9. Regarding the swelling fronts of the Aeroperl 300 pellets, no significant difference could be highlighted between the swelling fronts of the different formulations (Fig. 5.9b), there were no marked differences observed within given variability. The adsorbent concentration was therefore

not affecting the conversion of the solid core to a gel in a relevant way. All the pellets completely self-dispersed within 900 and 1000 s. In conclusion, the most important response parameter of self-dispersion was the erosion of the matrix that was faster in pure PVPVA pellet.

Fig. 5.9c, d show the evolution of the erosion (c) and swelling (d) fronts of extrudate pellets produced at different screw speeds, which did not reveal any marked effects. It therefore seemed that the composition had a more important impact on dissolution behavior than the screw speed.

Since the pellet composition seemed to be critical for self-dispersion behavior of the solid dosage form, self-dispersion of pellets containing different types of adsorbents was studied in a next step. Fig. 5.9e, f show the evolution of erosion (e) and swelling (f) fronts of extrudates containing 82/10/8% (w/w) PVPVA/Labrafac PG/adsorbent. Relevant differences could be observed between extrudates containing hydrophobic (Neusilin US2 and Aerosil R 972) and hydrophilic adsorbents. Indeed, pellets containing Aerosil R 972 or Neusilin US2 (hydrophobic) did not erode but swelled (Fig. 5.8b) and reached a maximum and constant diameter after approximately 700 s. Even after few hours in water the pellets did not erode. In contrast, pellets containing Aerosil 300 or Aeroperl 300 only slightly swelled (first 50 s) and eroded (Fig. 5.8a) until complete self-dispersion occurred within 900–1000 s. Florite R demonstrated an intermediate behavior (Fig. 5.9e–f). It swelled and eroded but an external opaque layer was still visible after complete water penetration in the matrix (Fig. 5.8c). This was probably due to the crystalline nature of Florite R that did not entirely disperse in the medium. However, unlike pellets containing Neusilin US2 and Aerosil R 972, the pellets containing Florite R completely self-dispersed after 1000 s since no gel layer was visible anymore.

In addition to the possibility of modifying the erosion rate by using an adsorbent/lipid combination, we found that the nature of the adsorbent can completely inhibit erosion. This is of great interest regarding formulation of poorly-water soluble drugs. Indeed, as shown by Joyce et al. [179] and Speybroeck et al. [180], the use of a lipid in combination with hydrophobic silica particles inhibited the lipid desorption during an *in vitro* digestion study. This was due to high interactions between the silica particles and the lipid. In our study, Aerosil R 972 and Neusilin US2 are hydrophobic adsorbents that might have high affinity to the lipophilic excipient i.e. Labrafac PG, which probably resulted to the absence of erosion of those pellets containing one of these more lipophilic adsorbents. This could have a negative effect on a poorly water-soluble drug regarding their release during formulation dispersion and possible digestion *in vivo*. Since poorly water-soluble drugs are often lipophilic, a silica/lipid solid dosage form is expected to

have the drug primarily in the lipid phase that is adsorbed on the inorganic carrier. If the lipid and adsorbent exhibit high affinity, strong interactions can be created that may hinder lipid dispersion and drug release [113]. The results of self-dispersion did not reveal significant correlations with results of the multifractal analysis. These two parts of the present work were deliberately chosen as complementary studies for an initial quality assessment of extrudates. It is, however, possible that a later formulation development for a specific drug may reveal correlations between multifractal measures and given drug dissolution. Such correlations may also be identified with other quality attributes of the extrudates and their final end products. In any case the basis of several quality tests for solid dosage forms is the sample microstructure and the corresponding basis for any drug dissolution testing is to a great extent the aqueous dispersion behavior and therefore both aspects require proper investigation and understanding.

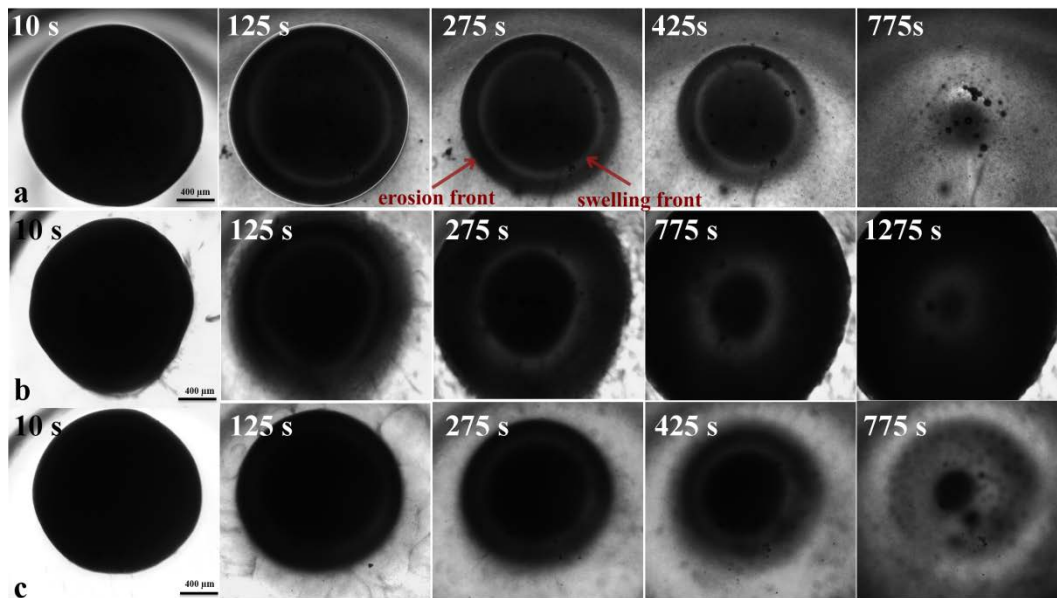


Fig. 5.8. Aqueous dispersion of extrudate pellets over time in 50 μL water without stirring. PVPVA/Labrafac PG/Aeroperl 300 (a), PVPVA/Labrafac PG/Neusilin US2 (b), and PVPVA/Labrafac PG/Florite R (c).

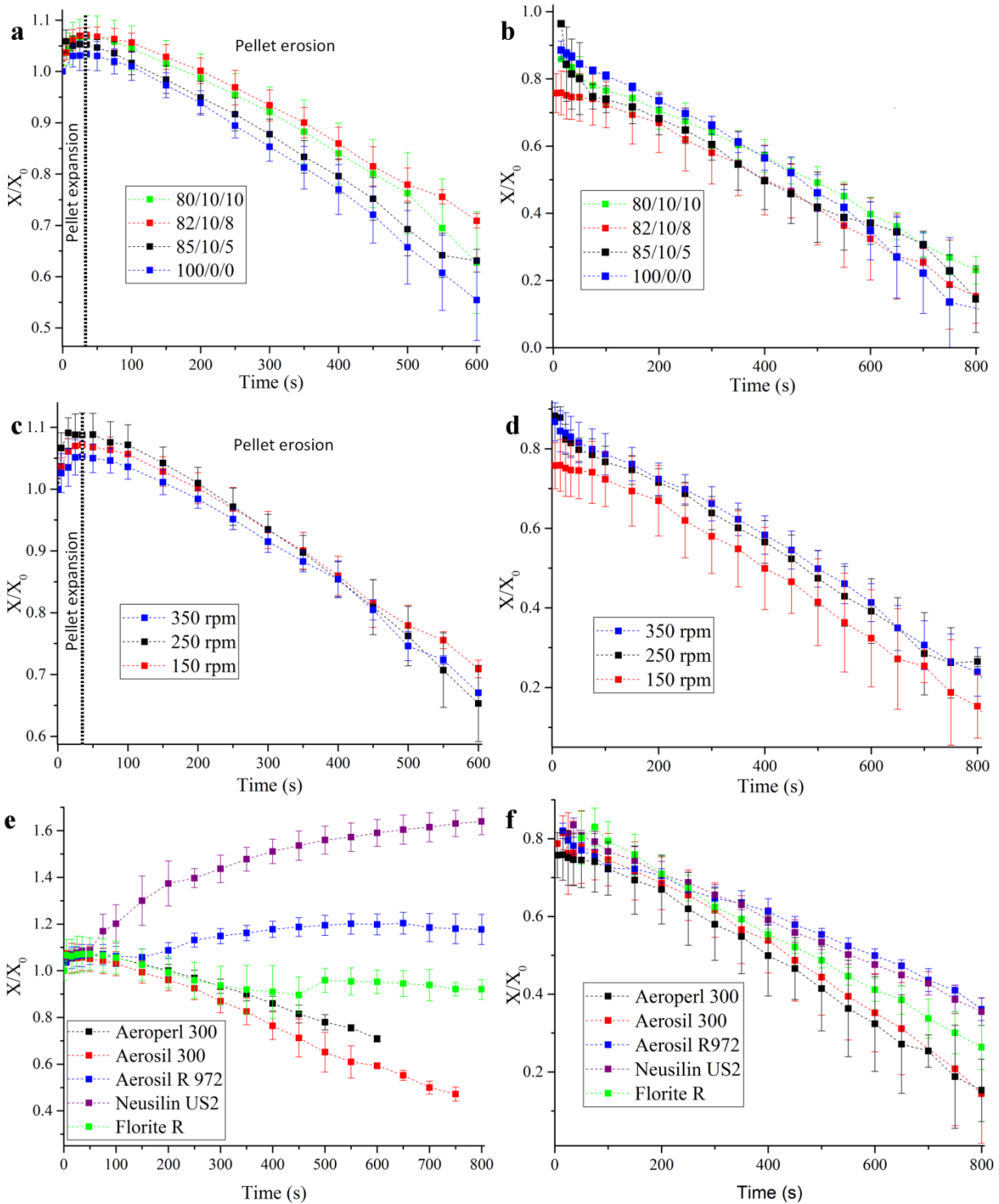


Fig. 5.9. Evolution of erosion (a, c) and swelling (b, d) fronts of pellets containing different Aeroperl 300 concentrations and of pure PVPVA (a, b), of pellets produced with different screw speeds (c, d), and of pellets containing different adsorbents (e, f) over time.

5.6. Conclusion

The aim of this work was to study the microstructure of extrudates pellets containing a lipid and an adsorbent by multifractal analysis and to evaluate their dispersion in aqueous medium. The tested extrudates revealed indeed a multifractal nature and relevant differences were identified. Adsorbent concentration, screw speed as well as physical properties of adsorbents had an effect on the microstructure. Further studies could also be done on the influence of screw design and feed rate, which are important parameters in HME processing. A better understanding of the microstructure is of great interest to a formulator since it can help tailoring the dosage form performance in line with the therapeutic objectives. The use of multifractal dimensions can in the future also help in modeling of such formulations since computational pharmaceutics is a thriving discipline. Any modeling must of course be based on proper understanding of a material structure and the presented multifractal analysis is advancement to this end. Multifractal analysis is a way to assign numbers to a complex microstructure, which can greatly help in microscopy and chemical imaging of pharmaceutical systems. The use of multifractal analysis in pharmaceutical technology is a new strategy so a traditional formulation and process development approach was only to study effects on the quality attributes, while the microstructure remained either unknown or it was not analyzed on a quantitative basis. The presented multifractal analysis may reveal changes in the microstructure even before the quality attributes are measured, which could even help beyond the development phase to assure a robust manufacturing. While multifractal analysis provided a morphological view on the system, the analysis of self-dispersion in water is a basic test for how components dynamically interact regarding any later-stage drug dissolution process. Interesting findings were made with respect to the interaction of more lipophilic adsorbents with lipids that should be considered for the development of pharmaceutical formulations. Such development should in the future not just be based on correlations of compositions/process parameters with quality attributes but a thorough characterization and understanding of the excipients and their microstructure should guide the way to a more efficient and robust pharmaceutical product development. The combination of multifractal analysis, and self-dispersion and erosion studies gave interesting results, which could further be used to formulate poorly water-soluble compounds of different natures, e.g. lipophilic, acidic, low molecular weight.

Appendix B

SEM pictures of the used adsorbent powders are presented in this Appendix B to illustrate their physical variety.

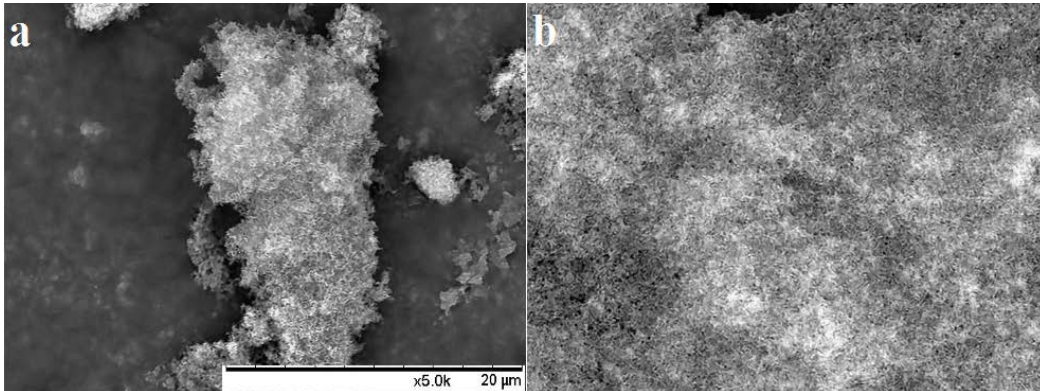


Fig. 5.10. SEM pictures of fumed Aerosil 300 (a), and Aerosil R 972 (b). Aerosil fumed silicates are very fine powders composed of aggregated and agglomerated primary particles. Primary particles could not be identified due to their very small size (< 50 nm)

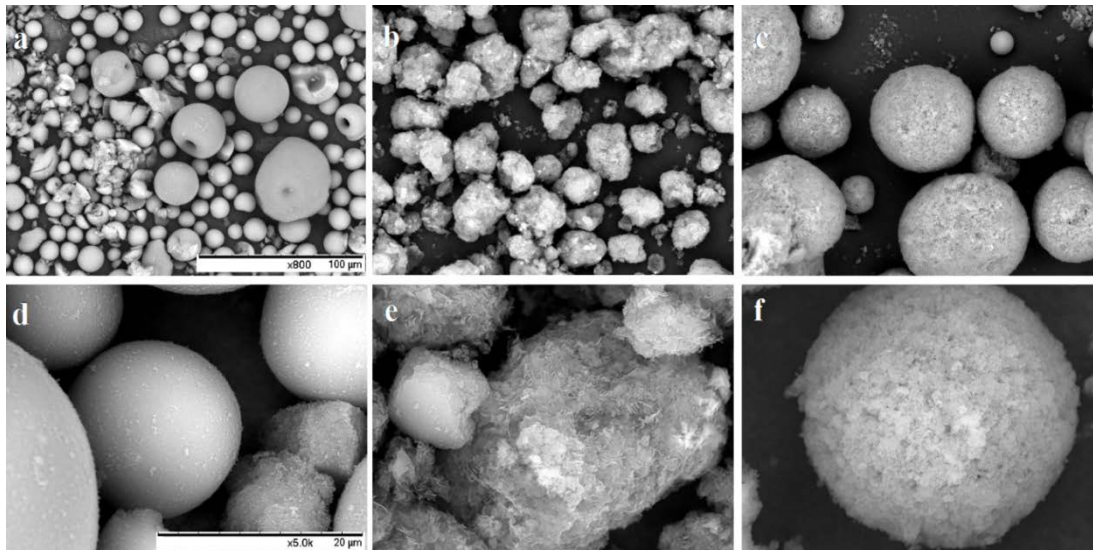


Fig. 5.11. SEM pictures of Aeroperl 300 (a, d), Florite R (b, e), and Neusilin US2 (c, f). Aeroperl 300 spherical granules have a rather smooth surface. Florite R particles exhibit irregular shape while the pore structure can be viewed as petaloid. Finally, the spherical Neusilin US2 particles display some porosity on their surface compared to Aeroperl 300.

Chapter 6

Multifractal and mechanical analysis of amorphous solid dispersions

Summary

The formulation of lipophilic and hydrophobic compounds is a challenge for pharmaceutical industries and it requires the development of complex formulations. Our first aim was to investigate hot-melt extrudates microstructure by means of multifractal analysis using scanning electron microscopy imaging. Since the microstructure can affect solid dosage form performance such as mechanical properties, a second objective was to study the influence of the type of adsorbent and of the presence of an amorphous compound on extrudate hardness. β -carotene (BC) was chosen as poorly water-soluble model compound. Formulations containing a polymer, a lipid and two different silica-based inorganic carriers were produced by hot-melt extrusion. Based on scanning electron microscopy/energy dispersive X-ray spectroscopy, the obtained images were analyzed using multifractal formalism. The breaking force of the strands was assessed by a three point bending test. Multifractal analysis and three point bending results showed that the nature of interparticle interactions in the inorganic carrier as well as the presence of amorphous BC had an influence on the microstructure and thus on the mechanical performance. The use of multifractal analysis and the study of the mechanical properties were complementary to better characterize and understand complex formulations obtained by hot-melt extrusion.

6.1. Introduction

More than 40% of newly developed chemical entities are poorly water-soluble, which often implies erratic absorption and a reduced oral bioavailability [66]. Some compounds exhibit limited water solubility because of solvation limitation as they are highly lipophilic, while other drugs are hydrophobic based on comparatively high crystal energy [181]. Particularly challenging are drugs that combine both lipophilicity and hydrophobicity, which requires special formulation strategies. One of the most successful oral formulation approaches of poorly-water soluble drugs is the solid dispersion (SD) technique [6]. It corresponds to the dispersion of an active compound in a solid matrix that is generally composed of a polymer and excipients. The most preferred type is here the amorphous SD, where the drug is dispersed either in an amorphous state or at a molecular level in an amorphous carrier. Among the additives that can be used, lipid excipients can be a key for the formulation of lipophilic compounds. Lipid excipients have been introduced in amorphous SD formulations by Serajuddin et al. [6] in the 1990's to overcome limitations encountered in systems using polymeric carriers only. Indeed, lipids can prevent drug recrystallization in the matrix and can be of further biopharmaceutical benefit. Such additives can increase drug solubilization upon aqueous dispersion and may circumvent precipitation, while another mechanism is an optional enhancement of membrane permeability [66,67]. Moreover, lipids have a low physiological toxicity, offer a wide range of physico-chemical properties and are inexpensive [69].

In this study, β -carotene (BC), also known as provitamin A, was selected as model compound that is lipophilic as well as hydrophobic. In a previous work, we already demonstrated that a specific combination of a polymer, a solid lipid and an inorganic adsorbent provided an amorphous SD of low-dose BC by hot-melt extrusion (HME) [16]. The key to success of this formulation strategy was the creation of designed lipid microdomains (DLM). This DLM delivery system is a molecularly designed formulation that tailors specific interactions between a solid fatty acid and an inorganic carrier. While the DLM formulation uses lipid in solid form, also liquid excipients could be of interest as direct solubilizer and polymer plasticizer. It was already reported that SD based on polymeric carriers have the tendency to be sticky and an intuitive expectation suggests that addition of a liquid lipid excipient may increase this undesired effect leading to difficulties of handling [35]. Therefore, the use of inorganic carriers with good oil adsorption capacity and that are already employed for the conversion of liquid to solid dosage

forms, can be a key to improve polymeric SD quality [182]. The combination of liquid lipid, polymer, and inorganic carrier has already been reported in a previous study [104]. The focus was on the influence of processing parameters and type of adsorbents on the microstructure of HME extrudates by introduction of multifractal analysis. Multifractals provide a powerful mathematical model to describe complex structures that cannot be described by the Euclidean geometry. Multifractals correspond to the superposition of homogeneous fractal objects that are characterized by their self-similarity or invariance under scale of magnification [156,183]. Fractal geometry has largely profited from the evolution of image analysis [157–159]. Optical microscopy, electron microscopy, atomic force microscopy, or confocal Raman spectroscopy are methods that provide morphological, structural or compositional information [162]. Fractals and multifractals of such imaging methods data are of particular interest for a better understanding of object microstructure, when a link to a mathematical dimension (or a set of dimensions) is possible. Multifractal analysis has been previously used mostly in food applications or in geosciences [159,169]. In the field of pharmaceuticals, the single fractal formalism has been applied to numerous applications such as drug dissolution and release [100,163,184,185] pharmacokinetics [186], pharmacodynamics [187], or surface ruggedness of solids [163]. The multifractal formalism has been introduced only recently [104]. The purpose of the current study is to follow-up on our previous work on HME formulations by comparing microstructural analysis and multifractal analysis with a mechanical property of the extrudates. A first aim is to study microstructures of hot-melt extrudates using a multifractal analysis of scanning electron microscopy (SEM)/energy dispersive X-ray spectroscopy (EDS) images. A polymer and a lipid excipient having solubility parameters close to that of BC were selected, and two types of silica-based adsorbents were chosen. The influence of the type of inorganic excipient and of the presence of amorphous BC on the SD microstructure was assessed. Finally, the breaking strength of the extrudates was measured and results were compared to results and insights gained from the microstructural analysis.

6.2. Materials and methods

6.2.1. Materials

Polyvinylpyrrolidone-vinylacetate (PVPVA; Kollidon VA 64) was purchased from BASF (Ludwigshafen, Germany). Propylene glycol dicaprylocaprate (Labrafac PG) was kindly donated by Gattefossé (Saint-Priest, France). Granulated form of colloidal silicon dioxide (Aeroperl 300 Pharma) was supplied by Evonik Industries (Hanau, Germany). Syloid XDP 3050 (Syloid XDP) was provided by Grace GmbH & Co. KG (Worms, Germany). Crystalline β -carotene (BC) was provided by DSM Nutritional Products Ltd. (Basel, Switzerland). N-hexane (purity 99%), dichloromethane (purity 99.5%), cyclohexane (purity 99.5%), methanol (purity 99.8%), ethanol (purity 99.5%) and acetonitrile (purity 99.9%) were obtained from Merck (Darmstadt, Germany). Butylated hydroxytoluene (purity 99%), tetrahydrofuran (purity 99.5%), N-ethyl-diisopropylamine (purity 98%), 2-propanol (purity 98%) and ammonium acetate (purity 98%) were purchased from Sigma–Aldrich (Steinheim, Germany).

6.2.2. Hot-melt extrusion

Prior to HME, physical mixtures were prepared by weighing and mixing different ratios of PVPVA, Labrafac PG, adsorbent and BC with a spatula. Formulation compositions are presented in Table 6.1. Premixes were manually fed into the hopper of a Thermo Scientific Haake MiniLab II conical, co-rotating, twin-screw microcompounder (Thermo Electron, Karlsruhe, Germany). After one minute of mixing time at 160°C and 150 rpm, the extrudate strand was allowed to exit from a 2 mm diameter die by opening the bypass valve. The extrudates were collected after cooling at ambient temperature. A fraction of the strands was pelletized using a Thermo Scientific Process 11 Variable length pelletizer (Karlsruhe, Germany) for further SEM/EDS analysis. Extrudates strands and pellets were stored in a fridge until analysis.

Table 6.1. Hot-melt extrusion formulations composition

Formulation	Adsorbent	Composition PVPVA/adsorbent/Labrafac PG/BC (%<i>, w/w</i>)
F1 [*]	Aeroperl 300	80/10/10/0
F2	Aeroperl 300	75/10/10/5
F3 ^{**}	Syloid XDP	80/10/10/0
F4	Syloid XDP	75/10/10/5
F5	/	95/0/0/5

^{*} drug-free reference formulation for F2

^{**} drug-free reference formulation for F4

6.2.3. Oil loading capacity

To determine the oil adsorbing capacity of the inorganic materials, we adapted a method from the literature [188]. In brief, 1 g of adsorbent was placed in a beaker and oil was added drop wise until a dry free-flowing paste-like mass was obtained.

6.2.4. BET powder specific surface area

The specific surface area of the two adsorbents was determined by physical adsorption of nitrogen gas using a Micromeritics Gemini V surface area and pore size analyzer (Norcross, USA). Powders were conditioned over night at 105°C in nitrogen prior to analysis. BET values were calculated by the software Gemini v2.00 (Table 6.2).

6.2.5. Mercury porosimetry

Pore analysis of Aeroperl 300 and Syloid XDP was performed by Quantachrome GmbH & Co. KG (LabSPA, Odelzhausen, Germany). Mercury porosimetry was conducted using a Quantachrome Poremaster 60 GT. The two adsorbents were conditioned at 150°C for five hours under vacuum prior to analysis. The Washburn equation was used to calculate pore volume and pore size (Table 6.2).

6.2.6. Differential scanning calorimetry

Thermal events in the extrudate strands and melting point of pure BC were assessed using a TA Instrument Discovery DSC (New Castle, USA). The extrudates strands and pure crystalline BC were accurately weighed ($5.5 \text{ g} \pm 0.5\text{g}$) in 50 μL aluminum pans and hermetically sealed. An empty pan was used as a reference. Samples were heated to 210°C using a heating rate of 20°C/min under a nitrogen flow of 20 mL/min.

6.2.7. X-ray powder diffraction

X-ray powder diffraction (XRPD) patterns were obtained by using a D2 Phaser diffractometer (Bruker AXS GmbH, Karlsruhe, Germany) configured with a fastlinear 1-D Lynxeye detector. The radiation was provided by a 1.8 kWCo KFL tube (wavelength = 1.79 Å) working with a Fe filter. The applied voltage and current were 30 kV and 10 mA, respectively. The powder samples were analyzed at room temperature over the 2θ range of 6–45°. The time per step was 0.6 s and the increment was 0.02° (2θ).

6.2.8. Raman spectroscopy

Raman spectra were collected employing a RamanRXN1 Analyzer (Kaiser Optical Systems Inc., Ann Arbor, MI, USA) equipped with a 785 nm NIR Invictus laser and a non-contact optic 0.4 NIR. Raman data were recorded with a resolution of 4 cm^{-1} using a 400 mW laser power in a spectral range of 100 to 1890 cm^{-1} . For data acquisition and analysis, the software iC Raman Instrument software (v4.1.910, Mettler-Toledo AutoChem Inc., Columbia, MD, USA) was used.

6.2.9. Scanning electron microscopy/energy X-ray dispersive spectroscopy

Extrudate pellets were observed with a Hitachi SEM TM3030 PLUS (Tokyo, Japan). A voltage of 15 kV and 150x magnification were used. EDS analysis was based on a Quantax 70 system (Bruker Nano GmbH, Berlin, Germany) consisting of an X Flash Min SVE signal processing unit, a scan generator and Megalink interface and an X Flash silicon drift detector 410/30H

Bruker Nano GmbH, Berlin, Germany). Samples were scanned during 6 min to map silicon (Si) atoms present in the inorganic materials.

6.2.10. Image processing and multifractal analysis

Prior to multifractal analysis, SEM/EDS pictures were processed using the image manipulation program GIMP (v2.8.14). The images were converted to binary pictures. Fig. 6.1 illustrates the conversion from a SEM/EDS picture (a) to a binary picture (b). The Image J plugin image analysis FracLac was employed to perform the box counting multifractal analysis. The black and white pictures were used and black color was set as background. The number of grid orientations, the maximum box size as % of pixels, and the moment q range were set to 4, 60, and $[-5; 5]$, respectively. Power series of box sizes was selected and box sizes were 2, 4, 16, 64 and 256 pixels. The special scan options “check pixel” and “tighten grid” were chosen. Fig. 6.1c, d show examples of grid sizes used in the box-counting method. Five extrudate pellets were analyzed for each formulation.

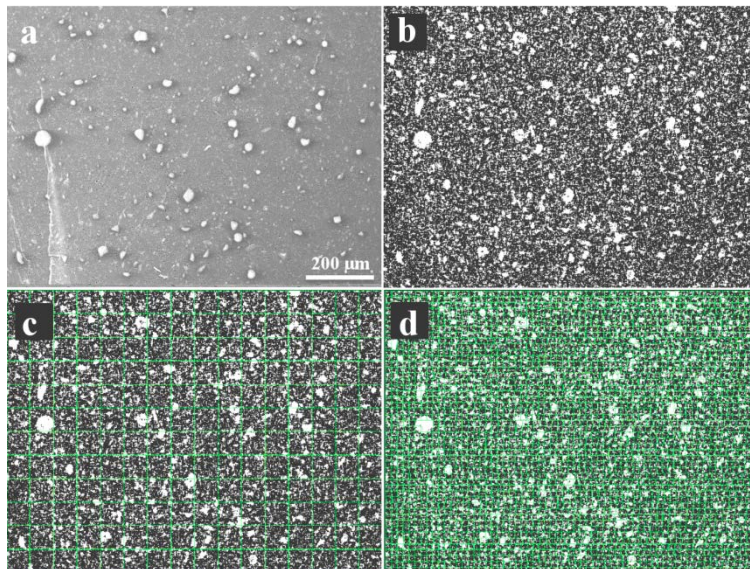


Fig. 6.1. Illustration of the conversion of a SEM/EDS 2-D picture (a) to a binary picture (b) and examples of box sizes used in the box-counting method (c, d). Only boxes containing at least one pixel are counted.

The box-counting method is one of the existing methods that allow for calculation of the fractal dimension using binary two-dimensional images. The approach consists of covering a 2-D image with boxes of sizes ε . The number N of boxes containing at least one pixel of the observed object is recorded and this procedure is repeated with a range of different box sizes [99]. The monofractal dimension D_0 is calculated from the following equation:

$$D_0 = \lim_{\varepsilon \rightarrow 0} \frac{\log N(\varepsilon)}{\log \frac{1}{\varepsilon}} \quad (6.1)$$

However, for the description of more complex structures, multifractal analysis can be used. Multifractal is an extension of fractal analysis, which decomposes self-similar measures into intertwined fractal sets that are characterized by their singularity strength and fractal dimension [157,159,169]. Multifractals can therefore be described as a superposition of homogeneous fractal objects and are characterized by a sequence of generalized fractal dimensions [159,183]. In multifractal analysis, the probability P_i of finding the object pixel in the i^{th} box is determined by:

$$P_i(\varepsilon) \sim \varepsilon^{\alpha_i} \quad (6.2)$$

with α_i Lipschitz-Hölder exponent corresponding to the density in the i^{th} box.

The number of boxes $N(\alpha)$ where P_i has singularity strengths between α and $\alpha + d\alpha$ is found to scale as:

$$N(\alpha) \sim \varepsilon^{-f(\alpha)} \quad (6.3)$$

where $f(\alpha)$ is the Hausdorff fractal dimension of the set of boxes with singularities α [169,170].

The box counting method determines the partition function $X(q, \varepsilon)$, which can be considered as the probability to find the object in the i^{th} box for different moments q varying in the $[-\infty; +\infty]$ interval. The partition function is expressed as followed:

$$X(q, \varepsilon) = \sum_{i=1}^{N(\varepsilon)} p_i^q(\varepsilon) \sim \varepsilon^{(q-1)D_q} \quad (6.4)$$

with D_q the generalized dimensions corresponding to the scaling exponents for the q^{th} moment of the measure. D_q is finally defined as:

$$D_q = \frac{1}{1-q} \lim_{\varepsilon \rightarrow 0} \frac{\log \sum_{i=1}^{N(\varepsilon)} p_i^q(\varepsilon)}{\log \varepsilon} \quad (6.5)$$

In the present work D_0 , D_1 and D_2 were of particular interest. D_0 also called capacity dimension, describes how a multifractal system covers the observed domain. D_1 is the information dimension (or Shannon entropy) that characterizes the degree of disorder in a distribution. Finally D_2 , which corresponds to the correlation dimension, indicates the degree of clustering. Higher D_0 , D_1 , and D_2 values indicate higher degree of space coverage, higher disorder and lower clustering level, respectively [171]. Fig. 6.2 depicts the difference between a multi- (F1) and a monofractal spectrum for which $D_2 \leq D_1 \leq D_0$, and $D_2 = D_1 = D_0$, respectively.

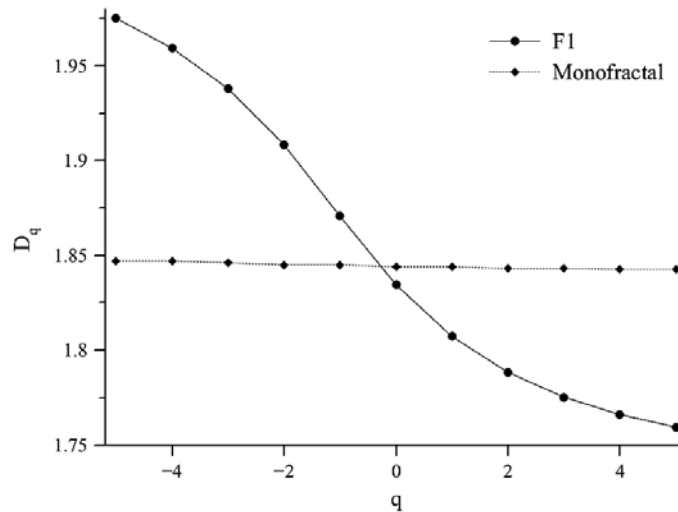


Fig. 6.2. Example of generalized dimensions D_q versus moment q for a multifractal (■) and a monofractal (▲) object.

6.2.11. Three point bending test

The breaking strength of extrudate strands was measured using a Stable Micro Systems TA-XT2i Texture Analyser (Surrey, England) equipped with a thin blade three point bend rig. The strands were cut into 1.5 cm pellets. The distance between the two thin blades was 1.0 cm. Since the thickness of the strands varied over their full length, the diameter was measured using a caliper. A force of 5 kg was employed. Pre-test speed and test speed were set up to 1 and 2 mm/s, respectively. The trigger force was 49 mN. The maximum recorded strength was taken as breaking force for each sample. The breaking strength index (BSI) was calculated using the following formula [189]:

$$BSI = \frac{\text{maximum recorded strength (mN)}}{\text{diameter (mm)}}$$

6.2.12. Reversed phase high-performance liquid chromatography

Reversed phase high-performance liquid chromatography (HPLC) was employed to evaluate BC degradation and cis-trans isomerization that could occur during the HME process. We employed the AOAC official method 2005.07 for analyzing BC in supplements and raw materials, which is based on reversed phase HPLC [138]. The mobile phase consisted of butylated hydroxytoluene (50 mg/L)/2-propanol (2%, v/v)/N-ethyl-diisopropylamine (0.02%, v/v)/0.2% ammonium acetate solution (2.5%, v/v)/acetonitrile (45.5%, v/v)/methanol (45.0%, v/v). BC was extracted from the SDs using butylated hydroxytoluene (100 mg/L)/water (6%, v/v)/ethanol (40%, v/v)/dichloromethane (54%, v/v).

6.3. Results and discussion

6.3.1. Characterization of BC physical state

The challenging physico-chemical properties of BC make it hard to obtain comparatively simple amorphous systems and more complex quaternary SDs have been identified recently as a

promising formulation principle [16]. An initial goal of the current work was therefore to produce BC amorphous SDs by combining a lipid, an adsorbent and a polymer. The lipid and polymer were selected according to their Hansen solubility parameters to ensure good miscibility during HME process. BC is a lipophilic compound with high melting point, thus the use of conventional polymeric formulations can be a challenge. There are only few polymers that have a solubility parameter close to the one of BC that is $17.5 \text{ MPa}^{1/2}$ (as estimated by Molecular Modeling Pro v6.2.6; Norgwyn Montgomery Software, USA). Greenhalgh et al. (1999), recommended that excipients should be selected so that the difference between excipient and compound solubility parameters is below $7 \text{ MPa}^{1/2}$. According to this rule, excipients having a solubility parameter between 10.5 and $24.5 \text{ MPa}^{1/2}$ are good candidates for BC formulation. Therefore, PVPVA and Labrafac PG, which have Hansen solubility parameters of 19.9 and $20.4 \text{ MPa}^{1/2}$, were selected.

In a first step, a formulation composed of 5% (w/w) BC and PVPVA alone (F5) was produced at 160°C and 150 rpm. The physical state of BC in the strands was initially evaluated by XRPD and DSC as classical characterization methods for SDs. Fig. 6.3 shows the XRPD diffractogram (a) and DSC thermogram (b) of F5. Even though the solubility parameter of PVPVA was expected to suggest miscibility of the excipient with BC according to the Greenhalgh et al. rule, the polymer alone did not enable converting BC in an amorphous state. Indeed, BC crystalline peaks (17 , 18 , 19.5 , 22 , 25.5 , 27.1 and 28.8° (2θ)) could still be observed in the extrudate diffractogram (Fig. 6.3a). This result was supported by the presence of BC melting point above 180°C in the DSC thermogram (Fig. 6.3b). A likely factor was the extrusion temperature that was below the BC melting point. An extrusion temperature above the BC melting point was avoided as it may result in a rapid, undesired isomerization and even degradation of BC. In a second step, a formulation composed of 85/10/5% (w/w) PVPVA/Labrafac PG/BC was produced but the resulting strand was oily and could therefore not be further analyzed. This observation confirmed the usefulness of adding an inorganic carrier to adsorb the excess of oil. Thus, two different adsorbents were evaluated, i.e. Aeroperl 300 and Syloid XDP. Table 6.2 summarizes the main physico-chemical properties of the two inorganic excipients. They have similar characteristics (e.g. chemical composition, pore volume, oil loading capacity), but differ in their manufacturing process. Aeroperl 300 is a granulated silica produced by a mechanical process, i.e. granulation of the fumed silica Aerosil 300; and Syloid XDP is a silica aerogel produced by a chemical process proprietary by Grace (Evonik Industries, 2013, Grace, 2015). Formulations F2 and F4 (Table 6.1) composed of 75/10/10/5% (w/w) PVPVA/Labrafac PG/adsorbent/BC were produced. They were

not oily and as shown in Fig. 6.3, no BC crystalline peak or melting point was visible. The combination of polymer/lipid and adsorbent obviously enabled amorphous SDs regardless of the adsorbent used.

Table 6.2. Physico-chemical properties of adsorbents

	Aeroperl 300	Syloid XDP
Type of silica	granulated form of colloidal silicon	silica aerogel
Manufacturing process	granulation of fumed silica particles	chemical process *
Particle shape **	spherical	irregular
Average particle size (laser diffraction; μm)	20-40 ^[1]	48-66 ^[2]
BET (N ₂) surface area (m ² /g)	263 \pm 1	300
Oil loading capacity (Labrafac PG; g/100g) ***	173 \pm 3	160 \pm 3
Pore structure	meso- and macropores	highly developed network of mesopores
Total pore volume (cm ³ /g) ****	1.65	1.66
Median large pore diameter (nm) ****	67.2	34.6
Median small pore diameter (nm) ****	15.7	8.1

* Proprietary by Grace

** Appendix C: Fig. 6.10

*** Maximum oil loading that still led to a dry free flowing powder (visual assessment)

**** Measured by Mercury intrusion porosimetry

[1] [44]

[2] [45]

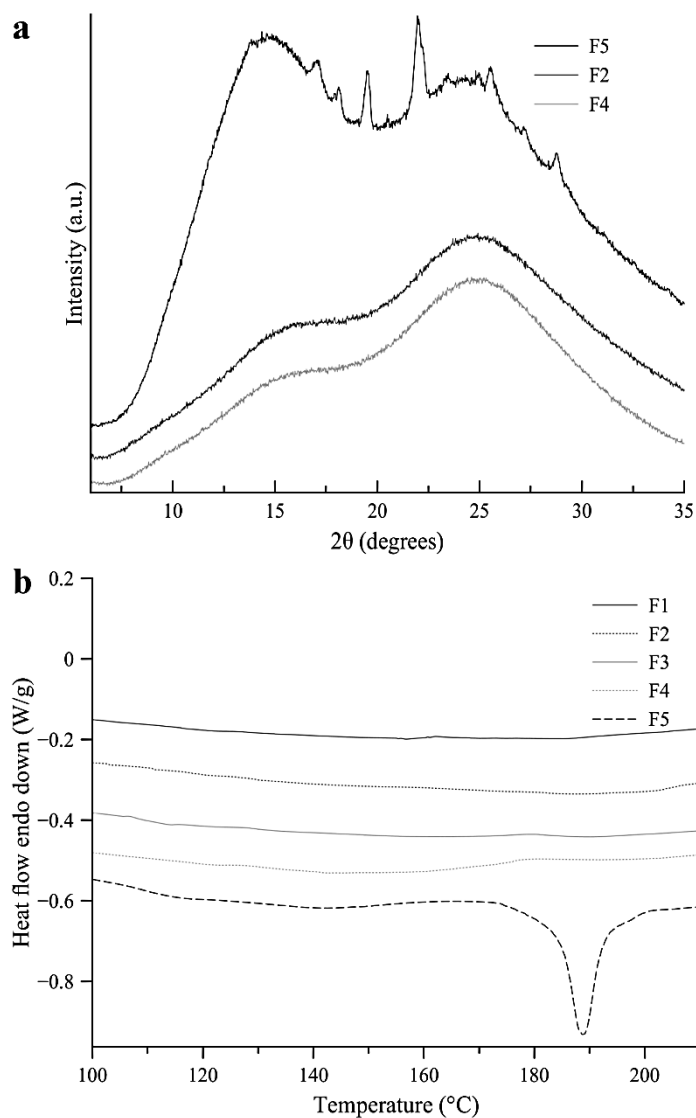


Fig. 6.3. XRPD diffractograms (a) and DSC thermograms (b) of extrudate formulations

BC is a non-polar molecule, Raman spectroscopy was therefore employed to assess the changes in BC vibrational spectrum according to its physical state in the extrudates. As shown by Pudney et al. (2011) and Lopez-Sanchez et al. (2011), changes affecting BC spectrum can be assigned to a solvated state of BC. Accordingly, they observed the same shift to higher frequency of the C=C stretch vibration band (around 1520 cm^{-1}) and found an increase in intensity of a band around 960 cm^{-1} (C-H out of plane wagging and C=C torsion), when BC was solvated in a lipid phase or dissolved in chloroform. In the present case, XRPD and DSC results showed that BC was

amorphous in F2 and F4 but still crystalline in F5. Therefore, changes should be seen in the Raman spectra of F2 and F4, whereas F5 spectra should be comparable to pure crystalline BC. Moreover, in order to study the influence of BC solubilization in Labrafac PG, BC was solubilized in the pure oil and the filtered solution was assessed by Raman spectroscopy. Fig. 6.4 shows the Raman spectra of the extrudates, of pure crystalline BC powder and of BC solubilized in Labrafac PG. Changes in the above-mentioned regions could effectively be observed in the amorphous SDs and BC/Labrafac PG solution compared to crystalline BC. Pure crystalline BC exhibited a band around 1514 cm^{-1} , whereas for F2, F4 and BC solution, this band was shifted to $1525\text{-}1526\text{ cm}^{-1}$ (Fig. 6.4a). A shift to higher frequency and broadening of the C=C stretch band can be assigned to the more relaxed conformation of BC when it is in a non-crystalline state, (i.e. in solution or amorphous) [191,192]. The second observation was an increase in the band intensity at around 960 cm^{-1} (Fig. 6.4b). The presence of a broad band in this region could also be observed in BC solution, whereas it was barely visible in F5 and for pure crystalline BC. Moreover, a smoothing of the bands between $850\text{ and }900\text{ cm}^{-1}$ (Fig. 6.4b), assigned to C-H out of plane wagging [193], could be observed in non-crystalline samples. All the changes seen in the Raman spectra of F2, F4, and BC in Labrafac PG confirmed an altered physical state of BC and suggest that interactions occurred between BC and the excipients to stabilize amorphous BC. Similarly to most of the unsaturated carotenoids, BC is prone to isomerization and oxidation. Light, oxygen and temperature are factors that can cause BC degradation [194]. Even though BC chemical stability was not within the scope of this study, it would be relevant to know if HME processing caused significant BC degradation. A chemical analysis was conducted using reversed phase HPLC analysis, which showed that BC recovery was $> 85\%$ in F2 and F4, and that no degradation occurred in F5. This confirmed that the absence of BC crystalline peaks in DSC and XRPD analysis indeed suggested an amorphous form and the analytical results were not influenced by BC degradation. Moreover, isomerization from trans- to cis-isomer was also assessed to verify that changes in Raman spectra of amorphous SDs were not due to BC isomerization. F2, F4 and F5 exhibited similar trans- to cis-isomerization (i.e. 40%) but F2 and F4 had similar Raman spectra, that were different from F5 spectra (Fig. 6.4). It can therefore be concluded that the chemical degradation was not responsible for band shifts, band broadening, or increase in band intensity. Finally, absence of BC isomerization in Labrafac PG solution and similarities observed with F2 and F4 Raman spectra demonstrated that the observed spectral changes were as expected caused by the physical state of BC that was interacting with the matrix.

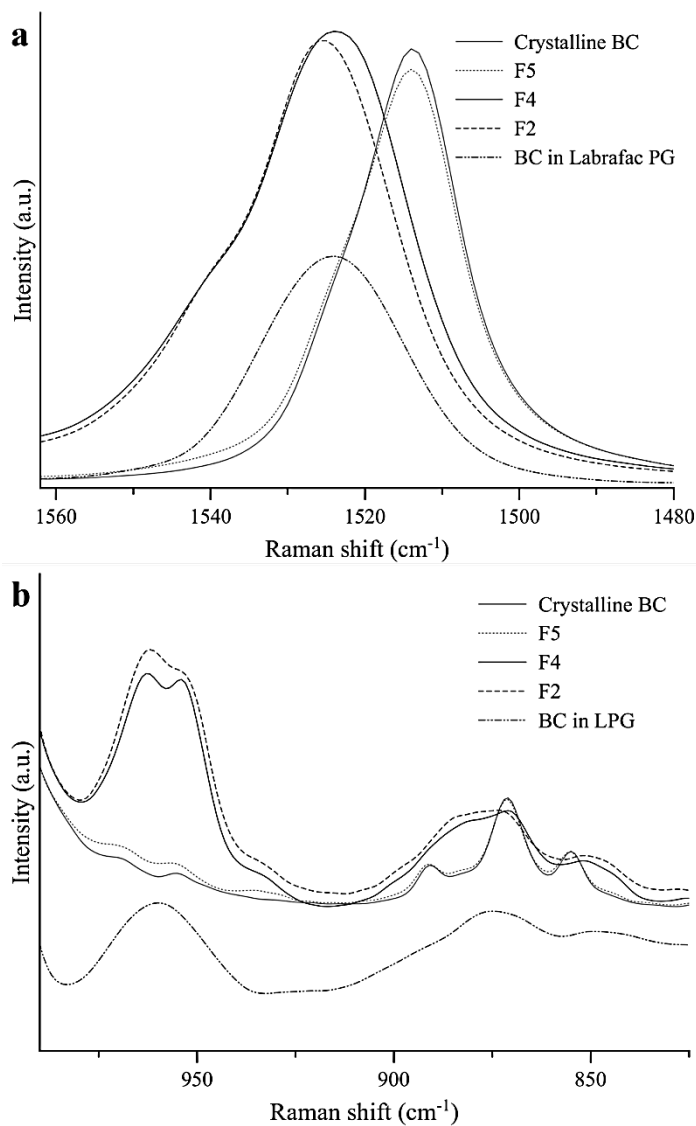


Fig. 6.4. Raman spectra of pure crystalline BC, extrudate strands and of BC dispersed in Labrafac PG in the 1500 cm⁻¹ (a) and in the 900 cm⁻¹ (b) regions.

The study of changes in PVPVA glass transition temperature (T_g) by DSC also suggested formation of interactions between BC and the matrix. Indeed, PVPVA had a T_g of 90°C that decreased to 74°C in the placebo samples F1 and F3. This was due to a plasticization effect of the oil/adsorbent mixtures. In presence of BC (F2 and F4), the T_g increased slightly to 78°C. Previous studies have demonstrated that an increase in polymer T_g can be due to an antiplasticization effect resulting from bonding between the polymer and other excipients or drugs, or it may be due to steric hindrance of the polymer chains [195].

All the analytical techniques used to assess BC physical state were in agreement and confirmed that BC amorphous SD could be obtained by using a rather complex formulation composed of oil, polymer and adsorbents.

6.3.2. Understanding the microstructure of hot-melt extrudates

6.3.2.1. Multifractal analysis of placebo extrudates

The key to success for obtaining the two amorphous BC SDs F2 and F4 was obviously to develop multicomponent formulations. Prior to SD analysis with BC, the placebo formulations were studied to understand the influence of the type of adsorbent on the microstructure. HME is a thermo-mechanical process, for which good excipient mixing results from the shear applied by two co-rotating screws. The applied shear as well as the nature of the excipients can therefore influence the formulation microstructure. In the present work, the extrudates differed in the type of adsorbents used. Aeroperl 300 and Syloid XDP were selected since they have similar physico-chemical properties (Table 6.2) but are produced by two different processes. Aeroperl 300 is manufactured by a mechanical process (i.e. granulation of Aerosil 300), whereas Syloid XDP is produced by a proprietary chemical reaction. These two manufacturing ways are expected to influence the type of interparticle interactions. Indeed, primary particles constituting of granulated silica-based adsorbent are stabilized by weak interactions (e.g., Van der Waals, H-bonds). In contrast, covalent bonds result in the structure of mesoporous silica-based adsorbent that are produced by a chemical reaction. As mentioned by Bumm, and Adler et al. [104,174], the screw speed can have an influence on particle breakage and thus on the final formulation microstructure. While exposed to shear stress, silica agglomerates can be partially destroyed and may return to their primary aggregated form [175]. Provided that weak interactions primarily exist in agglomerated silica particles, an intuitive expectation is that the shear during extrusion would have rather influenced the Aeroperl 300 formulation than the Syloid XDP system.

Fig. 6.5a, b depict F1 an F3 pellet cross sections observed by SEM and the corresponding EDS 2D-binary pictures (Fig. 6.5c, d). These systems exhibited a rather complex structure. Indeed, protruding silica particles could be seen on the SEM pictures (Fig. 6.5a, b) as well as on EDS pictures but with numerous other rather small entities (Fig. 6.5c, d). A quantitative differentiation

of the two placebo samples was therefore challenging based on simple image comparison. The recently introduced multifractal formalism in pharmaceuticals was here promising to distinguish formulation microstructures by means of the generalized dimensions D_0 , D_1 and D_2 [104].

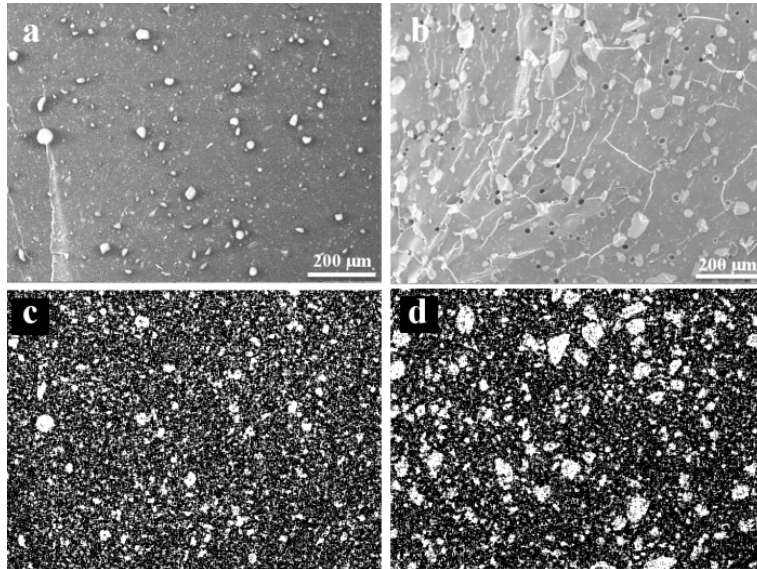


Fig. 6.5. SEM (a, b) and corresponding EDS 2-D binary pictures (c, d) of F1 (a, c) and F3 (b, d) formulations.

Accordingly, F1 and F3 were analyzed and thereby it was possible to assign numbers (i.e. dimensions) that could describe formulation or process effects on the microstructure. As a result, multifractal analysis confirmed that the type of adsorbent had an effect on the extrudate microstructure. Fig. 6.1 presents the generalized dimension Dq versus the moment q of F1 and results suggest that the formulation can be much better described as multifractal compared to a model assuming a single fractal dimension. This can be concluded since Dq clearly decreased while q increased and F2 exhibited the same behavior (data not shown). A zoom in D_0 , D_1 and D_2 multifractal region of F1 and F3 is depicted by Fig. 6.6. F1 exhibited higher generalized dimensions than F3, which corresponded to a higher space coverage (D_0), higher heterogeneity (D_1), and lower clustering level (D_2), respectively. This was in agreement with the assumption that Aeroperl 300 agglomerates were more prone to particle breakage than Syloid XDP particles.

This was hence likely to result in higher space coverage of Si atoms due to the presence of numerous smaller particles, as well as lower homogeneity and lower clustering level.

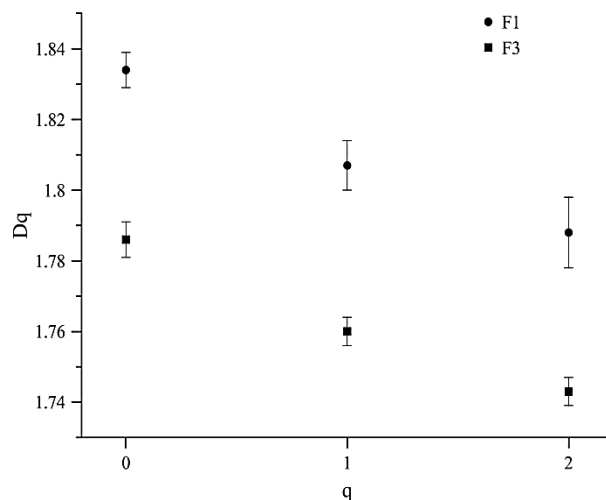


Fig. 6.6. Generalized multifractal dimensions Dq over the $[0,2]$ moment q range of formulations F1(●) and F3 (■).

The multifractal analysis provided a tool to assign numbers to the microstructure of the placebo extrudates and thereby enabled a better understanding of adsorbent effects. The differences observed in the microstructure were mainly due to the different types and strength of interparticle interactions. The use of multifractal could be of particular interest for scientists in formulation process research, since it could be used to study the impact of process parameters on different types of excipients to achieve a final dosage form of desired quality attributes.

6.3.2.2. Multifractal analysis of BC extrudates

Since BC amorphous SDs could be obtained by using both adsorbents, the second aim of the multifractal analysis was to assess the influence of BC on the microstructure.

SEM/EDS 2D-pictures of the two BC amorphous SDs (F2 and F4) pellet cross sections are shown in Fig. 6.7. The protruding inorganic particles that were previously visible in F1 and F3

(Fig. 6.5a, b) could not be so easily detected, most probably because of the presence of BC that might have been adsorbed (alone or in combination with Labrafac PG) to the inorganic excipient.

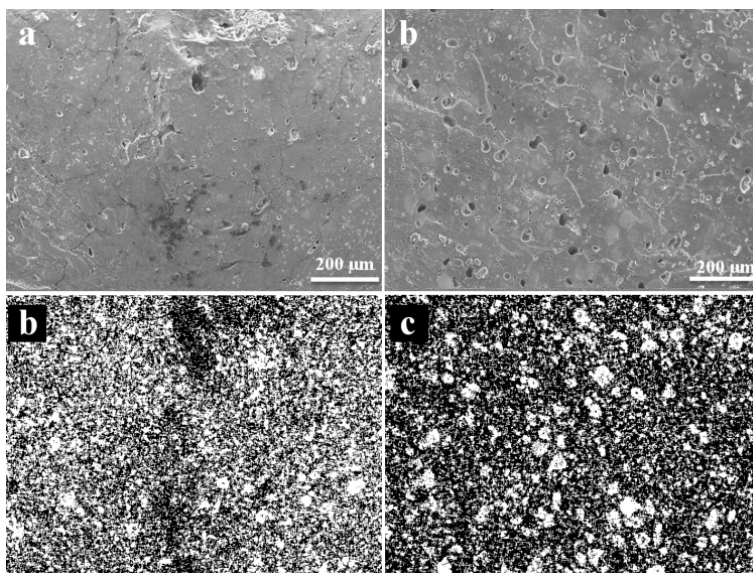


Fig. 6.7. SEM (a, b) and corresponding EDS 2-D binary pictures (c, d) of F2 (a, c) and F4 (b, d) formulations.

Multifractal analysis was again conducted to study the pellets microstructure. As shown in Fig. 6.8, the presence of BC exhibited a tendency towards higher capacity, D_0 , information, D_1 , and correlation, D_2 , dimensions. These findings showed that BC probably disturbed the overall mixing of silica particles, which resulted in the perturbation of adsorbent distribution and thus changes in the microstructure. As shown by Raman and DSC analyses, interactions between BC and the matrix were created during HME, which probably led to the observed changes in the microstructure. Moreover, both adsorbents had a porous structure, it is likely that BC could penetrate in the pores or be adsorbed on the adsorbent surfaces, which would have perturbed interactions of particles.

DSC and XRPD analyses could not detect any difference between F1/F3 or between F2/F4, whereas multifractal analysis suggested differences in their microstructure. Indeed, the multifractal analysis of placebo and BC extrudates demonstrated that both the type of adsorbent

and the presence of the active compound had an influence on the microstructure. The microstructure in turn can affect quality attributes of intermediate or final dosage forms. The use of inorganic particles can especially modify the mechanical properties of polymeric composite matrices so that hardness of extrudate strands was studied in particular.

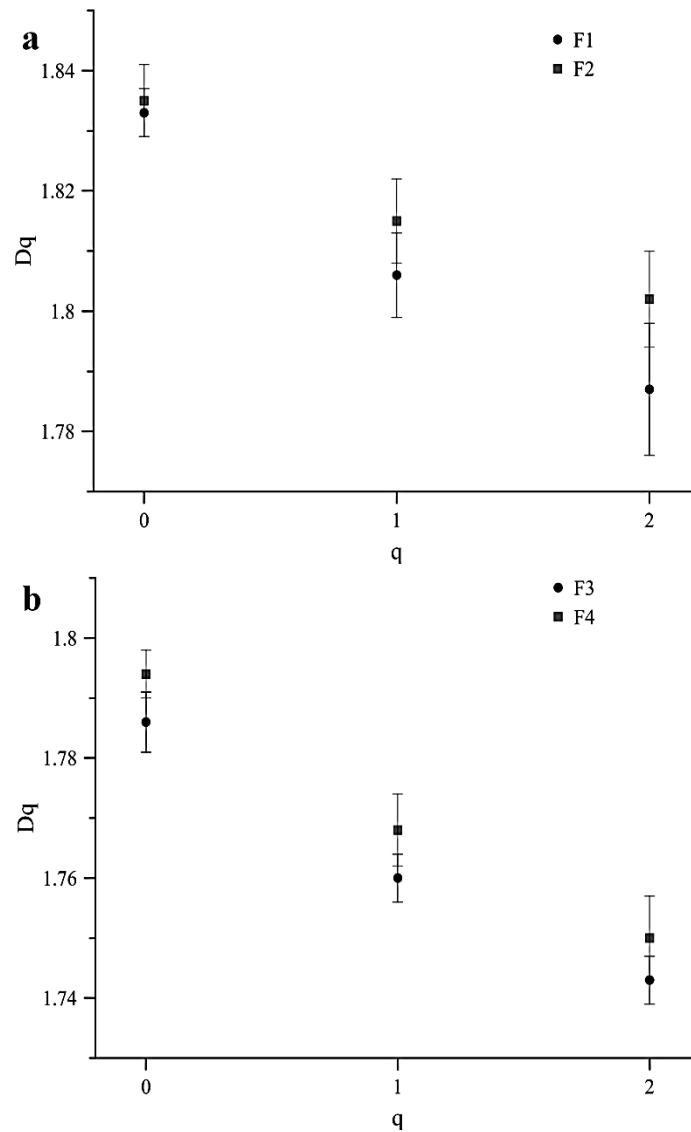


Fig. 6.8. Generalized multifractal dimensions Dq over the $[0,2]$ moment q range of formulations F1(■), F2 (■), F3 (●), and F4 (●).

6.3.3. Mechanical properties of hot-melt extrudates

The addition of inorganic excipients in a polymeric matrix is used in the field of composites and nanocomposites to reinforce or to modify the mechanical properties of polymers [196,197]. Thermoplastic polymers have generally poor mechanical properties, therefore inorganic particles can be added to provide higher strength. In the present case, the purpose of adding silica-based excipients in hot-melt extrudates was not to primarily modify the mechanical properties of the strands but to improve the premix powder flow and to adsorb an excess of oily components. However, since mechanical properties of polymer loaded with inorganic excipients are highly influenced by their microstructure [198] and since multifractal analysis revealed differences in the strand microstructure, it was of interest to study a mechanical property of the four HME formulations.

Three point bending was carried out by using a texture analyzer. The maximum force was recorded that corresponded to the extrudate bending point. Since variations in strand diameter were observed, the recorded peak breaking force was normalized by the strand diameter at the point of breakage for a relative data comparison. This value allowed the evaluation of strand hardness and was named BSI [189]. The strand composed of the pure polymer and F5 had very irregular shapes and therefore could not be analyzed with the texture analyzer. BSI values of F1-4 are presented in Fig. 6.9. Firstly, it occurs that F1 had higher BSI than F3. Accordingly, the formulation containing Aeroperl 300 was harder and needed higher force to break. Multifractal analysis showed that F1 exhibited higher space coverage and lower degree of clustering due to particle breakage compared to F3. As reported by Fu et al. (2008), particle size and loading may have an effect on material strength. Smaller particles result in higher strength and a higher particle loading also leads to enhanced mechanical properties. Aeroperl 300 sample exhibited a higher space coverage of Si atoms compared to Syloid XDP formulation. Higher space coverage provided more mechanical resistance and therefore is in line with the higher BSI value observed for F1. Besides particle size and loading, the particle shape can also play a role in the matrix strength. Oréface et al. (2001) observed that spherically shaped particles led to higher toughness than particles having a high aspect ratio (i.e. relation between width and height). Syloid XDP is composed of irregularly shaped particles (aspect ratio > 1), whereas Aeroperl 300 particles are spherical (aspect ratio = 1; cf. Appendix C: Fig. 6.10). They explained this effect by the susceptibility of irregular particles to induce cracks, which was in agreement with the lower BSI

value found for F3. Such cracks were previously observed in strands following pelletization, (e.g. Fig. 6.5b). Thus, comparing the multifractal data and the mechanical properties, it can be concluded that interactions of particles, their clustering as well as their shape were likely to explain the differences observed in BSI values for F1 and F3.

In a second step, the BSI of BC SDs was recorded. Both SDs exhibited higher BSI values than the corresponding placebo formulations. As highlighted by the multifractal analysis, BC might have helped in the overall silica particles mixing and grinding during HME since higher space coverage and lower degree of clustering were observed. Moreover, Raman spectroscopy and DSC analysis showed that BC was interacting with the matrix in F2 and F4. An enhancement of polymeric matrix strength has in a previous study been attributed to interactions with an excipient [199,200]. Such interactions appear to more generally reinforce the matrix mechanical properties, which leads to a higher strand hardness.

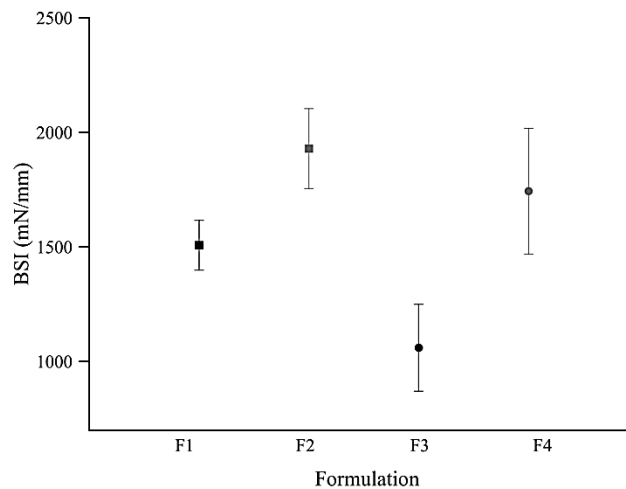


Fig. 6.9. . Breaking force index of extrudate formulations containing Aeroperl 300 (●) and Syloid XDP (■) obtained by three point bending test. F1-4 are coded according to Table 6.1.

From the three point bending test, it could be concluded that not only the microstructure (due to the inorganic carrier) but also the presence of BC/matrix interactions defined the SDs mechanical properties. The two methods were therefore complementary to understand the effect of the adsorbents and BC on the microstructure and the hardness of the extrudate strands.

6.4. Conclusion

The purpose of this study was to use multifractal analysis to better understand effects on the microstructure of hot-melt extrudates. Knowledge of the microstructure is of great interest for formulators since it can help to tailor the final dosage form according to desired product quality attributes. Multifractal analysis is here a powerful tool that allows assigning numbers to complex formulation structures. In the present case, microstructural differences were identified according to the type of adsorbent and due to the presence of BC. The shear stress induced by the screws had a more significant impact on granulated silica mixing and grinding than on silica gel. The presence of BC also influenced the overall distribution of silica excipients in the extrudates. The microstructure has usually a significant impact on quality attributes of pharmaceutical systems. Changes occurring within the microstructure could not only influence the final performance of pharmaceutical products, such as stability or drug release, but also impact the performance during downstream processing. Mechanical properties of materials are one of the most important parameter that should be taken into account prior to any downstream process. Since mechanical properties are conditioned by the microstructure, multifractal analysis was complemented by the assessment of the mechanical properties of the extrudate strands. Interesting correlations were observed and allow better understanding the impact of adsorbents and presence of an amorphous compound on the microstructure and the mechanical properties. The combination of both methods could further be used in the development of pharmaceutical products for which mechanical properties are of great interest, e.g. tablets or films. Future studies may extend the scope of microstructural analysis to elucidate effects on drug release.

Appendix C

SEM pictures of the pure adsorbent powders are presented in this Appendix C to illustrate their particle shape.

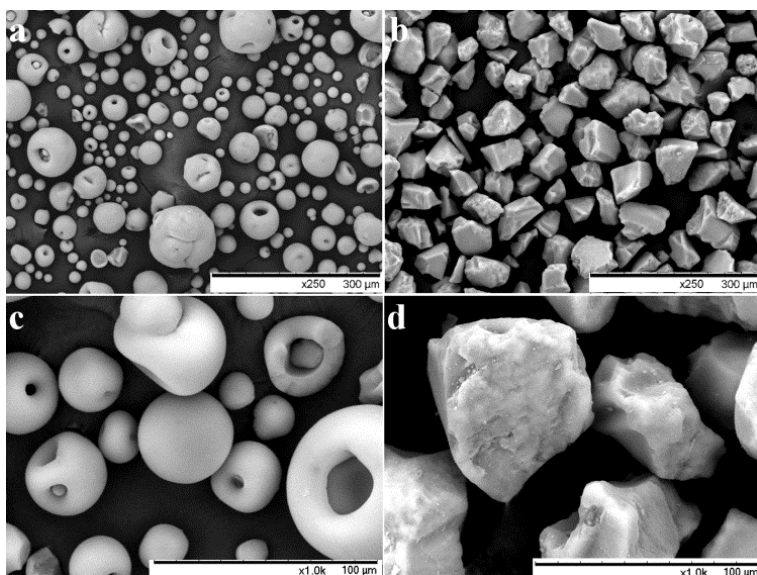


Fig. 6.10. SEM pictures of Aeroperl 300 (a, c), and Syloid XDP (b, d). Aeroperl 300 particles are spherical and exhibit a broad size distribution, whereas Syloid XDP particles have an irregular shape with consistent size.

Chapter 7

Final remarks and outlook

The formulation of poorly-water soluble compounds is one of the major challenges that the pharmaceutical industry is facing. Amorphous SD is one the most successful strategies that have been developed for solubility enhancement. However, some compounds require specific formulation considerations and simple polymeric systems usually employed in the development of SDs might be not sufficiently effective. Particularly complex is the formulation of APIs that combine both high crystallinity and lipophilicity. The present thesis focused on the development of new lipid-based types of SDs for such crystalline lipophilic compounds by means of HME. A second aim was to introduce novel analytical tools to better characterize complex solid dosage forms.

Lipid-based materials are potent excipients that can be used for the bioavailability enhancement of BCS class II APIs. Nevertheless, we observed that pure lipid systems could not form an amorphous SD of a primarily highly crystalline lipophilic compound by using a simple melting method. These findings were supported by the use of a novel detection tool. We observed that conventional method exhibited sensitivity limits that could lead to erroneous conclusion about the physical state of an API. Therefore, flow-through cross polarized imaging was introduced and we showed that it was an excellent tool to detect a low-dose crystalline compound in lipid matrices. It provided qualitative and quantitative information concerning the compound crystallinity. This new method has a great potential in the pharmaceutical technology for the detection of few crystalline particles that could lead to physical instability and thus to a likely altered bioavailability.

Simple lipids systems were not suitable for the development of amorphous SDs of a crystalline lipophilic compound, therefore specific excipient combinations were employed in HME process.

We targeted molecular interactions between a solid fatty-acid and an adsorbent in a polymeric matrix to create designed lipid microdomains (DLMs) for amorphous drug delivery. The creation of ion-dipole interactions was supported by FTIR spectroscopy. Additionally DSC, XRPD and AFM analysis showed that the lipid was in a non-crystalline form in the DLM delivery system. By combining analytical results, we concluded that the targeted interactions inhibited the lipid crystallization after HME, which resulted in the creation of disordered microdomains of lipid alkyl chains. The aim of creating DLMs was to generate a new pharmaceutical structure that is particularly suitable for inclusion of a poorly water-soluble compound. As expected, the DLM delivery system resulted in absence of model drug crystallinity, whereas this was not the case for the formulations containing crystalline lipid or polymeric matrix only.

We showed that the combination of a solid fatty acid, an adsorbent, and a polymer was a promising formulation approach for amorphous SD of challenging compounds. Therefore, this strategy was extended to the use of liquid lipids, which could act as polymer plasticizer and could further play the role as solubilizer for a poorly water-soluble compound. We showed that the formulations had complex structures and that a quantitative differentiation was not feasible using conventional visual assessment. Multifractal formalism was therefore introduced. It allowed assigning numbers on extrudates microstructure. Using three generalized multifractal dimensions, D_0 , D_1 and D_2 , we were able to describe the influence of the type of adsorbent, the adsorbent concentration and the screw speed on the microstructure. In a similar study, we also observed microstructural changes due the presence of amorphous API. Such direct quantification of microstructural changes is also of interest outside of the field of oral solid dispersions. It may be applicable to any field in which microstructural changes are expected to affect relevant quality attributes of a product. The present work further studied the self-dispersibility of extrudate products as it is of great importance for drug release. We assessed the erosion/dispersion behavior of the extrudate pellets as an early check in SD development. Even though no significant correlation with the multifractal analysis could be identified, an interesting finding was that the nature of the adsorbent could completely inhibit the pellet erosion and therefore could have an effect on drug release. We also complemented multifractal analysis by mechanical testing and found correlations with the microstructural study. All these methods were complementary and could further be used for a quality assessment of solid dosage forms.

The present thesis introduced a new flow-through technique that has the potential to be further used for lipid or any fluid systems. However, further technical development would be needed for its application to more viscous amorphous systems. This technique could be used in early phase development to anticipate quality failures of pharmaceutical dosage forms, which result from physical instabilities.

This thesis also proposed novel combinations of excipients for the formulation of amorphous SDs. Amorphous SDs are known to improve solubility of poorly-water soluble APIs. In this work the emphasis was on the physical characterization of BC in the extrudates and on a better understanding of complex microstructures. Further research could also address the dissolution of the novel formulations to evaluate to which extent BC solubility is enhanced. Using a conventional dissolution test could be of interest to assess the supersaturated state of BC and to observe a possible precipitation upon dissolution. However, for *in vitro/in vivo* correlation an *in vitro* digestion test would be recommended. BC is in fact highly lipophilic and it was demonstrated that its so-called bioaccessibility is greatly improved only when it is incorporated into mixed micelles [201,202]. Considering the complexity of the newly developed SDs, BC could either be associated with lipid into mixed micelles, be adsorbed onto the adsorbent surface, be associated with the polymer or be in the form of single molecules. A digestion test might therefore determine the bioavailable fraction of BC, which could be subject to a research continuation. The newly developed drug delivery systems could also be used to formulate other pharmaceutical compounds.

In general, this thesis offers interesting and promising formulation strategies for the formulation of crystalline lipophilic compounds. It also provided efficient characterization tools that could be used in the development of drug delivery systems during initial quality assessment as well as for long term stability evaluation.

Bibliography

- [1] R. Tiwari, G. Tiwari, B. Srivastava, A.K. Rai, Solid dispersions: An overview to modify bioavailability of poorly water soluble drugs, *Int. J. PharmTech Res.* 1 (2009) 1338–1349.
- [2] M.S. Ku, Use of the Biopharmaceutical Classification System in early drug development., *AAPS J.* 10 (2008) 208–12.
- [3] S. Bosselmann, R.O. Williams III, Rout- specific challenges in the delivery of poorly water-soluble drugs, in: R.O. Williams III, A. Watts, D.A. Miller (Eds.), *Formul. Poorly Water-Soluble Drugs*, Springer, 2012: pp. 1–26.
- [4] C.L.-N. Vo, C. Park, B.-J. Lee, Current trends and future perspectives of solid dispersions containing poorly water-soluble drugs., *Eur. J. Pharm. Biopharm.* 85 (2013) 799–813.
- [5] S. Janssens, G. Van den Mooter, Review: physical chemistry of solid dispersions., *J. Pharm. Pharmacol.* 61 (2009) 1571–1586.
- [6] A.T.M. Serajuddin, Solid dispersion of poorly water-soluble drugs: Early promises, subsequent problems, and recent breakthroughs, *J. Pharm. Sci.* 88 (1999) 1058–1066.
- [7] T. Vasconcelos, B. Sarmiento, P. Costa, Solid dispersions as strategy to improve oral bioavailability of poor water soluble drugs, *Drug Discov. Today.* 12 (2007) 1068–1075.
- [8] S.R.K. Vaka, M.M. Bommana, D. Desai, J. Djordjevic, W. Phuapradit, N. Shah, Excipients for amorphous solid dispersions, in: N. Shah, H. Sandhu, D.S. Choi, H. Chokshi, A.W. Malick (Eds.), *Amorph. Solid Dispersions Theory Pract.*, Springer, 2014: pp. 123–164.
- [9] M.M. Crowley, F. Zhang, M.A. Repka, S. Thumma, S.B. Upadhye, S. Kumar Battu, et al., Pharmaceutical Applications of Hot-Melt Extrusion: Part I, *Drug Dev. Ind. Pharm.* 33 (2007) 909–926.
- [10] C. Leuner, J. Dressman, Improving drug solubility for oral delivery using solid dispersions., *Eur. J. Pharm. Biopharm.* 50 (2000) 47–60.
- [11] A. Almeida, B. Claeys, J.P. Remon, C. Vervaet, Hot-melt extrusion developments in the pharmaceutical industry, in: D. Douroumis (Ed.), *Hot-Melt Extrus. Pharm. Appl.*, John Wiley & Sons, Ltd., 2012: pp. 43–69.
- [12] K. Kolter, M. Karl, A. Gryczke, Hot-melt extrusion with BASF Pharma polymers *Extrusion Compendium 2nd revised and enlarged edition*, 2012.
- [13] S. Ali, K. Kolter, Challenges and opportunities in oral formulation development, *Am.*

- Pharm. Rev. 15 (2012).
- [14] J.C. DiNunzio, D.A. Miller, Formulation development of amorphous solid dispersions prepared by melt extrusion, in: *Melt Extrus. Mater. Technol. Drug Prod. Des.*, 2013: pp. 161–203.
- [15] N. Shah, H. Sandhu, D.S. Choi, O. Kalb, S. Page, N. Wytenbach, Structured development approach for amorphous systems, in: R.O. Williams III, A.B. Watts, D.A. Miller (Eds.), *Formul. Poorly Water-Soluble Drugs*, Springer, 2012: pp. 267–310.
- [16] C. Adler, M. Schönenberger, A. Teleki, M. Kuentz, Molecularly designed lipid microdomains for solid dispersions using a polymer/inorganic carrier matrix produced by hot-melt extrusion, *Int. J. Pharm.* 499 (2016) 90–100.
- [17] J.P. Lakshman, Formulation, bioavailability, and manufacturing process enhancement: novel applications of melt extrusion in enabling product development, in: M.A. Repka, J. DiNunzio, N. Langley (Eds.), *Melt Extrus. Mater. Technol. Drug Prod. Des.*, Springer, 2013: pp. 329–362.
- [18] C. Adler, A. Teleki, M. Kuentz, Multifractal and mechanical analysis of amorphous solid dispersions, *Int. J. Pharm.* 523 (2017) 91–101. doi:10.1016/j.ijpharm.2017.03.014.
- [19] M. Kuentz, D.P. Elder, Methodology of oral formulation selection in the pharmaceutical industry, *Eur. J. Pharm. Sci.* 87 (2016) 136–163.
- [20] W.L. Chiou, S. Riegelman, Pharmaceutical Applications of Solid Dispersion Systems, *J. Pharm. Sci.* 60 (1971) 1281–1302.
- [21] C.A. McCarthy, R.J. Ahern, R. Dontireddy, K.B. Ryan, A.M. Crean, Mesoporous silica formulation strategies for drug dissolution enhancement: A review, *Expert Opin. Drug Deliv.* 13 (2016).
- [22] O.M.Y. Koo, *Pharmaceutical Excipients: Properties, Functionality, and Applications in Research and Industry*, Wiley, 2016.
- [23] O.G. Bhusnure, P.A. Kazi, S.B. Gholve, M.M.A.W. Ansari, K.S. N., SOLID DISPERSION: AN EVER GREEN METHOD FOR SOLUBILITY ENHANCEMENT OF POORLY WATER SOLUBLE DRUGS, *Int. Res. Pharm. Chem.* 4 (2014) 906–918.
- [24] T. Vasconcelos, B. Sarmiento, P. Costa, Solid Dispersions as Strategy to Improve Oral Bioavailability of Poor Water Soluble Drugs, *Drug Discov. Today.* 12 (2007) 1068–1075.
- [25] K. Sekiguchi, N. Obi, Studies on Absorption of Eutectic Mixture. I. A Comparison of the Behavior of Eutectic Mixture of Sulfathiazole and that of Ordinary Sulfathiazole in Man.,

- Chem. Pharm. Bull. (Tokyo). 9 (1961) 866–872.
- [26] T. Vasconcelos, B. Sarmiento, P. Costa, Solid Dispersions as Strategy to Improve Oral Bioavailability of Poor Water Soluble Drugs, *Drug Discov. Today*. 12 (2007) 1068–1075.
- [27] S. Sultana, A.H.M. Saifuddin, Review article: Solid dispersion currently practiced in pharmaceutical field, *Int. J. Adv. Res. Technol.* 5 (2016) 170–175.
- [28] H. Sandhu, N. Shah, H. Chokshi, A.W. Malick, Overview of Amorphous Solid Dispersion Technologies, in: N. Shah, H. Sandhu, D.S. Choi, H. Chokshi, M.A. Waseem (Eds.), *Amorph. Solid Dispersions Theory Pract.*, Springer, 2014: pp. 91–122.
- [29] N. Shah, H. Sandhu, W. Phuapradit, R. Pinal, R. Iyer, A. Albano, et al., Development of novel microprecipitated bulk powder (MBP) technology for manufacturing stable amorphous formulations of poorly soluble drugs, *Int. J. Pharm.* 438 (2012) 53–60.
- [30] ICH, Q3C Guideline for Residual Solvents (R5), *Int. Conf. Harmon. Tech. Requir. Regist. Pharm. Hum. Use.* (2011) 29.
- [31] N. Wytenbach, M. Kuentz, Glass-forming ability of compounds in marketed amorphous drug products, 2017.
- [32] S.A. Papadimitriou, D. Bikiaris, K. Avgoustakis, Microwave-induced enhancement of the dissolution rate of poorly water-soluble tibolone from poly(ethylene glycol) solid dispersions, *J. Appl. Polym. Sci.* 108 (2008) 1249–1258. doi:10.1002/app.27746.
- [33] M.K. Gupta, A. Vanwert, R.H. Bogner, Formation of physically stable amorphous drugs by milling with neusilin, *J. Pharm. Sci.* 92 (2003) 536–551.
- [34] A.-L. Lainé, D. Price, J. Davis, D. Roberts, R. Hudson, K. Back, et al., Enhanced oral delivery of celecoxib via the development of a supersaturable amorphous formulation utilising mesoporous silica and co-loaded HPMCAS, *Int. J. Pharm.* 512 (2016) 118–125.
- [35] H. Yan, E. Sun, L. Cui, X. Jia, X. Jin, Improvement in oral bioavailability and dissolution of tanshinone IIA by preparation of solid dispersions with porous silica, *J. Pharm. Pharmacol.* 67 (2015) 1207–1214.
- [36] W. Xu, J. Riikonen, V.-P. Lehto, Mesoporous systems for poorly soluble drugs, *Int. J. Pharm.* 453 (2013) 181–197.
- [37] A. Garcia-Bennett, A. Feiler, Mesoporous ASD: fundamentals, in: N. Shah, H. Sandhu, D. Soon Choi, H. Chokshi, A. Malick (Eds.), *Amorph. Solid Dispersions Theory Pract.*, Springer, 2014: pp. 637–693.
- [38] M. Kinoshita, K. Baba, A. Nagayasu, K. Yamabe, T. Shimooka, Y. Takeichi, et al.,

- Improvement of solubility and oral bioavailability of a poorly water-soluble drug, TAS-301, by its melt-adsorption on a porous calcium silicate, *J. Pharm. Sci.* 91 (2002) 362–370.
- [39] The speciality excipient Neusilin, (n.d.) Fuji Chemical Industry Co., Ltd.
- [40] A. Tan, S. Rao, C.A. Prestidge, Transforming lipid-based oral drug delivery systems into solid dosage forms: An overview of solid carriers, physicochemical properties, and biopharmaceutical performance, *Pharm. Res.* 30 (2013) 2993–3017.
- [41] H. Takeuchi, S. Nagira, H. Yamamoto, Y. Kawashima, Solid dispersion particles of amorphous indomethacin with fine porous silica particles by using spray-drying method, *Int. J. Pharm.* 293 (2005) 155–164.
- [42] Florite, (n.d.) Tomita Pharmaceutical Co., Ltd. www.tomitaph.co.jp.
- [43] J. Wang, D. Trinkle, G. Derbin, K. Martin, S. Sharif, P. Timmins, et al., Moisture adsorption and desorption properties of colloidal silicon dioxide and its impact on layer adhesion of a bilayer tablet formulation, *J. Excipients Food Chem.* 5 (2014) 21–31.
- [44] Evonik Industries, Aeroperl Granulated Fumed Oxides-Technical Information 1341, (2015) www.aerosil.com/sites/lists/RE/DocumentsSI/TI-1341.
- [45] Grace, Syloid Silicas- Pharmaceutical Excipients-Technical note 309d., (2015) www.grace.com/pharma-and-biotech/en-us/Documents/Syloid/M309d_Syloid_FP_XDP_Tech_Note_Oct.pdf.
- [46] Grace Materials and technologies, Syloid XDP 3050 Food additive and pharmaceutical excipient Product information, 2016. www.grace.com.
- [47] J. Forsgren, S. Frykstrand, K. Grandfield, A. Mihranyan, M. Strømme, A Template-Free, Ultra-Adsorbing, High Surface Area Carbonate Nanostructure, *PLoS One.* 8 (2013) e68486.
- [48] Merck Millipore, Make every drop count. Absorb more, achieve more with Parateck SLC, (n.d.). www.merckmillipore.com/parateckslc.
- [49] Evonik Industries, Speciality silica Sipernat and Sident, 2015. www.aerosil.com/product/aerosil/en/services/downloads/feed-food/Pages/default.aspx.
- [50] A. Feiler, Nonoporous silica advanced drug delivery, in: DDF Berlin, 2016. www.ddfevent.com/wp-content/uploads/2016/05/Adam-Feiler-Nanologica.pdf.
- [51] C.T. Kresge, M.E. Leonowicz, W.J. Roth, J.C. Vartuli, J.S. Beck, Ordered mesoporous molecular sieves synthesized by a liquid-crystal template mechanism, *Nature.* 359 (1992) 710–712.

- [52] D. Zhao, J. Feng, Q. Huo, N. Melosh, G.H. Fredrickson, B.F. Chmelka, et al., Triblock Copolymer Syntheses of Mesoporous Silica with Periodic 50 to 300 Angstrom Pores, *Science* (80-.). 279 (1998) 548 LP-552.
- [53] M. a Repka, S. Shah, J. Lu, S. Maddineni, J. Morott, K. Patwardhan, et al., Melt extrusion: process to product, *Expert Opin. Drug Deliv.* 9 (2012) 105–125.
- [54] S. Shah, M.A. Repka, Melt extrusion in drug delivery: three decades of progress, in: *Melt Extrus. Mater. Technol. Drug Prod. Des.*, 1st ed., Springer-Verlag New York, 2013: pp. 3–46.
- [55] S. Shah, M.A. Repka, Melt Extrusion in drug delivery: Three decades of progress, in: *Melt Extrus. Mater. Technol. Drug Prod. Des.*, 2013: pp. 3–46.
- [56] S. Madan, S. Madan, Hot melt extrusion and its pharmaceutical applications, *Asian J. Pharm. Sci.* 7 (2012) 123–133.
- [57] M. a Repka, S.K. Battu, S.B. Upadhye, S. Thumma, M.M. Crowley, F. Zhang, et al., Pharmaceutical applications of hot-melt extrusion: Part II., *Drug Dev. Ind. Pharm.* 33 (2007) 1043–1057.
- [58] Particle Sciences, Hot melt extrusion, *Tech. Br.* (2011) 3.
www.particlesciences.com/news/technical-briefs/2011/hot-melt-extrusion.html.
- [59] S. Shah, S. Maddineni, J. Lu, M.A. Repka, Melt extrusion with poorly soluble drugs, *Int. J. Pharm.* 453 (2013) 233–252.
- [60] W. Doetsch, Material handling and feeder technology, in: I. Ghebre-Selassie, C. Martin (Eds.), *Pharm. Extrus. Technol.*, Marcel Dek, 2013.
- [61] D. Leister, T. Geilen, G. Thobias, Twin-screw extruders for pharmaceutical hot-melt extrusion: Technology, techniques and practices, in: D. Douroumis (Ed.), *Hot-Melt Extrus. Pharm. Appl.*, Wiley, 2012: pp. 24–42.
- [62] M. Maniruzzaman, J.S. Boateng, M.J. Snowden, D. Douroumis, A review of hot-melt extrusion: process technology to pharmaceutical products., *ISRN Pharm.* 2012 (2012) 436763–436769.
- [63] C. Brown, J.C. DiNunzio, M. Eglesia, S. Forster, M. Lamm, M. Lowinger, et al., Hot-melt extrusion for solid dispersions: Composition and design considerations, in: N. Shah, H. Chokshi, H. Sandhu, A.W. Malick, D.S. Choi (Eds.), *Amorph. Solid Dispersions Theory Pract.*, Springer, 2014: pp. 196–230.
- [64] C. De Brabander, G. Van Den Mooter, C. Vervaet, J.P. Remon, Characterization of

- ibuprofen as a nontraditional plasticizer of ethyl cellulose, *J. Pharm. Sci.* 91 (2002) 1678–1685.
- [65] H. Arwidsson, O. Hjelstuen, D. Ingason, C. Graffner, Properties of ethyl cellulose films for extended release. II. Influence of plasticizer content and coalescence conditions when using aqueous dispersions, *Acta Pharm. Nord.* 3 (1991).
- [66] C.M. O’Driscoll, B.T. Griffin, Biopharmaceutical challenges associated with drugs with low aqueous solubility—The potential impact of lipid-based formulations, *Adv. Drug Deliv. Rev.* 60 (2008) 617–624.
- [67] M. Kuentz, Lipid-based formulations for oral delivery of lipophilic drugs, *Drug Discov. Today Technol.* 9 (2012) e97–e104.
- [68] M. Maniruzzaman, M.T. Islam, S. Halsey, D. Amin, D. Douroumis, Novel Controlled Release Polymer-Lipid Formulations Processed by Hot Melt Extrusion, *AAPS PharmSciTech.* 17 (2016) 191–199.
- [69] C. Reitz, P. Kleinebudde, Solid lipid extrusion of sustained release dosage forms, *Eur. J. Pharm. Biopharm.* 67 (2007) 440–448.
- [70] J. Krause, M. Thommes, J. Breitzkreutz, Immediate release pellets with lipid binders obtained by solvent-free cold extrusion, *Eur. J. Pharm. Biopharm.* 71 (2009) 138–144.
- [71] K. Vithani, M. Maniruzzaman, I.J. Slipper, S. Mostafa, C. Miolane, Y. Cuppok, et al., Sustained release solid lipid matrices processed by hot-melt extrusion (HME), *Colloids Surfaces B Biointerfaces.* 110 (2013) 403–410.
- [72] M.T. Islam, M. Maniruzzaman, S.A. Halsey, B.Z. Chowdhry, D. Douroumis, Development of sustained-release formulations processed by hot-melt extrusion by using a quality-by-design approach, *Drug Deliv. Transl. Res.* 4 (2014) 377–387.
- [73] P. Kleinebudde, Solid Lipid Extrusion, in: M.A. Repka, N. Langley, J. DiNunzio (Eds.), *Melt Extrus. Mater. Technol. Drug Prod. Des.*, Springer New York, 2013: pp. 299–328.
- [74] R. Laitinen, P.A. Priemel, S. Surwase, K. Graeser, C.J. Strachan, H. Groghanz, et al., Theoretical considerations in developing amorphous solid dispersions, in: N. Shah, H. Sandhu, D.S. Choi, H. Chokshi, M. A. Waseem (Eds.), *Amorph. Solid Dispersions Theory Pract.*, Springer New York, 2014: pp. 35–90.
- [75] A. Gryczke, Solubility parameters for prediction of drug/polymer miscibility in hot-melt extruded formulations, in: D. Douroumis (Ed.), *Hot-Melt Extrus. Pharm. Appl.*, John Wiley & Sons, Ltd., 2012: pp. 41–69.

- [76] K. Adamska, A. Voelkel, K. Héberger, Selection of solubility parameters for characterization of pharmaceutical excipients, *J. Chromatogr. A.* 1171 (2007) 90–97.
- [77] H.J. Lim, K. Lee, Y.S. Cho, Y.S. Kim, T. Kim, C.R. Park, Experimental consideration of the Hansen solubility parameters of as-produced multi-walled carbon nanotubes by inverse gas chromatography, *Phys Chem Chem Phys.* 16 (2014) 17466–17472.
- [78] J. Gupta, C. Nunes, S. Vyas, S. Jonnalagadda, Prediction of solubility parameters and miscibility of pharmaceutical compounds by molecular dynamics simulations, *J. Phys. Chem. B.* 115 (2011) 2014–2023.
- [79] K. Adamska, R. Bellinghausen, A. Voelkel, New procedure for the determination of Hansen solubility parameters by means of inverse gas chromatography, *J. Chromatogr. A.* 1195 (2008) 146–149.
- [80] S. Baghel, H. Cathcart, N.J. O'Reilly, Theoretical and experimental investigation of drug-polymer interaction and miscibility and its impact on drug supersaturation in aqueous medium, *Eur. J. Pharm. Biopharm.* 107 (2016) 16–31.
- [81] P.J. Marsac, T. Li, L.S. Taylor, Estimation of Drug--Polymer Miscibility and Solubility in Amorphous Solid Dispersions Using Experimentally Determined Interaction Parameters, *Pharm. Res.* 26 (2008) 139.
- [82] C.M. Hansen, Methods of characterization - Polymers, in: *Hansen Solubility Parameters A User's Handbook*, Second Ed., CRC Press, 2007: pp. 95–112.
- [83] D.J. Greenhalgh, A.C. Williams, P. Timmins, P. York, Solubility parameters as predictors of miscibility in solid dispersions, *J. Pharm. Sci.* 88 (1999) 1182–1190.
- [84] T. Kitak, A. Dumičić, O. Planinšek, R. Šibanc, S. Srčić, Determination of Solubility Parameters of Ibuprofen and Ibuprofen Lysinate, *Molecules.* 20 (2015) 21549–21568.
- [85] M.M. Knopp, N.E. Olesen, P. Holm, K. Löbmann, R. Holm, P. Langguth, et al., Evaluation of Drug–Polymer Solubility Curves Through Formal Statistical Analysis: Comparison of Preparation Techniques, *J. Pharm. Sci.* 104 (2015) 44–51.
- [86] S. Thakral, N.K. Thakral, Prediction of Drug-Polymer Miscibility through the use of Solubility Parameter based Flory-Huggins Interaction Parameter and the Experimental Validation: PEG as Model Polymer, *J. Pharm. Sci.* 102 (2013) 2254–2263.
- [87] P. Narayan, W.W. Porter, M. Brackhagen, C. Tucker, Polymers and surfactants, in: A. Newman (Ed.), *Pharm. Amorph. Solid Dispersions*, Wiley, Wiley, 2015: pp. 42–84.
- [88] M.C. Hansen, The Three-Dimensional Solubility Parameter - Key to Paint Component

- Affinities, *J. Paint Technol.* 39 (1967) 104–117.
- [89] D.W. van Krevelen, K. te Nijenhuis, Cohesive Properties and Solubility, in: Elsevier (Ed.), *Prop. Polym. Their Correl. with Chem. Struct. Their Numer. Estim. Predict. from Addit. Gr. Contrib.*, Elsevier Science, 2009: pp. 189–225.
- [90] B.A. Miller-Chou, J.L. Koenig, A review of polymer dissolution, *Prog. Polym. Sci.* 28 (2003) 1223–1270.
- [91] C.M. Hansen, *Hansen Solubility Parameters A User's Handbook*, 2013.
- [92] A. Forster, J. Hempenstall, I. Tucker, T. Rades, Selection of excipients for melt extrusion with two poorly water-soluble drugs by solubility parameter calculation and thermal analysis, *Int. J. Pharm.* 226 (2001) 147–161.
- [93] D.T. Friesen, R. Shanker, M. Crew, D.T. Smithey, W.J. Curatolo, J.A.S. Nightingale, Hydroxypropyl methylcellulose acetate succinate-based spray-dried dispersions: an overview., *Mol. Pharm.* 5 (2008) 1003–1019.
- [94] F.G. Vogt, Solid-state characterization of amorphous dispersions, in: A. Newman (Ed.), *Pharm. Amorph. Solid Dispersions*, Wiley, 2015: pp. 117–178.
- [95] R.A. Storey, I. Ymén, *Solid State Characterization of Pharmaceuticals*, 2011.
- [96] A. Newmann, E. Munson, Characterizing miscibility in amorphous solid dispersions, *Am. Pharm. Rev.* (2012). www.americanpharmaceuticalreview.com/Featured-Articles/112448-Characterizing-Miscibility-in-Amorphous-Solid-Dispersions.
- [97] D. Gramaglia, B.R. Conway, V.L. Kett, R.K. Malcolm, H.K. Batchelor, High speed DSC (hyper-DSC) as a tool to measure the solubility of a drug within a solid or semi-solid matrix, *Int. J. Pharm.* 301 (2005) 1–5.
- [98] S.R. Vippagunta, K.A. Maul, S. Tallavajhala, D.J.W. Grant, Solid-state characterization of nifedipine solid dispersions, *Int. J. Pharm.* 236 (2002) 111–123.
- [99] R. Lopes, N. Betrouni, Fractal and multifractal analysis: A review, *Med. Image Anal.* 13 (2009) 634–649.
- [100] N. Pippa, A. Dokoumetzidis, C. Demetzos, P. Macheras, On the ubiquitous presence of fractals and fractal concepts in pharmaceutical sciences: A review, *Int. J. Pharm.* 456 (2013) 340–352.
- [101] C. Tzoganakis, B.C. Price, S.G. Hatzikiriakos, Fractal analysis of the sharkskin phenomenon in polymer melt extrusion, *J. Rheol. (N. Y. N. Y.)* 37 (1993) 355–366.
- [102] A. Ekielski, K. Mishra, E. Biller, F. Ratajczyk, Utilizing fractal dimensions of extrudate

- sectional images for describing their textural properties, in: 15th International SGEMGeoConference Nano, Bio, Green Technol. Suitable Futur. Sect. Adv. Biotechnol., 2015.
- [103] A. Ekielski, Effect of selected parameters of double-screw extruder operation on fractal dimensions of the extrudate, *Ann. Warsaw Univ. Life Sci. SGGW, Agric.* 57 (2011) 41–47.
- [104] C. Adler, A. Teleki, M. Kuentz, Multifractal Characterization of Pharmaceutical Hot-Melt Extrudates, *Pharm. Res.* 34 (2017) 321–332. doi:10.1007/s11095-016-2064-4.
- [105] N. Fotaki, C.M. Long, K. Tang, H. Chokshi, Dissolution of amorphous solid dispersions: theory and practice, in: N. Shah, H. Chokshi, H. Sandhu, A.W. Malick, D.S. Choi (Eds.), *Amorph. Solid Dispersions Theory Pract.*, Springer, 2014: pp. 487–514.
- [106] The United States Pharmacopeia and the national formulary, USP (2009a), Dissolution. *Off. Compend. Stand. USP 32–NF 27.* (n.d.).
- [107] PhEUR (2011) European pharmacopoeia, Chapter 2.9.3 Dissolution Test Solid Dos. Forms, Strasbourg, Fr. Counc. Eur. Eur. Dir. Qual. Med. Healthc. (n.d.).
- [108] JP XV (2006) Japanese pharmacopoeia, Chapter 6.10 Dissolution Test. (n.d.).
- [109] Particle Sciences, In vitro dissolution testing for solid oral dosage forms, *Tech. Br.* 5 (2010).
- [110] K.P. O’Donell, R.O. Williams III, Optimizing the formulation of poorly water-soluble drugs, in: R.O. Williams III, A.B. Watts, D.A. Miller (Eds.), *Formul. Poorly Water-Soluble Drugs*, Springer, 2012: pp. 27–93.
- [111] J.T. Gautschi, Nonsink in vitro dissolution testing of amorphous solid dispersions, in: M.A. Repka, N. Langley, J. DiNunzio (Eds.), *Melt Extrus. Mater. Technol. Drug Prod. Des.*, Springer, 2013: pp. 205–220.
- [112] E.S. Kostewicz, B. Abrahamsson, M. Brewster, J. Brouwers, J. Butler, S. Carlert, et al., In vitro models for the prediction of in vivo performance of oral dosage forms, *Eur. J. Pharm. Sci.* 57 (2014) 342–366.
- [113] M. Pudlas, S.O. Kyeremateng, L.A.M. Williams, J.A. Kimber, H. van Lishaut, S.G. Kazarian, et al., Analyzing the impact of different excipients on drug release behavior in hot-melt extrusion formulations using FTIR spectroscopic imaging., *Eur. J. Pharm. Sci.* 67 (2015) 21–31.
- [114] F. Tres, J.D. Patient, P.M. Williams, K. Treacher, J. Booth, L.P. Hughes, et al., Monitoring

- the dissolution mechanisms of amorphous bicalutamide solid dispersions via real-time Raman mapping, *Mol. Pharm.* 12 (2015) 1512–1522.
- [115] J.P. Boetker, M. Savolainen, V. Koradia, F. Tian, T. Rades, A. Mullertz, et al., Insights into the early dissolution events of amlodipine using UV imaging and Raman spectroscopy., *Mol. Pharm.* 8 (2011) 1372–1380.
- [116] A. V. Rao, L.G. Rao, Carotenoids and human health, *Pharmacol. Res.* 55 (2007) 207–216.
- [117] J. Challem, M. Moneysmith, *User's Guide to Carotenoids and Flavonoids*, Basic Health Publications, Incorporated, 2005.
- [118] O.A. Eldahshan, A. Nasser, B. Singab, Carotenoids, *J. Pharmacogn. Phytochem.* 8192 (2013) 2668735–5.
- [119] T.L. Sourkes, The discovery and early history of carotene, *Bull. Hist. Chem.* 32 (2009) 32–38.
- [120] G.F. Stewart, B.S. Schweigert, J. Hawthorn, J.C. Bauernfeind, *Carotenoids as Colorants and Vitamin A Precursors: Technological and Nutritional Applications*, Elsevier Science, 2012.
- [121] I.W.G. on the Evaluation of Cancer-preventive Agents, I.A. for Research on Cancer, *Carotenoids*, International Agency for Research on Cancer, 1998.
- [122] J. Higdon, *Carotenoids- α -Carotene, β -Carotene, β -Cryptoxanthin, Lycopene, Lutein, and Zeaxanthin*, Linus Pauling Inst. (2004).
- [123] D.B. Rodriguez-Amaya, *Food Carotenoids: Chemistry, Biology and Technology*, Wiley, 2015.
- [124] S. Singh, R.S. Baghel, L. Yadav, A review on solid dispersion, *Int. J. Pharm. Life Sci.* 2 (2011) 1078–1095.
- [125] C. Timpe, Drug solubilization strategies applying nanoparticulate formulation and solid dispersion approaches in drug development, *Am. Pharm. Rev.* (2010).
- [126] M. Windbergs, C.J. Strachan, P. Kleinebudde, Understanding the solid-state behaviour of triglyceride solid lipid extrudates and its influence on dissolution, *Eur. J. Pharm. Biopharm.* 71 (2009) 80–87.
- [127] N. Khan, D.Q.M. Craig, Role of blooming in determining the storage stability of lipid-based dosage forms, *J. Pharm. Sci.* 93 (2004) 2962–2971.
- [128] R. Chadha, S. Bhandari, Drug-excipient compatibility screening--role of thermoanalytical and spectroscopic techniques., *J. Pharm. Biomed. Anal.* 87 (2014) 82–97.

- [129] J.L. Ford, T.E. Mann, Fast-Scan DSC and its role in pharmaceutical physical form characterisation and selection, *Adv. Drug Deliv. Rev.* 64 (2012) 422–430.
- [130] G.S. Oladiran, H.K. Batchelor, Determination of ibuprofen solubility in wax: A comparison of microscopic, thermal and release rate techniques, *Eur. J. Pharm. Biopharm.* 67 (2007) 106–111.
- [131] P. Liu, L. Yu, H. Liu, L. Chen, L. Li, Glass transition temperature of starch studied by a high-speed DSC, *Carbohydr. Polym.* 77 (2009) 250–253.
- [132] F. Theeuwes, A. Hussain, T. Higuchi, Quantitative analytical method for determination of drugs dispersed in polymers using differential scanning calorimetry, *J. Pharm. Sci.* 63 (1974) 427–429.
- [133] F.D. V. Jannin, M. Di Cuia, S. Chevrier, A. Faure, Y. Chavant, C. Voutsinas, Characterization of new self-emulsifying excipient to expand formulation options for poorly soluble drugs: Gelucire 48/16, AAPS, 2012.
- [134] D. Bikiaris, G.Z. Papageorgiou, A. Stergiou, E. Pavlidou, E. Karavas, F. Kanaze, et al., Physicochemical studies on solid dispersions of poorly water-soluble drugs: Evaluation of capabilities and limitations of thermal analysis techniques, *Thermochim. Acta.* 439 (2005) 58–67.
- [135] M.E. Lauer, M. Siam, J. Tardio, S. Page, J.H. Kindt, O. Grassmann, Rapid assessment of homogeneity and stability of amorphous solid dispersions by atomic force microscopy—from bench to batch, *Pharm. Res.* 30 (2013) 2010–22.
- [136] R. Jagtap, A. Ambre, Overview literature on atomic force microscopy (AFM): basics and its important applications for polymer characterization, *Indian J. Eng. Mater. Sci.* 13 (2006) 368–384.
- [137] A.G. Marangoni, L.H. Wesdorp, Structure and properties of fat crystals networks, in: Second edi, CRC Press, 2012: pp. 428–432.
- [138] J. Szpylka, J.W. DeVries, Determination of β -Carotene in Supplements and Raw Materials by Reversed-Phase High Pressure Liquid Chromatography: Collaborative Study, *J. AOAC Int.* 88 (2005) 1279–1291.
- [139] G.P. Andrews, H. Zhai, S. Tipping, D.S. Jones, Characterisation of the thermal, spectroscopic and drug dissolution properties of mefenamic acid and polyoxyethylene–polyoxypropylene solid dispersions, *J. Pharm. Sci.* 98 (2009) 4545–4556.
- [140] R.H. Müller, M. Radtke, S.A. Wissing, Solid lipid nanoparticles (SLN) and nanostructured

- lipid carriers (NLC) in cosmetic and dermatological preparations, *Adv. Drug Deliv. Rev.* 54 (2002) 131–155.
- [141] V. Jannin, J. Musakhanian, D. Marchaud, Approaches for the development of solid and semi-solid lipid-based formulations, *Adv. Drug Deliv. Rev.* 60 (2008) 734–746.
- [142] C.I. Braga, M.C. Rezende, M.L. Costa, Methodology for DSC calibration in high heating rates, *J. Aerosp. Technol. Manag.* 3 (2011) 179–192.
- [143] J.I. Langford, A.J.C. Wilson, Scherrer after sixty years: A survey and some new results in the determination of crystallite size, *J. Appl. Crystallogr.* 11 (1978) 102–113.
- [144] A.W. Burton, K. Ong, T. Rea, I.Y. Chan, On the estimation of average crystallite size of zeolites from the Scherrer equation: A critical evaluation of its application to zeolites with one-dimensional pore systems, *Microporous Mesoporous Mater.* 117 (2009) 75–90.
- [145] S. Qi, P. Belton, K. Nollenberger, A. Gryczke, D.M. Craig, Compositional Analysis of Low Quantities of Phase Separation in Hot-Melt-Extruded Solid Dispersions: A Combined Atomic Force Microscopy, Photothermal Fourier-Transform Infrared Microspectroscopy, and Localised Thermal Analysis Approach, *Pharm. Res.* 28 (2011) 2311–2326.
- [146] M.A. Emin, E. Mayer-Miebach, H.P. Schuchmann, Retention of β -carotene as a model substance for lipophilic phytochemicals during extrusion cooking, *LWT - Food Sci. Technol.* 48 (2012) 302–307.
- [147] J. Maclean, C. Medina, D. Daurio, F. Alvarez-Nunez, J. Jona, E. Munson, et al., Manufacture and performance evaluation of a stable amorphous complex of an acidic drug molecule and Neusilin, *J. Pharm. Sci.* 100 (2011) 3332–3344.
- [148] J. Sruti, C.N. Patra, S.K. Swain, S. Beg, H.R. Palatasingh, S.C. Dinda, et al., Improvement in Dissolution Rate of Cefuroxime Axetil by using Poloxamer 188 and Neusilin US2., *Indian J. Pharm. Sci.* 75 (2013) 67–75.
- [149] T. Ungár, Microstructural parameters from X-ray diffraction peak broadening, *Scr. Mater.* 51 (2004) 777–781.
- [150] D. Bahl, R.H. Bogner, Amorphization of indomethacin by co-grinding with Neusilin US2: Amorphization kinetics, physical stability and mechanism, *Pharm. Res.* 23 (2006) 2317–2325. doi:10.1007/s11095-006-9062-x.
- [151] T.A. Gavrilko, G.O. Puchkovska, V.I. Styopkin, T.V. Bezrodna, J. Baran, M. Drozd, Molecular dynamics and phase behavior of binary mixtures of fatty acids and cetyltrimethylammonium bromide as studied via Davydov splitting of molecular

- vibrational modes, *Ukr. J. Phys.* 58 (2013) 636–645.
- [152] P.D.A. Pudney, K.J. Mutch, S. Zhu, Characterising the phase behaviour of stearic acid and its triethanolamine soap and acid-soap by infrared spectroscopy., *Phys. Chem. Chem. Phys.* 11 (2009) 5010–5018.
- [153] M. Muchow, P. Maincent, R.H. Müller, Lipid nanoparticles with a solid matrix (SLN, NLC, LDC) for oral drug delivery., *Drug Dev. Ind. Pharm.* 34 (2008) 1394–1405.
- [154] C. Adler, M. Schönenberger, A. Teleki, B. Leuenberger, M. Kuentz, M. Schönenberger, et al., Flow-through cross-polarized imaging as a new tool to overcome the analytical sensitivity challenges of a low-dose crystalline compound in a lipid matrix., *J. Pharm. Biomed. Anal.* 115 (2015) 20–30.
- [155] B. Hancock, P. York, R. Rowe, The use of solubility parameters in pharmaceutical dosage form design, *Int. J. Pharm.* 148 (1997) 1–21. doi:10.1016/j.ijpharm.2006.11.034.
- [156] Q. Cheng, Multifractality and spatial statistics, *Comput. Geosci.* 25 (1999) 949–961.
- [157] A. Dathe, A.M. Tarquis, E. Perrier, Multifractal analysis of the pore- and solid-phases in binary two-dimensional images of natural porous structures, *Geoderma.* 134 (2006) 318–326.
- [158] A. Gómez-Carracedo, C. Alvarez-Lorenzo, R. Coca, R. Martínez-Pacheco, A. Concheiro, J.L. Gómez-Amoza, Fractal analysis of SEM images and mercury intrusion porosimetry data for the microstructural characterization of microcrystalline cellulose-based pellets, *Acta Mater.* 57 (2009) 295–303.
- [159] F. Mendoza, P. Verboven, Q.T. Ho, G. Kerckhofs, M. Wevers, B. Nicolai, Multifractal properties of pore-size distribution in apple tissue using X-ray imaging, *J. Food Eng.* 99 (2010) 206–215.
- [160] L. Valentini, G. Artioli, M. Voltolini, M.C. Dalconi, Multifractal Analysis of Calcium Silicate Hydrate (C-S-H) Mapped by X-ray Diffraction Microtomography, *J. Am. Ceram. Soc.* 95 (2012) 2647–2652.
- [161] V. Klang, C. Valenta, N.B. Matsko, Electron microscopy of pharmaceutical systems, *Micron.* 44 (2013) 45–74.
- [162] C.-W. Park, Y.-S. Rhee, F.G. Vogt, D. Hayes, J.B. Zwischenberger, P.P. DeLuca, et al., Advances in microscopy and complementary imaging techniques to assess the fate of drugs ex vivo in respiratory drug delivery: an invited paper., *Adv. Drug Deliv. Rev.* 64 (2012) 344–56.

- [163] R. Thibert, M. Akbarieh, R. Tawashi, Application of fractal dimension to the study of the surface ruggedness of granular solids and excipients, *J. Pharm. Sci.* 77 (1988) 724–726.
- [164] M. Stanković, H.W. Frijlink, W.L.J. Hinrichs, Polymeric formulations for drug release prepared by hot melt extrusion: application and characterization, *Drug Discov. Today*. (2015) 1–12.
- [165] C.L. Li, L.G. Martini, J.L. Ford, M. Roberts, The use of hypromellose in oral drug delivery, *J. Pharm. Pharmacol.* 57 (2005) 533–546.
- [166] P. Harmon, K. Galipeau, W. Xu, C. Brown, W.P. Wuelfing, Mechanism of Dissolution-Induced Nanoparticle Formation from a Copovidone-Based Amorphous Solid Dispersion, *Mol. Pharm.* 13 (2016) 1467–1481.
- [167] S. Bialleck, H. Rein, Drug release mechanisms of hot-melt extruded starch-based pellets, *Starch/Staerke*. 64 (2012) 408–419.
- [168] I. Bravo-Osuna, C. Ferrero, M.R. Jiménez-Castellanos, Drug release behaviour from methyl methacrylate-starch matrix tablets: Effect of polymer moisture content, *Eur. J. Pharm. Biopharm.* 69 (2008) 285–293.
- [169] A.N.D. Posadas, D. Giménez, M. Bittelli, C.M.P. Vaz, M. Flury, Multifractal Characterization of Soil Particle-Size Distributions, *Soil Sci. Soc. Am. J.* 65 (2001) 1361.
- [170] T.C. Halsey, M.H. Jensen, L.P. Kadanoff, I. Procaccia, B.I. Shraiman, Fractal measures and their singularities: The characterization of strange sets, *Nucl. Phys. B.* 2 (1987) 501–511.
- [171] J. Angulo, F. Esquivel, Multifractal Dimensional Dependence Assessment Based on Tsallis Mutual Information, *Entropy*. 17 (2015) 5382–5401.
- [172] D.L. Turcotte, Fractal models in the Earth sciences, *Tectonophysics*. 227 (1993) 234.
- [173] Basic characteristics of Aerosil fumed silica- Technical bulletin fine particles 11, (n.d.) Evonik Industries.
- [174] S.H. Bumm, Mixing studies and simulation of compounding chopped fiber and silica filler into thermoplastics in a modular co-rotating twin screw extruder, University of Akron, 2010.
- [175] Evonik Industries, Aerosil and Aeroperl Colloidal Silicon Dioxid for Pharmaceuticals- Technical Information TI 1281, (2013) www.aerosil.com/sites/lists/RE/DocumentsSI/TI-1281.
- [176] V.G. Kadajji, G. V. Betageri, Water soluble polymers for pharmaceutical applications,

- Polymers (Basel). 3 (2011) 1972–2009.
- [177] P. Colombo, R. Bettini, P. Santi, A. De Ascentiis, N.A. Peppas, Analysis of the swelling and release mechanisms from drug delivery systems with emphasis on drug solubility and water transport, *J. Control. Release*. 39 (1996) 231–237.
- [178] P. Colombo, R. Bettini, P. Santi, N.A. Peppas, Swellable matrices for controlled drug delivery: Gel-layer behaviour, mechanisms and optimal performance, *Pharm. Sci. Technol. Today*. 3 (2000) 198–204.
- [179] P. Joyce, A. Tan, C.P. Whitby, C.A. Prestidge, The Role of Porous Nanostructure in Controlling Lipase-Mediated Digestion of Lipid Loaded into Silica Particles, *Langmuir*. 30 (2014) 2779–2788.
- [180] M. Van Speybroeck, H.D. Williams, T.-H. Nguyen, M.U. Anby, C.J.H. Porter, P. Augustijns, Incomplete Desorption of Liquid Excipients Reduces the in Vitro and in Vivo Performance of Self-Emulsifying Drug Delivery Systems Solidified by Adsorption onto an Inorganic Mesoporous Carrier, *Mol. Pharm*. 9 (2012) 2750–2760.
- [181] C.A.S. Bergström, C.M. Wassvik, K. Johansson, I. Hubatsch, Poorly soluble marketed drugs display solvation limited solubility, *J. Med. Chem*. 50 (2007) 5858–5862.
- [182] C. Kutza, H. Metz, J. Kutza, F. Syrowatka, K. Mäder, Toward a detailed characterization of oil adsorbates as “solid liquids,” *Eur. J. Pharm. Biopharm*. 84 (2013) 172–182.
- [183] P. Lopez-Sanchez, S. Schumm, P.D. a Pudney, J. Hazekamp, Carotene location in processed food samples measured by Cryo In-SEM Raman., *Analyst*. 136 (2011) 3694–3697.
- [184] G. Valsami, P. Macheras, Determination of fractal reaction dimension in dissolution studies, *Eur. J. Pharm. Sci*. 3 (1995) 163–169.
- [185] K. Kosmidis, P. Argyrakis, P. Macheras, Fractal kinetics in drug release from finite fractal matrices, *J. Chem. Phys*. 119 (2003) 6373–6377.
- [186] A. Dokoumetzidis, P. Macheras, The changing face of the rate concept in biopharmaceutical sciences: from classical to fractal and finally to fractional., *Pharm. Res*. 28 (2011) 1229–1232.
- [187] A. Dokoumetzidis, A. Iliadis, P. Macheras, Nonlinear dynamics and chaos theory: concepts and applications relevant to pharmacodynamics, *Pharm Res*. 18 (2001) 415–426.
- [188] Y. Choudhari, U. Reddy, F. Monsuur, T. Pauly, H. Hofer, W. McCarthy, Comparative evaluation of porous silica based carriers for lipids and liquid drug formulations,

- Mesoporous Biomater. 1 (2014) 61–74.
- [189] M. Brncic, B. Tripalo, S. Rimac Brncic, S. Karlovic, A. Zupan, Z. Herceg, Evaluation of textural properties for whey enriched direct extruded and puffed corn based products, *Bulg. J. Agric. Sci.* 15 (2009) 204–213.
- [190] P.D.A. Pudney, L. Gambelli, M.J. Gidley, Confocal Raman microspectroscopic study of the molecular status of carotenoids in tomato fruits and foods, *Appl. Spectrosc.* 65 (2011) 127–134.
- [191] R.J. Weesie, J.C. Merlin, J. Lugtenburg, G. Britton, F.J. Jansen, J.P. Cornard, Semiempirical and Raman spectroscopic studies of carotenoids., *Biospectroscopy*. 5 (1999) 19–33.
- [192] N. Chieng, T. Rades, J. Aaltonen, An overview of recent studies on the analysis of pharmaceutical polymorphs, *J. Pharm. Biomed. Anal.* 55 (2011) 618–644.
- [193] M. Maguregui, U. Knuutinen, J. Trebolazabala, H. Morillas, K. Castro, I. Martinez-Arkarazo, et al., Use of in situ and confocal Raman spectroscopy to study the nature and distribution of carotenoids in brown patinas from a deteriorated wall painting in Marcus Lucretius House (Pompeii), *Anal. Bioanal. Chem.* 402 (2012) 1529–1539.
- [194] D.B. Rodriguez-Amaya, I.L.S. Institute, O. (Project), *A Guide to Carotenoid Analysis in Foods*, ILSI Press, 2001.
- [195] L.A. Felton, J.W. McGinity, *Aqueous Polymeric Coatings for Pharmaceutical Dosage Forms*, Third Edition, in: CRC Press, 2008.
- [196] S.Y. Fu, X.Q. Feng, B. Lauke, Y.W. Mai, Effects of particle size, particle/matrix interface adhesion and particle loading on mechanical properties of particulate-polymer composites, *Compos. Part B Eng.* 39 (2008) 933–961.
- [197] R.L. Oréfice, L.L. Hench, A.B. Brennan, Effect of particle morphology on the mechanical and thermo-mechanical behavior of polymer composites, *J. Brazilian Soc. Mech. Sci.* 23 (2001) 1–8.
- [198] S.C. Tjong, Structural and mechanical properties of polymer nanocomposites, *Mater. Sci. Eng. R Reports*. 53 (2006) 73–197.
- [199] R.C.R. Nunes, J.L.C. Fonseca, M.R. Pereira, Polymer–filler interactions and mechanical properties of a polyurethane elastomer, *Polym. Test.* 19 (2000) 93–103.
- [200] S.-F. Chou, K.A. Woodrow, Relationships between mechanical properties and drug release from electrospun fibers of PCL and PLGA blends, *J. Mech. Behav. Biomed. Mater.* 65

- (2017) 724–733.
- [201] R. Zhang, Z. Zhang, L. Zou, H. Xiao, G. Zhang, E.A. Decker, et al., Enhancing Nutraceutical Bioavailability from Raw and Cooked Vegetables Using Excipient Emulsions: Influence of Lipid Type on Carotenoid Bioaccessibility from Carrots., *J. Agric. Food Chem.* 63 (2015) 10508–10517.
- [202] Z. Zhang, R. Zhang, D.J. McClements, Encapsulation of β -carotene in alginate-based hydrogel beads: Impact on physicochemical stability and bioaccessibility, *Food Hydrocoll.* 61 (2016) 1–10.

List of abbreviations

AFM	Atomic force microscopy
AMS	Aluminum magnesium silicate
ANOVA	Analysis of variance
API	Active pharmaceutical ingredient
ATR-FTIR	Attenuated total reflectance Fourier-transform infrared spectroscopy
BC	β -carotene
BCS	Biopharmaceutical classification system
BSI	Breaking force index
CED	Cohesive energy density
DSC	Differential scanning calorimetry
DLM	Designed lipid microdomain
EDS	Energy dispersive X-Ray spectroscopy
FTIR	Fourier-transform infrared spectroscopy
HME	Hot-melt extrusion
HPC	Hydroxypropylcellulose
HPLC	High performance liquid chromatography
HDSC	High-speed differential scanning calorimetry
MDSC	Modulated differential scanning calorimetry
NCE	New chemical entity
NMR	Nuclear magnetic resonance
PLM	Polarized light microscopy
PM	Physical mixture
PVPVA	Polyvinylpyrrolidone vinyl acetate
RP-HPLC	Reverse-phase high performance liquid chromatography
SA	Stearic acid
SCF	Supercritical fluid
SD	Solid dispersion
SEM	Scanning electron microscopy
SFC	Solid fat content
TD-NMR	Time-domain nuclear magnetic resonance

TGA Thermogravimetric analysis

XRPD X-ray powder diffraction

List of symbols

$f(a)$	Hausdorff fractal dimension
n_{drug}	Number of mole of drug
$n_{polymer}$	Number of mole of polymer
q	Moment
w	Weight
D	Fractal dimension
D_0	Capacity dimension
D_1	Information dimension
D_2	Correlation dimension
D_q	Generalized multifractal dimension
E_v	Energy of vaporization
E_{hi}	Group contribution for hydrogen bonding interactions
F_{di}	Group contribution for dispersive interactions
F_{pi}	Group contribution for polar interactions
ΔG_m	Free energy of mixing
ΔH_m	Enthalpy of mixing
M_w	Molecular weight
N	Number of boxes of size ε
Oil	TD-NMR signal intensity of the oil
P_i	Probability of finding the object pixel in the i^{th} box of size ε
R	Gas constant
$Sample$	TD-NMR signal intensity of the sample
Si	Silicon
T	Temperature of NMR analysis
T_g	Glass transition temperature

T_m	Melting temperature
V_m	Molar volume
X_0	Diameter of dried pellet
X	Pellet diameter at time of analysis
$X(q, \varepsilon)$	Partition function
α_i	Leipschitz-Hölder exponent
δ	Solubility parameter
δ_d	Partial solubility parameter accounting for dispersion effects
δ_h	Partial solubility parameter accounting for hydrogen bonding
δ_p	Partial solubility parameter accounting for polar effects
$\Delta\delta_t$	Total 3-D Hansen solubility parameter
ε	Difference between drug and polymer total solubility parameters
φ_d	Volume fraction of drug
φ_p	Volume fraction of polymer
χ_{dp}	Flory-Huggins interaction parameter

List of figures

Fig. 2.1. Illustration of the different types of amorphous SDs	6
Fig. 2.2. Number of publications since 1980 to current on the topic of HME	13
Fig. 2.3. Scheme of a twin-screw extruder and downstream processes.	14
Fig. 2.4. Example of a laboratory scale twin-screw extruder.....	15
Fig. 2.5. Example of a microcompounder and barrel design	15
Fig. 2.6. Example of screw configuration showing the different subsections of twin-screw extrusion process.	16
Fig. 2.7. Commonly used screw elements in pharmaceutical HME process.	17
Fig. 2.8. T_m/T_g of drug as a function of Log P and related drug loading range.	27
Fig. 2.9. Chemical structure of all-trans BC.....	32
Fig. 3.1. Schematic of XPT-C cross-polarized particle analyzer	41
Fig. 3.2. SFC profiles of pure Gelucire 50/13 and Geleol as a function of temperature obtained by TD-NMR.	42
Fig. 3.3. 3D-laser scanning images of pure Gelucire 50/13 and Geleol.....	44
Fig. 3.4. DSC thermograms of Gelucire 50/13 and Geleol SDs and PMs	45
Fig. 3.5. XRPD diffractograms of Gelucire 50/13 and Geleol SDs BC, as well as of pure BC	49
Fig. 3.6. Polarized light micrographs of molten Gelucire 50/13 and Geleol SDs.....	50
Fig. 3.7. 3D-laser scanning images of Gelucire 50/13 and Geleol SDs	51
Fig. 3.8. AFM superposed topography and phase images of Gelucire 50/13 and Geleol SDs	52
Fig. 3.9. 3D-laser scanning images and AFM superposed topography and phase images of Gelucire 50/13 and Geleol SDs	53
Fig. 3.10. Number of particles per gram of molten Gelucire 50/13 and Geleol as function of BC concentration	56
Fig. 4.1. SFC profile as a function of temperature measured by TD-NMR and XRPD diffractogram of pure SA	65
Fig. 4.2. XRPD diffractogram of extrudates containing different ratios of HPC, SA and AMS..	66
Fig. 4.3. Room temperature ATR-FTIR absorption spectra of pure SA, and HPC/SA/AMS extrudates in the regions of C=O and COO ⁻ stretching, and area under the curve corresponding to dimer band and carboxylate band as a function of formulation composition	68

Fig. 4.4. Room temperature ATR-FTIR absorption spectra of pure SA, and HPC/SA/AMS extrudates in the regions of CH stretching, and CH rocking vibrations.....	69
Fig. 4.5. ATR-FTIR absorption spectra of SA as a function of temperature, and of the DLM formulation at room temperature in the regions of C=O and COO ⁻ stretching vibrations.....	71
Fig. 4.6. ATR-FTIR absorption spectra of SA as a function of the temperature, and of the DLM formulation at room temperature in the regions of CH stretching, and CH rocking vibrations.....	72
Fig. 4.7. AFM 3D height images of extrudates composed of HPC/SA/AMS formulations, and DLM system.....	73
Fig. 4.8. SEM and corresponding EDS pictures of 80/20% (w/w) HPC/AMS and DLM system.	74
Fig. 4.9. XRPD diffractograms of pure BC and of extrudates containing 3% (w/w) BC.....	75
Fig. 4.10. Room temperature ATR-FTIR spectra of placebo DLM formulation and DLM formulation containing 3% (w/w) BC.....	76
Fig. 4.11. AFM phase images of extrudates.....	77
Fig. 4.12. Schematic of H-bond and ion-dipole interactions between SA and AMS in the DLM system.....	78
Fig. 4.13. Room temperature ATR-FTIR absorption spectra of SA, and HPC/AMS/SA extrudates in the region of C-O-H bending and stretching as well as CH scissoring and wagging vibrations.	83
Fig. 4.14. ATR-FTIR absorption spectra of pure SA and of the DLM formulation as a function of temperature in the region of C-O-H bending and stretching as well as CH scissoring and wagging vibrations.....	84
Fig. 5.1. D_q versus moment q for a multifractal and a monofractal.	90
Fig. 5.2. Illustration of the conversion of a SEM/EDS 2D-picture to a binary picture and examples of box sizes used in the box-counting method	93
Fig. 5.3. SEM/EDS 2D-pictures of Si distribution in extrudates	94
Fig. 5.4. D_q over the [-5;5] moment q range of formulations prepared at 150 rpm.	95
Fig. 5.5. D_q spectrum over the [-5;5] moment q range of formulations prepared using 150, 250, and 350 rpm screw speeds.....	97
Fig. 5.6. SEM/EDS 2D-pictures of Si distribution in extrudates containing different adsorbents	98
Fig. 5.7. D_q spectrum over the [-5;5] moment q range of formulations containing different adsorbents.....	99
Fig. 5.8. Aqueous dispersion of extrudate pellets over time in water	102

Fig. 5.9. Evolution of erosion and swelling fronts of pellets over time.....	103
Fig. 5.10. SEM pictures of fumed Aerosil 300, and Aerosil R 972	105
Fig. 5.11. SEM pictures of Aeroperl 300, Florite R, and Neusilin US2	105
Fig. 6.1. Illustration of the conversion of a SEM/EDS 2-D picture to a binary picture and examples of box sizes used in the box-counting method	112
Fig. 6.2. Example of D_q versus q for a multifractal and a monofractal object.....	114
Fig. 6.3. XDPR diffractograms and DSC thermograms of extrudate formulations	118
Fig. 6.4. Raman spectra of pure BC, extrudate strands and of BC dispersed in Labrafac PG.	120
Fig. 6.5. SEM and corresponding EDS 2-D binary pictures of F1 and F3	122
Fig. 6.6. D_q over the [0,2] moment q range of formulations F1 and F3.....	123
Fig. 6.7. SEM and corresponding EDS 2-D binary pictures of F2 and F4 formulations.....	124
Fig. 6.8. Generalized multifractal dimensions Dq over the moment q range of extrudates.....	125
Fig. 6.9. BSI of extrudate formulations obtained by three point bending test	127
Fig. 6.10. SEM pictures of Aeroperl 300 and Syloid XDP	129

List of tables

Table 2.1. Classification and properties of solid dispersions	7
Table 2.2. Processing technologies used in amorphous solid dispersion manufacturing.....	9
Table 2.3. List of inorganic excipients commonly used in pharmaceutical formulation	11
Table 2.4. Common pharmaceutical polymers used in hot-melt extrusion processes	19
Table 2.5. Common pharmaceutical functional additives used in hot-melt extrusion	20
Table 2.6. Commonly used lipid-based excipients	21
Table 2.7. Commonly used computational and experimental methods for the estimation of drug-polymer miscibility	23
Table 2.8. Relevant characteristics of polymers, additives and API used in hot-melt extrusion]..	27
Table 2.9. Common analytical methods used to investigate hot-melt extrusion formulations	30
Table 2.10. Physico-chemical properties of β -Carotene	32
Table 3.1. Melting peak and onset temperature of the raw materials obtained by DSC at heating rates of 5 C/min and 150°C/min.....	43
Table 3.2. Enthalpy of melting of the lipid-based solid dispersions containing different concentrations of β -Carotene (BC) (150°C/min heating rate).	47
Table 4.1. Formulation composition of extrudate strands produced by HME.....	61
Table 5.1. Adsorbents used in the extrudate formulations	91
Table 5.2. Composition of the extrudates and screw speeds used during HME process	91
Table 6.1. Hot-melt extrusion formulations composition	110
Table 6.2. Physico-chemical properties of adsorbents.....	117

Acknowledgements

I would like to express my gratitude to all persons who supported me and encouraged me during my PhD.

I gratefully acknowledge Prof. Dr. Imanidis for giving me the chance to complete my PhD at the University of Basel and at the University of Applied Sciences and Arts Northwestern Switzerland. I appreciated all our fruitful scientific discussions and your continuous good mood.

Many thanks also go to Prof. Dr. Martin Kuentz who gave me a lot of freedom and trusted me during these PhD years. I enjoyed our scientific discussions as well as your constant optimism and enthusiasm. I am grateful to you since you helped me to find a balance between perfectionism and efficacy.

Thanks go also to Dr. Alexandra Teleki without whom I would not have had the chance to start my PhD in Basel. I spent a great time in your team in DSM Nutritional Products during which I learnt a lot and gained self-confidence. I really appreciated our collaboration during this project and I thank you for your valuable inputs.

I would like to acknowledge Dr. Bruno Leuenberger for his expertise and help at the beginning of my Thesis.

Thanks also go to Dr. Elger Funda and Dr. Christian Schäfer, for their valuable inputs and for their support.

Many thanks also to the Analytical Research Center of DSM Nutritional Products for the HPLC analysis.

I also thank Henry Rieger, Simon Spreiter and Alain Mauranne for their precious help.

I am also grateful to Prof. Dr. Karine Mougin for having accepted to be the co-referent of my thesis.

Many thanks also to Dr. Monika Schönenberger for having taken the time to analyze my complex samples.

I also would like to acknowledge Theodore Bühler who introduced me to numerous analytical techniques.

To my IPT colleagues, I would like to say thank you for the nice and convivial moments we spent together. I liked the lunch and coffee breaks, the breakfasts and Christmas dinners. It was a pleasure to learn to know all of you. Angela, Barbora, Benjamin L., Benjamin Z., Berndt, Carla,

Claudia, David, Dominik, Felix, Georg, Jael, Jan, Jonas, Katka, Kira, Lena, Martin C., Martin N., Martin K., Matthias, Michael, Nicolas, Oliver, Patricia, Renata N., Renata A. V., Sandra, Sheela, Simone, Susanne, Tarik, Tahir, Ursula, Veronika, Wiebke, Zdravka, Thank you!! Special thanks go to Andreas, my lab-mate, with whom I spent amazing moments. It was so pleasant to share the lab with you.

A ma famille, j'aimerais dire un grand merci pour m'avoir toujours encouragée. Même si vous ne savez pas exactement ce que j'ai fait durant ces années de thèse, vous avez été présents dans les bons moments comme dans les périodes un peu plus difficiles.

Enfin, j'aimerais te remercier Thibault d'avoir accepté mon rythme de travail et de m'avoir encouragée et rassurée lorsque j'en avais besoin. Ta présence a été précieuse pour mener à bien ce projet de vie qui m'ouvre maintenant de nouveaux horizons.

Curriculum Vitae

Camille Adler

2 Impasse des Cerisiers

68490 Hombourg

camiadler68@gmail.com

Born in Mulhouse, France

4th May 1988

Education

PhD in Pharmaceutical Technology

Oct 2013 - May 2017

University of Basel and University of Applied Sciences and Arts Northwestern Switzerland

Master in Chemical Engineering

Sept 2009 – Sept 2013

Engineering School of Chemistry (ENSCMu), Mulhouse, France

Bachelor in Chemistry

Sept 2007 – Jun 2009

Technical and Scientific University (FST), Mulhouse, France

Gymnasium

Sept 2003 – Jun 2006

Lycée Jeanne d'Arc, Mulhouse, France

Work Experience

Graduate Research Internship

Feb - Aug 2013

DSM Nutritional Products, Nutrition R&D Center Formulation and Application, Kaiseraugst

Industry Internship

Jul 2012

Zülpich Kappa Papier, Zülpich, Germany

Research Internship

Jun 2012

Institute of Materials Science of Mulhouse (IS2M), France

Industry Internship

Jul 2010

Millenium Inorganic Chemicals (Cristal Global), Analysis laboratory, Thann, France

List of Publications and Patents

- C. Adler, M. Kuentz, and A. Teleki. Novel extrudates WO2017005622 A1, 2017.
- C. Adler, A. Teleki, and M. Kuentz, Multifractal and mechanical analysis of amorphous solid dispersions, *Int. J. Pharm.* 523 (2017) 91-101.
- A. Teleki and C. Adler, Formulation of sparingly soluble compounds by hot-melt extrusion, WO 2015071394 A1, 2016.
- C. Adler, A. Teleki, and M. Kuentz, Multifractal Characterization of Pharmaceutical Hot-Melt Extrudates, *Pharm. Res.* 34 (2017) 321–332.
- C. Adler, M. Schönenberger, A. Teleki, and M. Kuentz, Molecularly designed lipid microdomains for solid dispersions using a polymer/inorganic carrier matrix produced by hot-melt extrusion, *Int. J. Pharm.* 499 (2016) 90–100.
- C. Adler, M. Schönenberger, A. Teleki, B. Leuenberger, and M. Kuentz, Flow-through cross-polarized imaging as a new tool to overcome the analytical sensitivity challenges of a low-dose crystalline compound in a lipid matrix., *J. Pharm. Biomed. Anal.* 115 (2015) 20–30.

List of Posters and Oral Presentations

- C. Adler, A. Teleki, and M. Kuentz. The multifractal nature of amorphous hot-melt extrudates (Poster presentation).
Annual Research Meeting, Department of Pharmaceutical Sciences, University of Basel, Switzerland, 2017.

- C. Adler. Designed lipid microdomains: A new formulation approach for poorly water-soluble compounds (Oral presentation).
Forschungsevent, School of Life Sciences, University of Applied Sciences and Arts Northwestern Switzerland, 2016.
- C. Adler, A. Teleki, and M. Kuentz. Multifractal analysis and dispersion imaging of pharmaceutical hot-melt extrudates (Poster presentation).
9th Swiss Pharma Science Day, Bern Switzerland, 2016.
- C. Adler, A. Teleki, and M. Kuentz. Designing a lipid microstructure on an inorganic carrier for solid drug dispersion formulation (Poster presentation).
Formula VIII, Barcelona, Spain, 2016.
- C. Adler, A. Teleki, M. Schönenberger, and M. Kuentz. Designing lipid microdomains on an inorganic carrier by hot-melt extrusion (Poster presentation).
10th World Meeting on Pharmaceutics, Biopharmaceutics and Pharmaceutical Technology, Glasgow, United Kingdom, 2016.
- C. Adler. Designing a lipid microstructure on an inorganic carrier for solid drug dispersion formulation (Oral presentation).
Annual Research Meeting, Department of Pharmaceutical Sciences, University of Basel, Switzerland, 2016.
- C. Adler, A. Teleki, M. Schönenberger, and M. Kuentz. A new polymer/lipid system for hot-melt extrusion by designing a microstructure on an inorganic carrier (Poster presentation).
Annual Research Meeting, Department of Pharmaceutical Sciences, University of Basel, Switzerland, 2016.
- C. Adler, A. Teleki, M. Schönenberger, and M. Kuentz. Designing lipid microdomains on an inorganic carrier by hot-melt extrusion (Poster presentation).
8th Swiss Pharma Science Day, Bern Switzerland, 2015.

- C. Adler. Flow-through cross-polarized imaging as a new tool to overcome the analytical sensitivity challenges of a low-dose crystalline compound in a lipid matrix (Oral presentation).
Forschungsseminar, School of Life Sciences, University of Applied Sciences and Arts Northwestern Switzerland, 2015.
- C. Adler, A. Teleki, B. Leuenberger, and M. Kuentz. Introducing flow-through cross-polarized imaging to analyze a low-dose crystalline drug in a lipid matrix (Poster presentation).
Controlled Release Society German Chapter Annual Meeting, Muttenz, Switzerland, 2015.
- C. Adler, A. Teleki, M. Schönenberger, and M. Kuentz. Overcoming the challenges of analytical characterization sensitivity of a low dose active compound in a lipid matrix (Poster presentation).
7th Swiss Pharma Science Day, Bern Switzerland, 2014
- C. Adler, A. Teleki, and M. Kuentz. Dissolution study of hot melt extrudates using water vapor sorption analysis and automated microscopic imaging (Poster presentation).
2nd Poorly Soluble Drugs Workshop, Lille, France 2014.
- C. Adler, A. Teleki, and M. Kuentz. Comparison of hot-melt extrudates dissolution using water sorption analysis and automated microscopic imaging (Poster presentation).
9th World Meeting on Pharmaceutics, Biopharmaceutics and Pharmaceutical Technology, Lisbon, Portugal 2014.
- C. Adler, A. Teleki, and M. Kuentz. Comparison of hot-melt extrudates dissolution using water sorption analysis and automated microscopic imaging (Poster presentation).
Annual Research Meeting, Department of Pharmaceutical Sciences, University of Basel, Switzerland, 2014.

Awards

- Noelting Prize for a deserving graduated student given by the Association of Chemistry of Mulhouse, 2013
- Top student in graduate class for Master in Chemical Engineering, Mulhouse, France, 2009 – 2013.
- Top student in undergraduate class for Bachelor in Chemistry, Mulhouse, France, 2007 – 2009.
- Scientific Baccalauréat Diploma with highest honors, 2006.